Mapping Complex Brain Torque Components and Their Genetic Architecture and Phenomic Associations in 24,112 Individuals

Supplement 1

Zhao *et al.*

This file includes:

Supplementary Methods Materials and
Supplementary References
Figures S1 to S32
Tables S1 to S7 and S15 to S18
Legends for Tables S8 to S14 and S19 to S29 (provided in separate Excel files)

Supplementary Methods and Materials

Study Population

The current study utilized neuroimaging data of 24,112 subjects from 6 cohorts: the Adolescent Brain Cognitive Development (ABCD), the Human Connectome Project (HCP), the International *Consortium for* Brain Mapping (ICBM), the Pediatric Imaging, Neurocognition, and Genetics (PING), the Philadelphia Neurodevelopmental Cohort (PNC) and the UK Biobank (UKB). Table S1 provides population characteristics of each cohort. All study procedures were approved by the institutional review boards of the participating institutions of these projects, and all participants provided written informed consent.

Adolescent Brain Cognitive Development

The Adolescent Brain and Cognitive Development Study (ABCD) (1) is a multi-site, longitudinal neuroimaging study following 9–10 year-old youth through adolescence. The ABCD study team employed a rigorous epidemiologically informed school-based recruitment strategy, designed with consideration of the demographic composition of the 21 ABCD sites. This study employed the baseline structural brain MRI dataset of 2,891 subjects from the release 1.0. Details about MRI acquisition protocols are available in (2). Parental informed consent and child assent were obtained from all participants and approved by centralized and institutional review boards at each data collection site. We discarded 12 subjects due to failed image processing or incomplete metadata and other 110 subjects who were identified as outliers in terms of brain torque (BT) measures (> mean±3SD), resulting in a sample of 2,769 subjects (age range 9 – 11 years, 1,449 males). Handedness was evaluated using the ABCD Youth Edinburgh Handedness Inventory (EHI) Short Form (3) and the sample were classified into left-handed (N = 196), right-handed (N = 2,181) and mixed-handed (N = 392). In ABCD, child psychopathological symptoms/behaviors were evaluated using the parent-reported child behavior checklist (CBCL (4)). The ABCD CBCL contains 20 items, including 8 syndrome scales (Anxious/Depressed, Withdrawn/Depressed, Somatic Complaints, Social Problems, Thought Problems, Attention Problems, Aggressive Behavior, Rule-breaking Behavior), 1 total score summarizing all 8 syndrome scales, 2 broad-band scales (Internalizing and Externalizing Problems) as well as 6 DSM-oriented scales (Depressive Problems, Anxiety Problems, Somatic Problems, Attention-Deficit/Hyperactivity Disorder (ADHD), Oppositional Defiant Disorder (ODD), and Conduct Disorder), and 3 2007 scales (Sluggish Cognitive Tempo (SCT), Obsessive-Compulsive Problems (OCD) and Stress Problems). All CBCL items were recorded as t-scores. Details about the ABCD cohort are available at https://abcdstudy.org.

Human Connectome Project

The Human Connectome Project (HCP) (5) is a project to map the neural pathways that underlie brain function and behavior using high-quality neuroimaging data (https://humanconnectome.org/). The details about the HCP dataset are available in the HCP reference manual (https://www.humanconnectome.org/study/hcp-young-adult/document/900-subjects-data-release). All subjects provided written informed consent on forms approved by the Institutional Review Board of Washington University. This study relied on 897 HCP subjects with structural brain imaging from the HCP S900 release (age range 22-37 years, 393 males). In HCP, the strength of hand preference had been assessed with EHI (3), resulting in scores ranging from -100 (strong left-hand preference) to 100 (strong right-hand preference). According to the EHI (6), subjects were classified into left-, right- and mixed-handers based the scores (left: -100 to -60, N = 46; mixed: -60 to 60, N = 195; right: 60 to 100, N = 656). 37 HCP subjects identified as outliers in terms of BT measures were discarded in the current study.

International Consortium for Brain Mapping

The International Consortium for Brain Mapping (ICBM) project developed a probabilistic reference system for the human brain (7). We included structural MRI scans of 641 subjects from the ICBM database. 229 subjects for whom MR image processing was failed and 41 subjects who

were outliers in terms of BT measures were discarded in the current study, leaving 371 subjects (age range 18 – 80 years, 197 males). Handedness was quantified with a Laterality Quotient (LQ) using EHI (3) and the sample were classified into left-handed (N = 34), right-handed (N = 333) and mixed-handed (N = 4). All subjects gave informed consent according to institutional guidelines. Details about the dataset are available at https://ida.loni.usc.edu/.

Pediatric Imaging, Neurocognition, and Genetics

The Pediatric Imaging, Neurocognition, and Genetics (PING) data repository is a resource of standardized and curated data of brain MRI, genomics, and developmental and neuropsychological assessments for a large cohort of developing children aged 3 – 20 years (8). Participants and their parents gave their written informed consent or assent to participate in study procedures. Written parental informed consent was obtained for all PING subjects below the age of 18, and child assent was also obtained for all participants between the ages of 7 and 17. Written informed consent was obtained directly from all participants aged 18 years or older. Handedness was reported by parents or guardians of the minor participants and participants aged 18 and over when they complete the PING Study Demographics and Child Health History Questionnaire. Detailed information about the PING dataset is available at https://chd.ucsd.edu/research/ping.html and in (8). This study utilized structural brain MRI scans of 693 PING participants. We removed 3 participants due failed MRI processing and other 23 participants who were outliers in terms of BT measures, resulting a sample of 677 subjects (age range 3 – 21 years, 355 males, 70 left-handers, 577 right-handers, 30 mixed-handers).

Philadelphia Neurodevelopmental Cohort

The Philadelphia Neurodevelopmental Cohort (PNC) is a large-scale initiative that seeks to describe how genetics impact trajectories of brain development and cognitive functioning in adolescence, and understand how abnormal trajectories of development are associated with psychiatric symptomatology (9, 10). Signed informed consent or assent and parental consent (for participants under age 18) were obtained for all participants. In PNC, all neuroimaging scans were acquired at a single site, on a single scanner, in a short period of time that did not span any software or hardware upgrades (10). Of the initial 1,445 subjects who completed imaging, 448 subjects were excluded because of a history of potential abnormal brain development or a history of medical problems that may affect the brain. We further excluded 20 subjects with failed MRI processing and 55 subjects as outliers of BT measures, leaving 922 subjects (age range 8 – 23, 428 males, 126 left-handers, 796 right-handers). Measures of handedness were based on self-reports of dominant handedness. In PNC, child psychopathological symptoms/behaviors were evaluated using a structured screening interview GOASSESS (11). The psychopathology screen in GOASSESS assessed lifetime occurrence of major domains of psychopathology including psychosis spectrum symptoms, mood (major depressive episode, mania), anxiety (agoraphobia, generalized anxiety, panic, specific phobia, social phobia, separation anxiety), behavioral disorders (oppositional defiant, attention deficit/hyperactivity, conduct), eating disorders (anorexia, bulimia), and suicidal thinking and behavior. 112 item-level symptoms were used in this study as suggested in recent factor analyses of these clinical data (12, 13). Details about the PNC dataset are available at https://www.med.upenn.edu/bbl/philadelphianeurodevelopmentalcohort.html.

UK Biobank

UK Biobank (UKB) is a large-scale biomedical database and research resource, containing in-depth genetic and health information from about 500,000 UK participants. The present analyses were conducted under UKB application number 25641. Ethical approval was obtained from the research ethics committee (REC reference 11/NW/0382). All participants provided informed consent to participate. Further information on the consent procedure can be found at http://biobank.ctsu.ox.ac.uk/crystal/field.cgi?id=200. This study used brain MRI imaging data (14, 15) (UK Biobank data-field: 110) from the 2018 August release of 22,392 participants (http://biobank.ctsu.ox.ac.uk/crystal/label.cgi?id=110). Details of the MRI acquisition is described in the UK Biobank Brain Imaging Documentation (http://biobank.ctsu.ox.ac.uk/crystal/refer.cgi?id=1977) and in a protocol form

(http://biobank.ctsu.ox.ac.uk/crystal/refer.cgi?id=2367). This study discarded 1,002 participants whose MRI scans did not pass manual quality assessment, 1,148 participants due to data withdraw from UKB or failed image processing, and other 1719 participants who were identified as outliers in terms of BT measures, resulting a sample of 18,513 subjects with age range from 44 to 81 years, and 8,908 male subjects. Handedness was assessed based on responses to the question (UK Biobank data-field: 1707): "*Are you right or left handed?*" with four response options: "*Right-handed*", "*Left-handed*", "*Use both right and left equally*", and "*Prefer not to answer*". Those who preferred not to answer were excluded for association analysis with handedness, leaving 16,489 right-handers, 1747 left-handers, and 277 mixed-handers with BT measures. We also employed genome-wide genotyping data as described at http://www.ukbiobank.ac.uk/scientists-3/genetic-data/, as well as other phenotypic data, including brain MRI measures of GM morphologies, WM microstructures, T2*, and task-based BOLD (blood-oxygen-level dependent) effects (14, 15), questionnaires of health and lifestyle, sociodemographic factors, physical and cognitive measures, and etc. In addition to the above exclusion criteria, 795 participants who reported a diagnosis of neurological and/or psychiatric disorder at scanning (UKB data-field: 20002) were discarded in the analyses of population-level average torque patterns and the effects of age, sex, handedness and TIV, and in the genetic analyses (excluded disorders are listed in Table S23). These participants were included in the phenome-wide scans for exploring possible associations with clinical traits.

MRI processing for BT measurements

Different BT components were measured in the 6 neuroimaging datasets using a framework integrating a set of automatic 3D brain shape analysis approaches introduced in recent studies (16-19) (Fig. 1).

All MR images were first preprocessed using the FSL software (20) v5.0 (https://fsl.fmrib.ox.ac.uk/fsl/fslwiki/) to align brain volumes to the standard MNI template (MNI152 nonlinear asymmetric template 6th generation, see https://fsl.fmrib.ox.ac.uk/fsl/fslwiki/Atlases) using 7 degrees of freedom transformations (i.e., 3 translations, 3 rotations, and 1 uniform scaling) (Fig. 1-A). This preprocessing normalized individual brains into a common coordinate system without distorting the morphological shapes. Next, the normalized images were processed using the FreeSurfer software package (21) v6.0 (https://surfer.nmr.mgh.harvard.edu) to reconstruct cortical hemispheric surfaces (Fig. 1-B). The FreeSurfer workflow includes motion correction and averaging of volumetric T1-weighted images (22), removal of non-brain tissue (23), automated Talairach transformation, brain volume segmentation (24, 25), intensity normalization (26), tessellation of the boundary between gray matter (GM) and white matter (WM), automated topology correction (27) and surface deformation following intensity gradients to optimally place the GM/WM and GM/cerebrospinal fluid borders at the location where the greatest shift in intensity defines the transition to the other tissue class (28). Each hemispheric GM and WM surface is composed of 163,842 vertices arranged as 327,680 triangles. Once the surface models are complete, a number of deformable procedures were performed for further data processing and analysis, including surface inflation, registration to a spherical atlas using individual cortical folding patterns to match cortical geometry across subjects (29).

Accurate definition of the mid-sagittal plane (MSP) is essential for the accuracy of BT measurements, because computation of the angle of interhemispheric fissure bending and surface positional asymmetry relies on it. As a result of the linear spatial normalization using FSL, the x, y and z axes of the MNI coordinate system by default correspond to the left-right, anterior-posterior and dorsal-ventral directions of the brain and the plane x=0 represents the MSP. However, the linear registration is often insufficient to align the true brain MSP to x=0 due to the asymmetric nature of the brain (30, 31). To address the potential deviation, the MSP was defined as the least squares plane that best fits the vertices on the two hemispheric medial surfaces (excluding the frontal and occipital poles where the interhemispheric fissure bending is maximum) lying within 5 mm to x=0 in the MNI space. Then, the brain orientation was refined by rotating the brain surface with an 3D angle between the plane x=0 and the estimated MSP (Fig. 1-D).

To measure gross lobar torque features, a morphologic closing operation was applied to the pial surfaces of smoothed hemispheric volumes in order to fill the sulci (https://surfer.nmr.mgh.harvard.edu/fswiki/LGI) (Fig. 1-E). Petalia and shift were computed as the respective displacements of the left and right frontal and occipital extreme points along the antero-posterior and dorso-ventral axes respectively (Fig. 1-F). In (17, 18), to measure frontal and occipital bending, planes were first fitted to the vertices of the medial surfaces of the left and right hemispheres in the first (frontal) and last (occipital) quarters of the anterior-posterior length of the brain, next angles between the fitted planes' normals and the normal of MSP were calculated for the left and right hemispheres separately, then the angles were averaged between the two hemispheres as the measure of bending. The frontal/occipital bending is a geometric distortion observed in the axial view (32). However, rotation of these fitted planes relative to MSP is not restricted to be in the axial view (around the Z-axis) only, because of the irregular geometry of the cortical surface. Thus, the direction of the fitted plane's normal is uncertain in the 3D space, consequently the normal-based measure could not directly reflect the true bending in the left or right direction (Fig. S26). To address this issue, we measured the bending with a different procedure: 1) extract the points with the shortest distances to both the left and right hemispheric surfaces from the image background to capture the longitudinal shape of the interhemispheric fissure (33), 2) fit planes to these points in the frontal and occipital regions, 3) the frontal and occipital bending were measured as the angles between these fitted planes and the MSP in the axial view (Fig. 1-F).

Left-right tissue distribution asymmetry (TDA) was measured on a cross-sectional basis, where each cerebral hemisphere was independently and evenly cut into 60 contagious slices (ribbons of the hemispheric pial surface) perpendicular to the antero-posterior axis (Fig. 1-G). Each slice has a dimension of about 3 mm (similar to the widths of major sulci (34)) along the anterior-posterior axis, as measured on the MNI152 brain template. For each slice, a bounding box covering the slice surface was generated with three edges parallel to the x, y, and z axes. The width of each bounding box was measured as the sectional hemispheric width at the corresponding brain slice. The sectional hemispheric perimeter was measured as the average length of the hemispheric pial surface at two ends of each slice. The profile of both width and perimeter measures for the contiguous slices represents the variation of the cerebral hemisphere external morphology along the antero-posterior direction. The difference of the measures between the left and right cerebral hemispheres reflected the bilateral variation of the cerebral surface.

Positional differences between the two cerebral hemispheres were computed at each vertex to quantify relative displacements along the left-right, antero-posterior and ventro-dorsal axes (Fig. 1-H). The left-right positional asymmetry ($Asym_{LR}$) was computed as the distance of a vertex on the left hemispheric surface to the MSP subtracted from that of its corresponding vertex on the right hemispheric surface. The antero-posterior positional asymmetry ($Asym_{AP}$) and dorsal-ventral positional asymmetry ($Asym_{DV}$) were calculated as the projections of the displacement vector between the left and right corresponding vertices along the anterior-posterior and dorso-ventral axes. In particular, the vertex-wise interhemispheric correspondences were obtained by nonlinearly registering both hemispheric surfaces to the same symmetrical reference based on local folding patterns (35) (Fig. 1-C). These vertex-wise measures of surface positional asymmetry (SPA) were smoothed on the tessellated surfaces using a Gaussian kernel with the full width half maximum (FWHM) of 20 mm to increase the signal-to-noise ratio and to reduce the impact of mis-registration. Additionally, we computed mean $Asym_{LR}$, $Asym_{AP}$ and $Asym_{DV}$ within 74 brain regions defined by the FreeSurfer Destrieux atlas (36). These regional SPA measures were used as substitutes for the vertex-wise measures in the analyses of BT features' intercorrelations and phenomic and genomic associations to overcome the computational challenge in these high-dimensional analyses.

Because a 7 degrees of freedom transformation was performed at the beginning of this workflow (see above), all the BT measures were divided by the uniform scaling factor obtained in the linear spatial normalization so as to recover the BT measures to the native dimensions, except the

angular measures of frontal and occipital bending that are independent of global scaling. All the BT profiles were measured using programs written in Matlab (R2019b). All the procedure for MRI processing and BT measurements were implemented on the LONI pipeline system for high-performance parallel computing (http://pipeline.loni.usc.edu) (37, 38). To exclude possible outliers in terms of BT measures, we excluded the subjects with at least one lobar measure exceeded 3 standard deviations from the mean in each individual cohort. We also evaluated if BT measures would change with inter-individual variation in brain image quality. A highly reliable measure of image quality (39) - the Euler number (40) was extracted from each subject's FreeSurfer output. The FreeSurfer's Euler number summarizes the topological complexity of reconstructed cortical surfaces. Correlations between BT measures and the Euler number were assessed in each individual data set. No significant correlations with Euler number were found in all datasets ($|r| < 0.2$) (Fig. S27-S32).

Statistical analysis for BT and effects of age, sex, handedness and TIV

To determine population-level, average patterns of BT, one-sample t-tests were applied to individual and pooled data sets to examine the null hypothesis that the mean of each BT measure differs from zero. Correlations between all BT features of petalia, bending, shift, sectional TDA and regional SPA were assessed. For a general view, we also assessed correlations between the major BT components, including the lobar measures of petalia, bending, shift and global summary metrics of TDA and SPA. For an individual, the summary metrics of TDA were computed as the maximal sectional hemispheric width/perimeter asymmetry in the anterior (front 30 slices) and posterior (back 30 slices) portions of the brain. To compute the summary metrics of SPA for an individual, the map of vertex-wise, population-average beta values for SPA estimated using linear regression were multiplied by the individual's SPA map, then these products were summed over all vertices.

To characterize the complex (linear and nonlinear), lifespan age trajectories of BT using the pooled sample, linear regression models were constructed with a step-down model selection procedure testing for cubic, quadratic and linear age effects, for each lobar profile, at each brain slice for sectional TDA, and at each cortical surface vertex for SPA. Such method has been commonly used in previous studies of complex brain structural trajectories in neurodevelopment (41) and aging (42, 43). The full model for a BT measure T is

$$T = intercept + \beta_1 Age + \beta_2 Age^2 + \beta_3 Age^3 + e,$$

where e is the residual error, and the intercept and β terms are the fixed effects. If the cubic age effect was not significant, the cubic term was removed and we stepped down to the quadratic model and so on. The analyses were repeated controlling for sex, handedness and total Intracranial volume (TIV) as covariates. Additionally, since there were twins and siblings (from ABCD and HCP) contained in the sample, we included family as a random effect to account for the family structure. MRI acquisition sites and scanners were not included in this lifespan analysis using the pooled sample because of their pronounced associations with age ($r > 0.79$) caused by the lack of age overlapping across the individual datasets (Table S1). To validate if the results would be confounded by sites/scanners, age effects were retested in 3 separate age windows (3-22, 18-40, 40-81 years) using subsamples with maximally overlapped age ranges and adjusting for sites/scanners and other covariates described above. The subsamples for 3-22 years consisted of the ABCD, PING and PNC cohorts (N = 4,368), for 18-40 years consisted of the HCP and a part of ICBM cohorts (N = 1,132), and for 40-81 years consisted of the UKB and a part of ICBM cohorts (N = 17,817).

To investigate effects of sex, handedness, sex-by-handedness interaction and TIV in the pooled sample (N = 23,317), we repeated the linear regressions with these terms as the fixed effects and adjusting for linear, quadratic and cubic age effects, sites and scanners and a random variable of family. Sex and handedness differences in variance and prevalence of BT features were examined using variance ratio test (F-test) and Chi-squared two-sample test respectively.

We corrected for multiple comparisons for BT measures at different scales separately. For lobar and sectional measures, Bonferroni correction was applied to set a significance

threshold adjusting for the number of profiles (P < 0.05/6 lobar measures and P < 0.05/60 × 2 sectional measures). Vertex-wise statistical results were corrected across the cortical surface using the random field theory (RFT) method (44) that adapts to spatial correlations of the surface data. The critical threshold was set to RFT-corrected P < 0.05/3 to further correct for the 3 positional asymmetry dimensions. Significant vertex-wise sex and handedness differences in variance of SPA were detected at false discovery rate (FDR) < 0.05/3. All linear regression analyses were conducted using our Neuroimaging PheWAS system, which is a cloud-computing platform for big-data, brain-wide imaging association studies (for details, see http://phewas.loni.usc.edu/phewas/ and (45)).

Phenome scan analyses

Phenome scan analyses were conducted for the BT measures (6 lobar measures + 60×2 TDA + 74×3 regional SPA = 348 profiles in total) derived from the UKB dataset using the Phenome Scan Analysis Tool (46) (PHESANT, https://github.com/MRCIEU/PHESANT) so as to search for other related variables in addition to age, sex, handedness and genetic factors. 6,334 phenomic variables of sociodemographics, lifestyle, environment, cognitive functions, health and medical information, and medical imaging markers were extracted from the UKB database. 795 participants, who reported a diagnosis of neurological and/or psychiatric disorder and were excluded in other analyses, were included here to enable to explore possible associations with clinical traits. PHESANT was specifically designed for performing comprehensive phenome scans across the complex UKB data fields, using an automated, rule-based method to determine how to test variables of different types. A detailed description of PHESANT's automated rule-based method is given in (46). PHESANT estimates the bivariate association of each BT measure with each phenotypic variable in the dataset using linear, logistic, ordered logistic, and multinominal logistic regression for continuous, binary, ordered categorical, and unordered categorical data types respectively. Prior to testing, an inverse normal rank transform is applied to variables of the continuous data type, to ensure they are normally distributed. All analyses were adjusted for age, age^2, sex, handedness, TIV, the first ten genetic principal components, imaging-related variables (15, 47) including MRI acquisition center (UKB data-field: 54-2.0), X/Y/Z brain center of gravity (UKB data-fields: 25756, 25757 and 25758), scanner table position (UKB data-field: 25759), T1 signal-to-noise ratio (UKB data field: 25734), T1 contrast-to-noise ratio (UKB data-field: 25735), mean rfMRI head motion (UKB data-field: 25741) and mean tfMRI head motion (UKB data-field: 25742). Phenome-wide significance was determined using a critical threshold adjusting for the 6,334 phenotypes and the 348 BT measures (P < 0.05/6334/348 = 2.27e-8).

Associations between BT features and child psychopathological symptoms/behaviors were tested using the ABCD and PNC datasets. The psychopathological measures included 20 ABCD CBCL scales and 112 PNC GOASSESS items, as described in above section of Study Population. These analyses were conducted using multiple linear regression as implemented in the Neuroimaging PheWAS tool (45), adjusting for age, age^2, sex, handedness, TIV, the first ten genetic principal components. For ABCD, we also adjusted for scanners and imaging sites, and the random effect of family membership. Scanners/sites were not included in the model for PNC, as all imaging data from the PNC were acquired at a single site, on a single scanner, in a short period of time that did not span any software or hardware upgrades (10). In addition, the analyses were repeated to assess effects of age (8-22 years)-by-psychopathology interactions on BT features using the PNC dataset (not using the ABCD dataset because of its focused age range (9-10 years)). Significant associations and interactions were determined using a critical threshold adjusting for the number of psychopathological measures (20 for ABCD and 112 for PNC) and the 348 BT measures.

Genomic Data and Processing

This study employed genomic data from the ABCD, PING, PNC and UKB datasets. ABCD participants were genotyped using the Affymetrix NIDA Smokescreen array, consisting of 733,293 SNP markers. For PING participants, genotyping was performed on the Illumina Human660W-

Quad BeadChip with 550,000 SNPs. Of the initial 1,445 PNC participants recruited for brain imaging, 657 were genotyped on the Illumina HumanHap 610 array; 399 on the Illumina HumanHap 550 array; 281 on the Illumina Human Omni Express array and 108 on the Affymetrix Axiom array. Prior to imputation, the ABCD, PING and PNC datasets were filtered using the standard GWAS quality control (QC) protocol (48, 49), so as to exclude samples with low individual call rate < 90%, sex discrepancy, outlying heterozygosity (> mean±3SD), non-European ancestry (genetic principal component analysis outliers whose values of the first 2 PCs exceeded the median ± 5×interquartile range of the reference European sample (1000G Phase3 v5)) and/or being related to another sample (PI_HAT > 0.2), and to remove variants with high missingness (>10%), low minor allele frequency (MAF < 0.05) and/or strong deviation from Hardy-Weinberg equilibrium (P < 1e-5). Then the filtered genotyping datasets were phased with Eagle v2.4 and imputed using Minimac4 for the Haplotype Reference Consortium (HRC) r1.1 reference Panel via the Michigan Imputation Server (50) (https://imputationserver.sph.umich.edu/). UK Biobank participants were genotyped using the Affymetrix UK BiLEVE Axiom array (on an initial ~50,000 participants) and the Affymetrix UK Biobank Axiom array (on the remaining ~450,000 participants). The two arrays are very similar with over 95% common marker content. In total, about 800,000 markers were genotyped for each participant. The UK Biobank team first imputed the genotyping data using the HRC reference panel and then imputed the SNPs not in the HRC panel using a combined UK10K + 1000 Genomes panel. The imputation process produced a dataset (V3, released in March 2018) with >92 million autosomal SNPs. Detailed information and documentation on the genotyping, imputation and QC for the UK Biobank data set are available at (https://www.ukbiobank.ac.uk/enable-your-research/about-our-data/genetic-data). Post-imputation sample and variant QC was performed to delete subjects missing more than 10% of total imputed genotypes and without valid BT measures, and to remove multiallelic variants and variants with an imputation information score < 0.7, missingness rate > 10%, MAF < 1% and/or HWE P < 1e-7. As in other UK Biobank GWASs, e.g. (51), we also removed samples without a UK ancestry as determined by the in.white.British.ancestry.subset variable in the file ukb_sqc_v2.txt provided by the UK Biobank. Finally, the processed datasets consisted of 1,399 ABCD samples with 7,016,694 variants, 350 PING participants with 7,383,086 variants, 422 PNC samples with 7,224,238 variants and 18,206 UKB participants with 11,195,104 variants. The pre- (for ABCD, PING and PNC) and post-imputation QC (for all 4 datasets) described above was performed using the PLINK2.0 software (52) (https://www.cog-genomics.org/plink/2.0/).

Heritability estimation

We estimated the narrow-sense (pedigree-based) heritability of the BT features using the twin data of the ABCD and HCP cohorts. For ABCD samples, zygosity was determined using the probability of identity-by-descent (IBD) extracted from the genome-wide genotyping data of 2,652 subjects with brain MRI. According to the protocol introduced in the ABCD data release note - NDA 2.0.1 Genetics, we identified full siblings or dizygotic (DZ) twins with a threshold of IBD > 0.4 and monozygotic (MZ) twins with a threshold of IBD > 0.8 rather at 0.5 and 1, considering the existence of inherent noise in the genotyping data caused by the identify-by-state estimations. 120 MZ twin pairs and 379 full sibling or DZ twin pairs were identified in the ABCD participants. In HCP S900 samples, twin statuses were self-reported. However, in the later S1200 release, zygosity was updated based on genotyping data available from blood and saliva samples of some HCP subjects. 36 twin pairs who self-reported as DZ twins were found to be genetically MZ. Taking this change into account, the S900 subjects with brain MRI included 179 twin pairs (114 MZ with 99 siblings and 6 half siblings and 65 DZ with 55 siblings and 9 half siblings), 273 siblings, 10 half siblings and 87 unpaired individuals. Pedigree-based heritability was estimated using the variance component analysis method as implemented in SOLAR-Eclipse (53)(v8.4.2, http://solar-eclipse-genetics.org**).** Each BT measure was entered into a linear mixed-effects model as a dependent variable. The model included fixed effects of age, age^2, sex, handedness and TIV, and a random effect of genetic similarity that was determined by pedigrees. Genetic similarity is coded as 1 for MZ twins who share 100% of their DNA sequence, and as 0.5 for DZ twins and siblings who share on average 50%, and as 0 for unrelated individuals. Heritability statistics were corrected for multiple comparisons using Bonferroni correction for lobar and

sectional measures adjusting for the number of profiles (P < 0.05/6 lobar measures and P < 0.05/(60×2) sectional measures) and using FDR for vertex-wise results (FDR < 0.05/3 across the cortical surface and adjusting for the 3 positional asymmetry dimensions).

We also estimated SNP-based heritability of the BT features using the LD-score regression (LDSC) (54) (https://github.com/bulik/ldsc) with the GWAS summary statistics for UKB and the meta-GWAS summary statistics. SNP-based heritability were also estimated using the genome-based restricted maximum likelihood (GREML) analysis implemented in GCTA (55) (v1.93.2beta, https://cnsgenomics.com/software/gcta/#Overview) with the QCed genotyping dataset from UKB. In the GCTA-GREML analysis, a set of confounding factors (the same ones used in the GWAS analysis for UKB, see bellow) were included, which were age, age^2, sex, handedness, TIV, the first ten genetic principal components, imaging-related variables (15, 47) such as MRI acquisition center (UKB data-field: 54-2.0), X/Y/Z brain center of gravity (UKB data-fields: 25756, 25757 and 25758), scanner table position (UKB data-field: 25759), T1 signal-to-noise ratio (UKB data field: 25734), T1 contrast-to-noise ratio (UKB data-field: 25735), mean rfMRI head motion (UKB data-field: 25741) and mean tfMRI head motion (UKB data-field: 25742). The analysis for SNP-based heritability was not applied to the ABCD, PNC and PING cohorts because of their insufficient sample sizes in the filtered genomic datasets, which would result in nonsensical estimates, i.e., h^2_{SNP} values will be out of the 0-100% range and/or with very large variance (SE > 30%).

Genome-wide association analysis

Genome-wide association study (GWAS) analyses on different BT measures were conducted for the ABCD, PING, PNC, UKB samples using generalized linear regression adjusting for age, age^2, sex, handedness, TIV, the first ten genetic principal components and imaging-related variables if needed, as implemented in the PLINK2.0. Especially, the imaging-related variables included in the regression model were, for ABCD and PING, scanner device and imaging sites; for UKB, as suggested in (15, 47), imaging center (UKB data-field: 54-2.0), X/Y/Z brain center of gravity (UKB data-fields: 25756, 25757 and 25758), scanner table position (UKB data-field: 25759), T1 signal-to-noise ratio (UKB data field: 25734), T1 contrast-to-noise ratio (UKB data-field: 25735), mean rfMRI head motion (UKB data-field: 25741) and mean tfMRI head motion (UKB data-field: 25742). Since all imaging data from the PNC were acquired at a single site, on a single scanner, in a short period of time that did not span any software or hardware upgrades (10), scanner/site was not included in the GWAS model for PNC. The cubic age term was not included in the model as there was no cubic age effect in the individual samples. We then used METAL (56) (v2020-05-05, https://genome.sph.umich.edu/wiki/METAL) to perform meta-analyses using the z-scores method, based on p-values, sample size and direction of effect, with genomic control correction. We discarded variants that existed in only one individual GWAS to ensure that the loci identified by the meta-analysis are replicated in at least two datasets. This provided overall P-values on 7,393,766 high-quality genotyped and imputed autosomal SNPs. Significant genetic associations were first identified using the commonly used genome-wide significance threshold P < 5e-08, which accounts for the number of SNPs tested in modern GWAS and the correlation structure between SNPs in European ancestry populations (57). For a more conservative discovery, we further adjusted the threshold with a Bonferroni factor that accounts for the number of BT measures tested (6 lobar measures, 60 × 2 sectional TDA measures, and 74 × 3 regional mean SPA measures), giving a threshold of P < 5e-8/348 = 1.44e-10. The clumping function in PLINK using an LD r^2 cut off of 0.2 and a 500 kb sliding window was implemented to identify independent leading SNPs in each LD block. Association lookups were performed for all leading SNPs via the NHGRI-EBI catalog of published GWASs (58) (http://www.ebi.ac.uk/gwas/) to check whether these SNPs had been previously associated with any traits.

Gene-based association analysis

Gene-based association analysis was conducted using MAGMA (59) (v1.07, https://ctg.cncr.nl/software/magma). The gene-based statistics were derived using the summary statistics from each meta-analysis. Genetic variants were assigned to genes based on their position according to the NCBI 37.3 build, with a gene window of 5 kb upstream and downstream of transcript end sites for each gene, resulting a total of 18,359 protein coding genes. The

European panel of the 1000 Genomes data (60) (phase 1, release 3) was used as a reference panel to account for linkage disequilibrium. A significance threshold for gene-based associations was calculated using the Bonferroni method to correct for multiple testing across the genes ($P < 0.05/18359 = 2.72e-6$), and a further Bonferroni adjustment was also applied for the number of BT measures tested ($P < 0.05/18359/348 = 7.83-9$). Association lookups was performed in the NHGRI-EBI GWAS catalog again to explore previously reported associations of the genes identified here.

Gene-set enrichment analysis

MAGMA gene-set enrichment analysis (61, 62) was performed on the genome-wide, gene-based statistics to explore implicated biological pathways, examining 7,563 Gene Ontology 'biological process' sets from the Molecular Signatures Database (63) (MSigDB, v7.2, https://www.gsea-msigdb.org/gsea/msigdb). Briefly, for each BT profile, the gene-wise association statistics computed in the above gene-based association analysis were quantified as Z-scores using a probit transformation mapping stronger associations onto higher Z-scores. Then, for each gene set, a linear regression model was implemented on a gene-level data matrix of gene-set indicator variables (coded 1 for genes in that gene set and 0 otherwise) to test whether the mean association of genes in the gene set is greater than that of genes not in the gene set. Significant gene-set enrichments were assessed at a significance threshold adjusting for multiple testing across the gene sets ($P < 0.05/7563 = 6.61e-6$), and further adjusting for the number of BT measures tested ($P < 0.05/7563/348 = 1.90e-9$).

Gene-property analysis

We also preformed MAGMA gene-property analysis (61, 62) on the genome-wide, gene-based statistics to assess relationships between the gene-BT associations in our data and the gene expression levels at different brain developmental stages from the BrainSpan data (64) (https://www.brainspan.org). The BrainSpan dataset comprised brain tissue gene expression values at 31 age stages, from 8 postconceptional weeks (pcw) to 40 years. The gene-property analysis is essentially the same model as the above competitive gene-set analysis, but using continuous gene-set predictor variables (gene expression values at each age stage here) rather than binary indicators. This approach tested for the degree to which the genetic association of a gene changes as the value for the tested variable increases (62). Significance of gene property effects were determined controlling for multiple testing across the age groups ($P < 0.05/31 = 0.0016$), and further controlling for the number of BT measures tested ($P < 0.05/31/348 = 4.63e-6$).

Genetic correlation analysis

We estimated genetic correlations between the BT features studied here and 9 complex traits that were widely related to brain asymmetry previously. We fetched GWAS summary statistics of recent large-scale studies on these traits: Educational Attainment (65) (N = 1,131,881), Intelligence (66) (N = 269,867), attention deficit hyperactivity disorder (67) (N=55,374), autism spectrum disorder (68) (N = 46,350), Schizophrenia (69) (N = 306,011), Bipolar Disorder (70) (N = 51,710), Major Depression (71) (N = 480,359), Neuroticism (72) (N = 449,484) and Alzheimer's Disease (73) (N = 455,258), from https://www.thessgac.org/data, https://www.med.unc.edu/pgc/ and https://ctg.cncr.nl/software/summary_statistics. These summary statistics were correlated with the meta-GWAS summary statistics for BT measures obtained in this study using LDSC (54). Significant genetic correlations were tested using a significant threshold correcting for the 9 traits and 348 BT measures tested here ($P < 0.05/9/348 = 1.60e-5$).

Supplementary References

1. Volkow ND, Koob GF, Croyle RT, Bianchi DW, Gordon JA, Koroshetz WJ, et al. (2018): The conception of the ABCD study: From substance use to a broad NIH collaboration. *Dev Cogn Neurosci*. 32:4-7.
2. Casey BJ, Cannonier T, Conley MI, Cohen AO, Barch DM, Heitzeg MM, et al. (2018): The Adolescent Brain Cognitive Development (ABCD) study: Imaging acquisition across 21 sites. *Dev Cogn Neurosci*. 32:43-54.
3. Oldfield RC (1971): The assessment and analysis of handedness: the Edinburgh inventory. *Neuropsychologia*. 9:97-113.
4. Achenbach TM, Rescorla LA (2003): Manual for the ASEBA Adult Forms & Profiles. University of Vermont, Research Center for Children, Youth, and Families, Burlington, VT.
5. Van Essen DC, Ugurbil K, Auerbach E, Barch D, Behrens TE, Bucholz R, et al. (2012): The Human Connectome Project: a data acquisition perspective. *Neuroimage*. 62:2222-2231.
6. Veale JF (2014): Edinburgh Handedness Inventory - Short Form: a revised version based on confirmatory factor analysis. *Laterality*. 19:164-177.
7. Mazziotta J, Toga A, Evans A, Fox P, Lancaster J, Zilles K, et al. (2001): A probabilistic atlas and reference system for the human brain: International Consortium for Brain Mapping (ICBM). *Philos Trans R Soc Lond B Biol Sci*. 356:1293-1322.
8. Jernigan TL, Brown TT, Hagler DJ, Jr., Akshoomoff N, Bartsch H, Newman E, et al. (2016): The Pediatric Imaging, Neurocognition, and Genetics (PING) Data Repository. *Neuroimage*. 124:1149-1154.
9. Satterthwaite TD, Connolly JJ, Ruparel K, Calkins ME, Jackson C, Elliott MA, et al. (2016): The Philadelphia Neurodevelopmental Cohort: A publicly available resource for the study of normal and abnormal brain development in youth. *Neuroimage*. 124:1115-1119.
10. Satterthwaite TD, Elliott MA, Ruparel K, Loughead J, Prabhakaran K, Calkins ME, et al. (2014): Neuroimaging of the Philadelphia neurodevelopmental cohort. *Neuroimage*. 86:544-553.
11. Calkins ME, Merikangas KR, Moore TM, Burstein M, Behr MA, Satterthwaite TD, et al. (2015): The Philadelphia Neurodevelopmental Cohort: constructing a deep phenotyping collaborative. *J Child Psychol Psychiatry*. 56:1356-1369.
12. Shanmugan S, Wolf DH, Calkins ME, Moore TM, Ruparel K, Hopson RD, et al. (2016): Common and Dissociable Mechanisms of Executive System Dysfunction Across Psychiatric Disorders in Youth. *Am J Psychiatry*. 173:517-526.
13. Xia CH, Ma Z, Ciric R, Gu S, Betzel RF, Kaczkurkin AN, et al. (2018): Linked dimensions of psychopathology and connectivity in functional brain networks. *Nat Commun*. 9:3003.
14. Alfaro-Almagro F, Jenkinson M, Bangerter NK, Andersson JLR, Griffanti L, Douaud G, et al. (2018): Image processing and Quality Control for the first 10,000 brain imaging datasets from UK Biobank. *Neuroimage*. 166:400-424.
15. Miller KL, Alfaro-Almagro F, Bangerter NK, Thomas DL, Yacoub E, Xu J, et al. (2016): Multimodal population brain imaging in the UK Biobank prospective epidemiological study. *Nat Neurosci*. 19:1523-1536.
16. Xiang L, Crow T, Roberts N (2019): Automatic analysis of cross-sectional cerebral asymmetry on 3D in vivo MRI scans of human and chimpanzee. *J Neurosci Res*. 97:673-682.
17. Xiang L, Crow T, Roberts N (2019): Cerebral torque is human specific and unrelated to brain size. *Brain Struct Funct*. 224:1141-1150.
18. Hou L, Xiang L, Crow TJ, Leroy F, Rivière D, Mangin JF, et al. (2019): Measurement of Sylvian Fissure asymmetry and occipital bending in humans and Pan troglodytes. *Neuroimage*. 184:855-870.
19. Li X, Crow TJ, Hopkins WD, Gong Q, Roberts N (2018): Human torque is not present in chimpanzee brain. *Neuroimage*. 165:285-293.
20. Jenkinson M, Beckmann CF, Behrens TE, Woolrich MW, Smith SM (2012): Fsl. *Neuroimage*. 62:782-790.
21. Fischl B (2012): FreeSurfer. *Neuroimage*. 62:774-781.

22. Reuter M, Rosas HD, Fischl B (2010): Highly accurate inverse consistent registration: a robust approach. *Neuroimage*. 53:1181-1196.
23. Segonne F, Dale AM, Busa E, Glessner M, Salat D, Hahn HK, et al. (2004): A hybrid approach to the skull stripping problem in MRI. *Neuroimage*. 22:1060-1075.
24. Fischl B, Salat DH, Busa E, Albert M, Dieterich M, Haselgrove C, et al. (2002): Whole brain segmentation: automated labeling of neuroanatomical structures in the human brain. *Neuron*. 33:341-355.
25. Fischl B, Salat DH, van der Kouwe AJ, Makris N, Segonne F, Quinn BT, et al. (2004): Sequence-independent segmentation of magnetic resonance images. *Neuroimage*. 23 Suppl 1:S69-84.
26. Sled JG, Zijdenbos AP, Evans AC (1998): A nonparametric method for automatic correction of intensity nonuniformity in MRI data. *IEEE Trans Med Imaging*. 17:87-97.
27. Segonne F, Pacheco J, Fischl B (2007): Geometrically accurate topology-correction of cortical surfaces using nonseparating loops. *IEEE Trans Med Imaging*. 26:518-529.
28. Fischl B, Dale AM (2000): Measuring the thickness of the human cerebral cortex from magnetic resonance images. *Proc Natl Acad Sci U S A*. 97:11050-11055.
29. Fischl B, Sereno MI, Tootell RB, Dale AM (1999): High-resolution intersubject averaging and a coordinate system for the cortical surface. *Hum Brain Mapp*. 8:272-284.
30. Balzeau A, Gilissen E (2010): Endocranial shape asymmetries in Pan paniscus, Pan troglodytes and Gorilla gorilla assessed via skull based landmark analysis. *J Hum Evol*. 59:54-69.
31. Zhao L, Ruotsalainen U, Hirvonen J, Hietala J, Tohka J (2010): Automatic cerebral and cerebellar hemisphere segmentation in 3D MRI: adaptive disconnection algorithm. *Med Image Anal*. 14:360-372.
32. Toga AW, Thompson PM (2003): Mapping brain asymmetry. *Nat Rev Neurosci*. 4:37-48.
33. Zhao L, Hietala J, Tohka J (2009): Shape analysis of human brain interhemispheric fissure bending in MRI. *Med Image Comput Comput Assist Interv*. 12:216-223.
34. Tang H, Liu T, Liu H, Jiang J, Cheng J, Niu H, et al. (2021): A slower rate of sulcal widening in the brains of the nondemented oldest old. *Neuroimage*. 229:117740.
35. Greve DN, Van der Haegen L, Cai Q, Stufflebeam S, Sabuncu MR, Fischl B, et al. (2013): A surface-based analysis of language lateralization and cortical asymmetry. *J Cogn Neurosci*. 25:1477-1492.
36. Destrieux C, Fischl B, Dale A, Halgren E (2010): Automatic parcellation of human cortical gyri and sulci using standard anatomical nomenclature. *Neuroimage*. 53:1-15.
37. Dinov I, Lozev K, Petrosyan P, Liu Z, Eggert P, Pierce J, et al. (2010): Neuroimaging study designs, computational analyses and data provenance using the LONI pipeline. *PLoS One*. 5.
38. Dinov ID, Van Horn JD, Lozev KM, Magsipoc R, Petrosyan P, Liu Z, et al. (2009): Efficient, Distributed and Interactive Neuroimaging Data Analysis Using the LONI Pipeline. *Front Neuroinform*. 3:22.
39. Rosen AFG, Roalf DR, Ruparel K, Blake J, Seelaus K, Villa LP, et al. (2018): Quantitative assessment of structural image quality. *Neuroimage*. 169:407-418.
40. Dale AM, Fischl B, Sereno MI (1999): Cortical surface-based analysis. I. Segmentation and surface reconstruction. *Neuroimage*. 9:179-194.
41. Shaw P, Kabani NJ, Lerch JP, Eckstrand K, Lenroot R, Gogtay N, et al. (2008): Neurodevelopmental trajectories of the human cerebral cortex. *J Neurosci*. 28:3586-3594.
42. Pfefferbaum A, Rohlfing T, Rosenbloom MJ, Chu W, Colrain IM, Sullivan EV (2013): Variation in longitudinal trajectories of regional brain volumes of healthy men and women (ages 10 to 85 years) measured with atlas-based parcellation of MRI. *Neuroimage*. 65:176-193.
43. Zhao L, Matloff W, Ning K, Kim H, Dinov ID, Toga AW (2019): Age-Related Differences in Brain Morphology and the Modifiers in Middle-Aged and Older Adults. *Cereb Cortex*. 29:4169-4193.
44. Worsley KJ, Evans AC, Marrett S, Neelin P (1992): A three-dimensional statistical analysis for CBF activation studies in human brain. *J Cereb Blood Flow Metab*. 12:900-918.

45. Zhao L, Batta I, Matloff W, O'Driscoll C, Hobel S, Toga AW (2020): Neuroimaging PheWAS (Phenome-Wide Association Study): A Free Cloud-Computing Platform for Big-Data, Brain-Wide Imaging Association Studies. *Neuroinformatics*.
46. Millard LAC, Davies NM, Gaunt TR, Davey Smith G, Tilling K (2018): Software Application Profile: PHESANT: a tool for performing automated phenome scans in UK Biobank. *Int J Epidemiol*. 47:29-35.
47. Smith SM, Douaud G, Chen W, Hanayik T, Alfaro-Almagro F, Sharp K, et al. (2021): An expanded set of genome-wide association studies of brain imaging phenotypes in UK Biobank. *Nat Neurosci*. 24:737-745.
48. Anderson CA, Pettersson FH, Clarke GM, Cardon LR, Morris AP, Zondervan KT (2010): Data quality control in genetic case-control association studies. *Nat Protoc*. 5:1564-1573.
49. Marees AT, de Kluiver H, Stringer S, Vorspan F, Curis E, Marie-Claire C, et al. (2018): A tutorial on conducting genome-wide association studies: Quality control and statistical analysis. *Int J Methods Psychiatr Res*. 27:e1608.
50. Das S, Forer L, Schönherr S, Sidore C, Locke AE, Kwong A, et al. (2016): Next-generation genotype imputation service and methods. *Nat Genet*. 48:1284-1287.
51. Elliott LT, Sharp K, Alfaro-Almagro F, Shi S, Miller KL, Douaud G, et al. (2018): Genome-wide association studies of brain imaging phenotypes in UK Biobank. *Nature*. 562:210-216.
52. Chang CC, Chow CC, Tellier LC, Vattikuti S, Purcell SM, Lee JJ (2015): Second-generation PLINK: rising to the challenge of larger and richer datasets. *Gigascience*. 4:7.
53. Kochunov P, Jahanshad N, Marcus D, Winkler A, Sprooten E, Nichols TE, et al. (2015): Heritability of fractional anisotropy in human white matter: a comparison of Human Connectome Project and ENIGMA-DTI data. *Neuroimage*. 111:300-311.
54. Finucane HK, Bulik-Sullivan B, Gusev A, Trynka G, Reshef Y, Loh PR, et al. (2015): Partitioning heritability by functional annotation using genome-wide association summary statistics. *Nat Genet*. 47:1228-1235.
55. Yang J, Lee SH, Goddard ME, Visscher PM (2011): GCTA: a tool for genome-wide complex trait analysis. *Am J Hum Genet*. 88:76-82.
56. Willer CJ, Li Y, Abecasis GR (2010): METAL: fast and efficient meta-analysis of genomewide association scans. *Bioinformatics*. 26:2190-2191.
57. Hoggart CJ, Clark TG, De Iorio M, Whittaker JC, Balding DJ (2008): Genome-wide significance for dense SNP and resequencing data. *Genet Epidemiol*. 32:179-185.
58. Buniello A, MacArthur JAL, Cerezo M, Harris LW, Hayhurst J, Malangone C, et al. (2019): The NHGRI-EBI GWAS Catalog of published genome-wide association studies, targeted arrays and summary statistics 2019. *Nucleic Acids Res*. 47:D1005-D1012.
59. de Leeuw CA, Mooij JM, Heskes T, Posthuma D (2015): MAGMA: generalized gene-set analysis of GWAS data. *PLoS Comput Biol*. 11:e1004219.
60. Abecasis GR, Auton A, Brooks LD, DePristo MA, Durbin RM, Handsaker RE, et al. (2012): An integrated map of genetic variation from 1,092 human genomes. *Nature*. 491:56-65.
61. de Leeuw CA, Neale BM, Heskes T, Posthuma D (2016): The statistical properties of gene-set analysis. *Nat Rev Genet*. 17:353-364.
62. de Leeuw CA, Stringer S, Dekkers IA, Heskes T, Posthuma D (2018): Conditional and interaction gene-set analysis reveals novel functional pathways for blood pressure. *Nat Commun*. 9:3768.
63. Liberzon A, Subramanian A, Pinchback R, Thorvaldsdóttir H, Tamayo P, Mesirov JP (2011): Molecular signatures database (MSigDB) 3.0. *Bioinformatics*. 27:1739-1740.
64. Miller JA, Ding SL, Sunkin SM, Smith KA, Ng L, Szafer A, et al. (2014): Transcriptional landscape of the prenatal human brain. *Nature*. 508:199-206.
65. Lee JJ, Wedow R, Okbay A, Kong E, Maghzian O, Zacher M, et al. (2018): Gene discovery and polygenic prediction from a genome-wide association study of educational attainment in 1.1 million individuals. *Nat Genet*. 50:1112-1121.
66. Savage JE, Jansen PR, Stringer S, Watanabe K, Bryois J, de Leeuw CA, et al. (2018): Genome-wide association meta-analysis in 269,867 individuals identifies new genetic and functional links to intelligence. *Nat Genet*. 50:912-919.

67. Demontis D, Walters RK, Martin J, Mattheisen M, Als TD, Agerbo E, et al. (2019): Discovery of the first genome-wide significant risk loci for attention deficit/hyperactivity disorder. *Nat Genet*. 51:63-75.
68. Grove J, Ripke S, Als TD, Mattheisen M, Walters RK, Won H, et al. (2019): Identification of common genetic risk variants for autism spectrum disorder. *Nat Genet*. 51:431-444.
69. Ripke S, Walters J, O'Donovan M (2020): Mapping genomic loci prioritises genes and implicates synaptic biology in schizophrenia. *medRxiv*.
70. Stahl EA, Breen G, Forstner AJ, McQuillin A, Ripke S, Trubetskoy V, et al. (2019): Genome-wide association study identifies 30 loci associated with bipolar disorder. *Nat Genet*. 51:793-803.
71. Wray NR, Ripke S, Mattheisen M, Trzaskowski M, Byrne EM, Abdellaoui A, et al. (2018): Genome-wide association analyses identify 44 risk variants and refine the genetic architecture of major depression. *Nat Genet*. 50:668-681.
72. Nagel M, Jansen PR, Stringer S, Watanabe K, de Leeuw CA, Bryois J, et al. (2018): Meta-analysis of genome-wide association studies for neuroticism in 449,484 individuals identifies novel genetic loci and pathways. *Nat Genet*. 50:920-927.
73. Jansen IE, Savage JE, Watanabe K, Bryois J, Williams DM, Steinberg S, et al. (2019): Genome-wide meta-analysis identifies new loci and functional pathways influencing Alzheimer's disease risk. *Nat Genet*. 51:404-413.

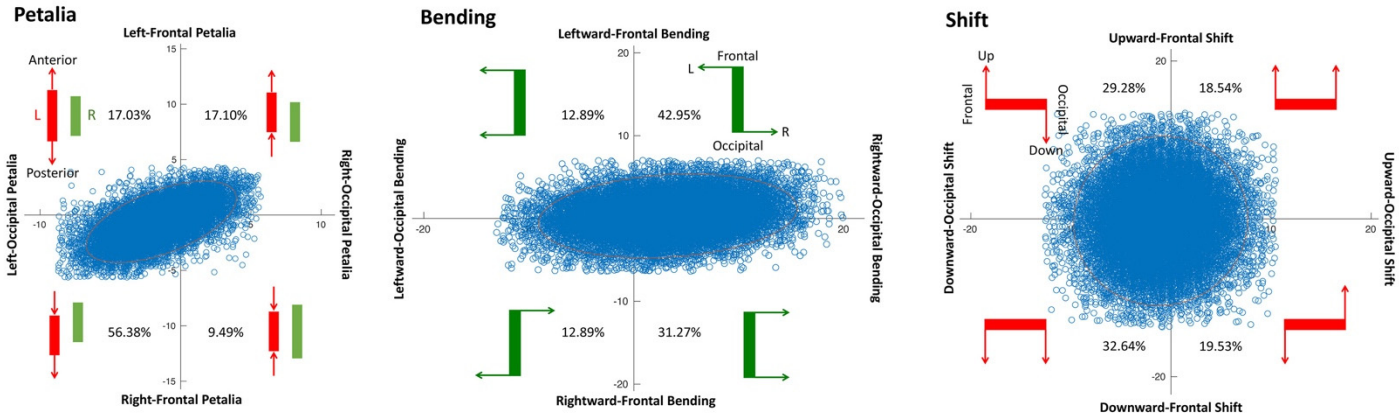

Figure S1. Plots of occipital (x-axis) and frontal (y-axis) petalia, bending and shift with 95% confidence ellipses in the pooled sample. Population prevalence of each brain torque configuration is annotated in the plots.

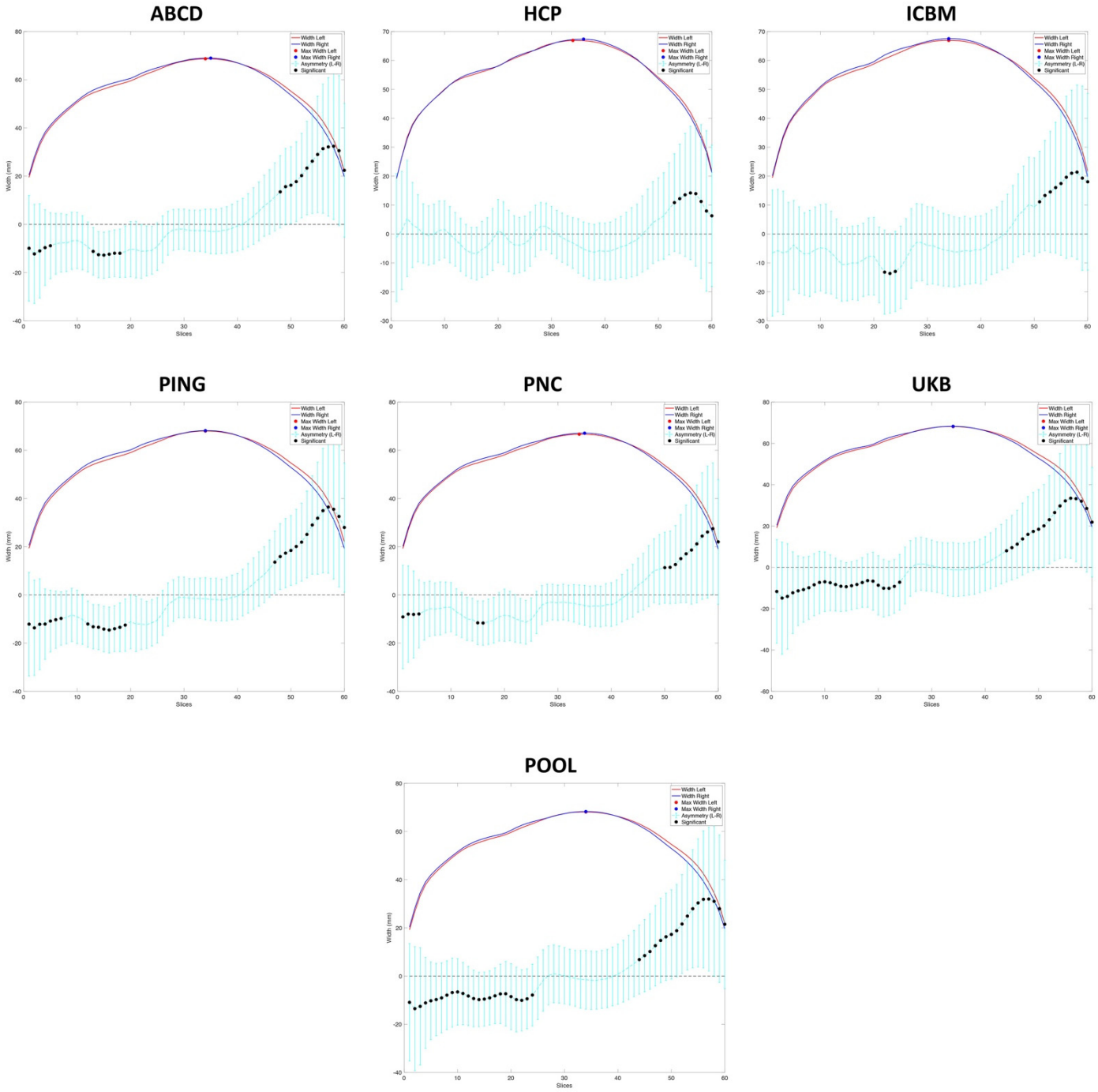

Figure S2-A. Population-level average sectional width asymmetry in the individual and pooled datasets. Significant sectional asymmetries ($P < 0.05/120$ and asymmetry/(left+right) > 2%) are marked with black dots.

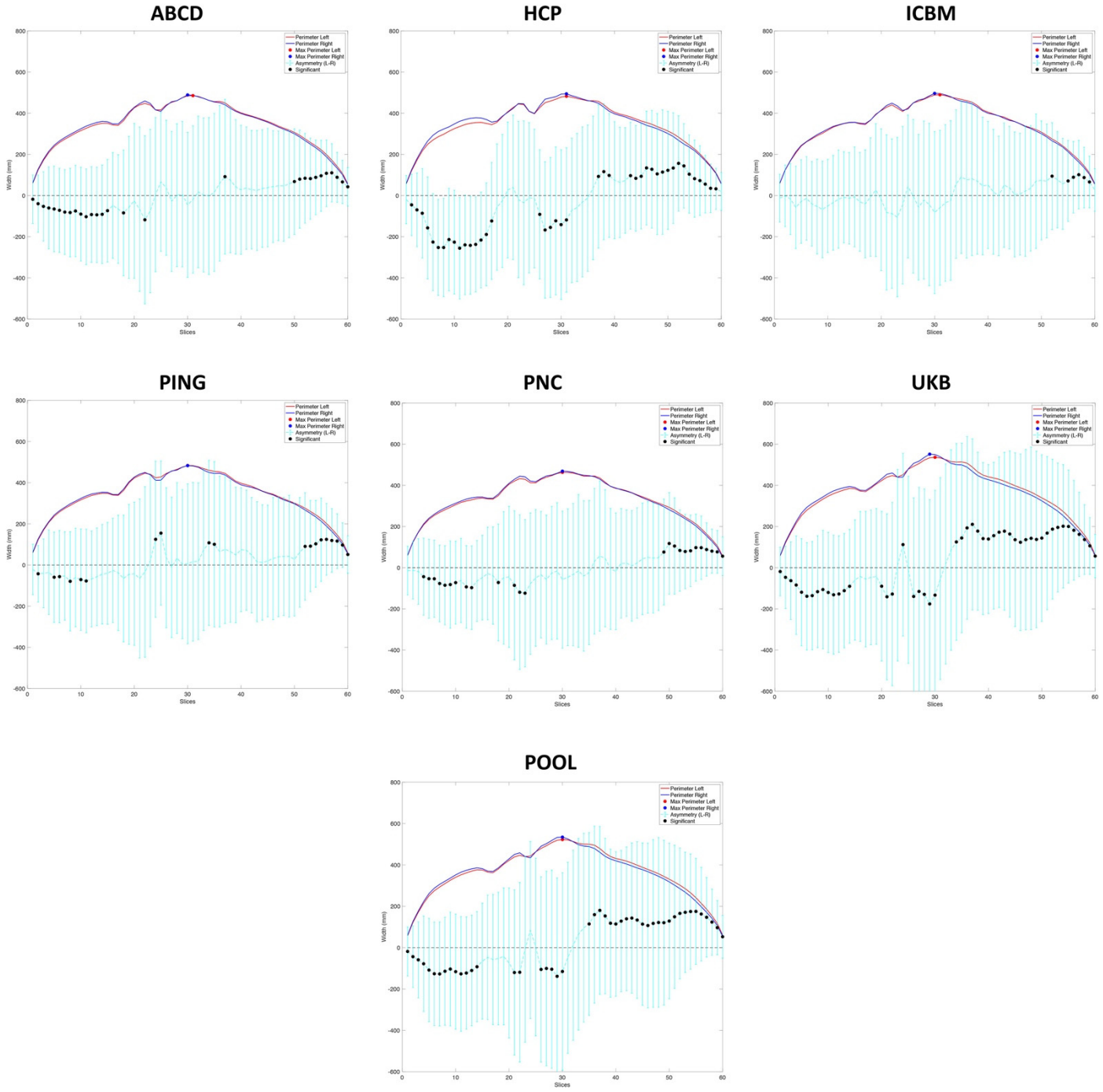

Figure S2-B: Population-level average sectional perimeter asymmetry in the individual and pooled datasets. Significant sectional asymmetries ($P < 0.05/120$ and asymmetry/(left+right) > 2%) are marked with black dots.

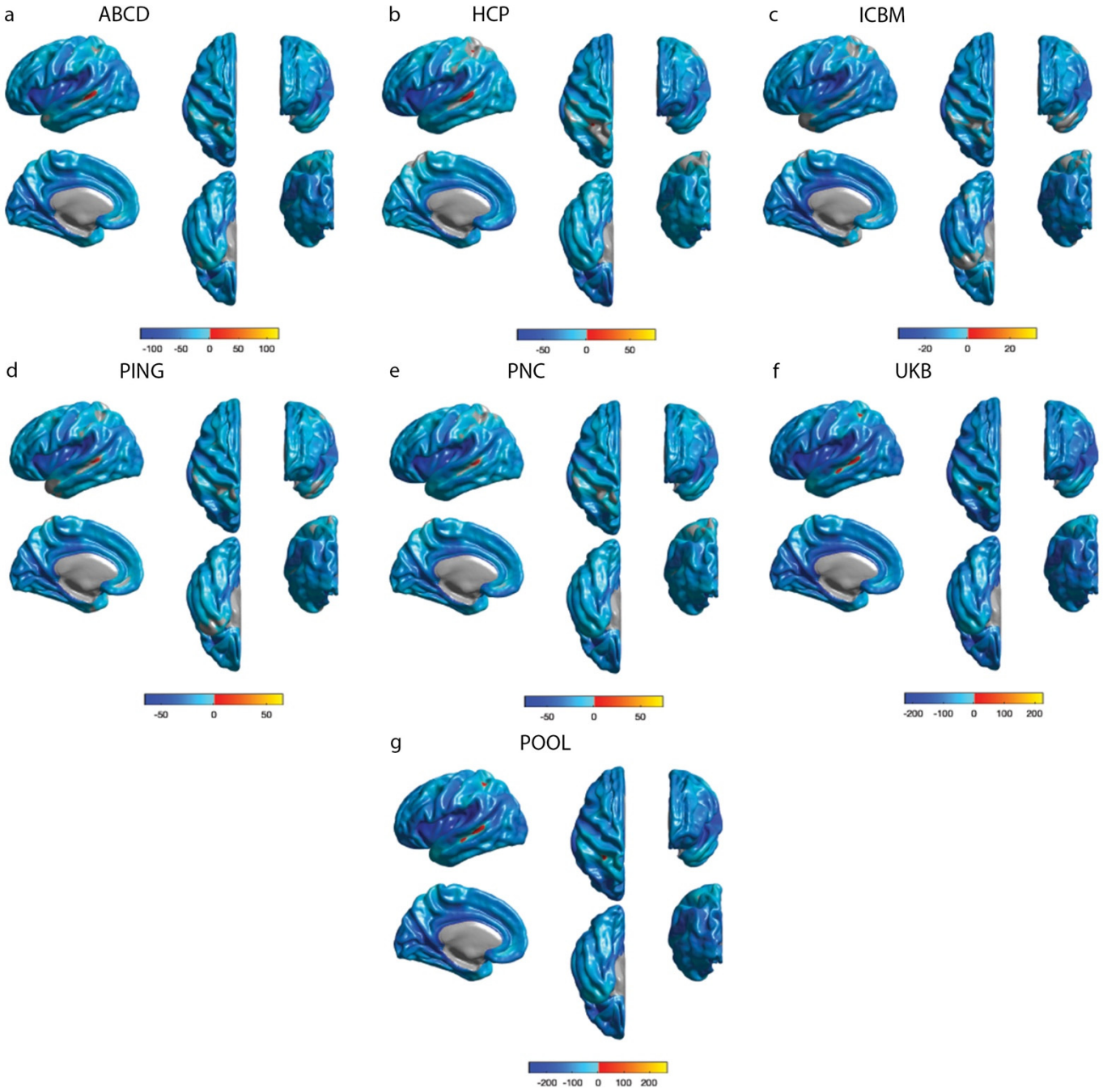

Figure S3-A. Population-level average surface positional asymmetry along the left-right axis in the individual and pooled datasets. Color bars represent T statistics (thresholded at random field theory corrected $P < 0.05/3$). Red-yellow and blue-cyan shows leftward and rightward displacements of the left hemisphere relative to the right respectively.

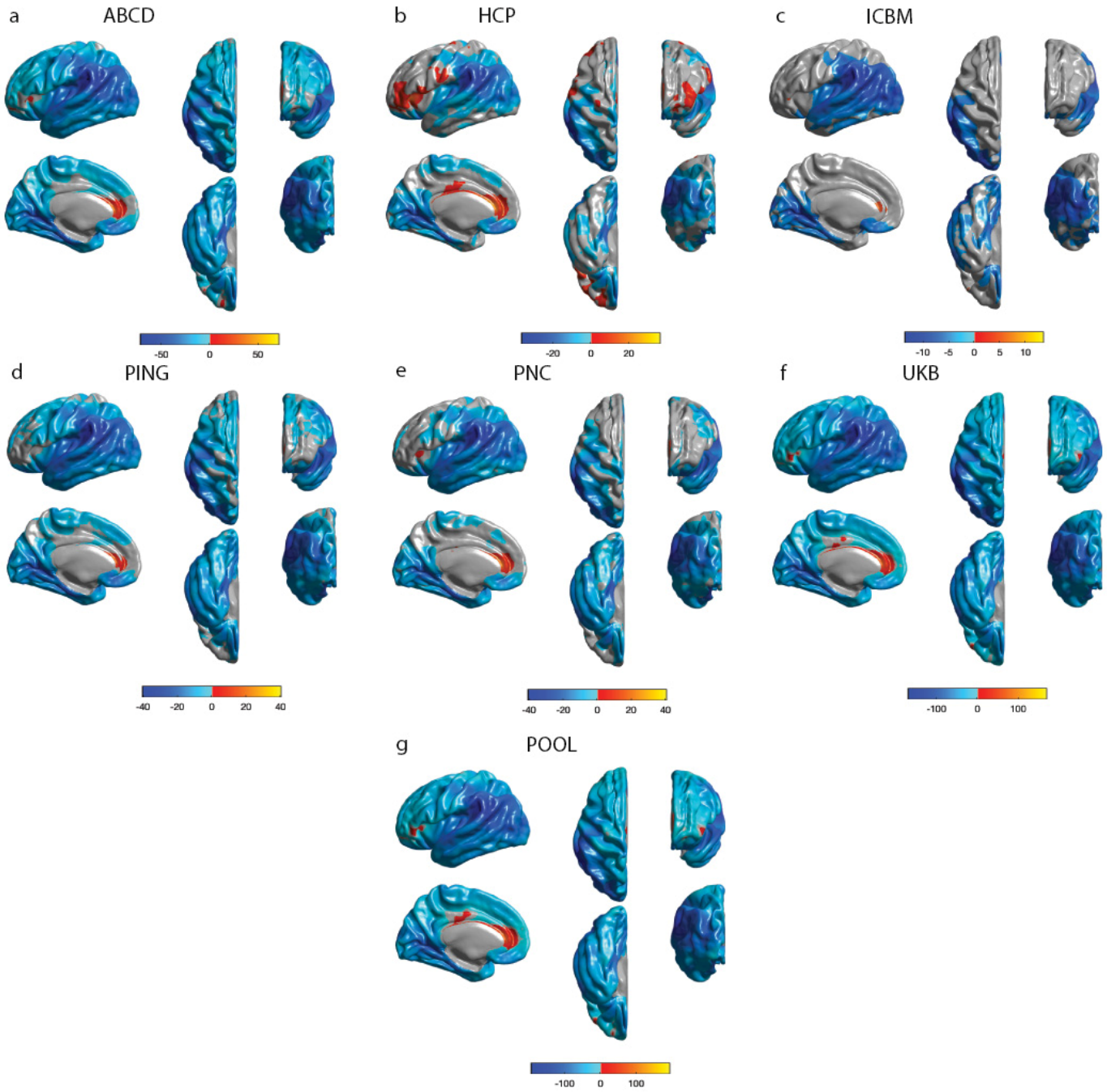

Figure 3-B. Population-level average surface positional asymmetry along the antero-posterior axis in the individual and pooled datasets. Color bars represent T statistics (thresholded at random field theory corrected $P < 0.05/3$). Red-yellow and blue-cyan show forward and backward displacements of the left hemisphere relative to the right respectively.

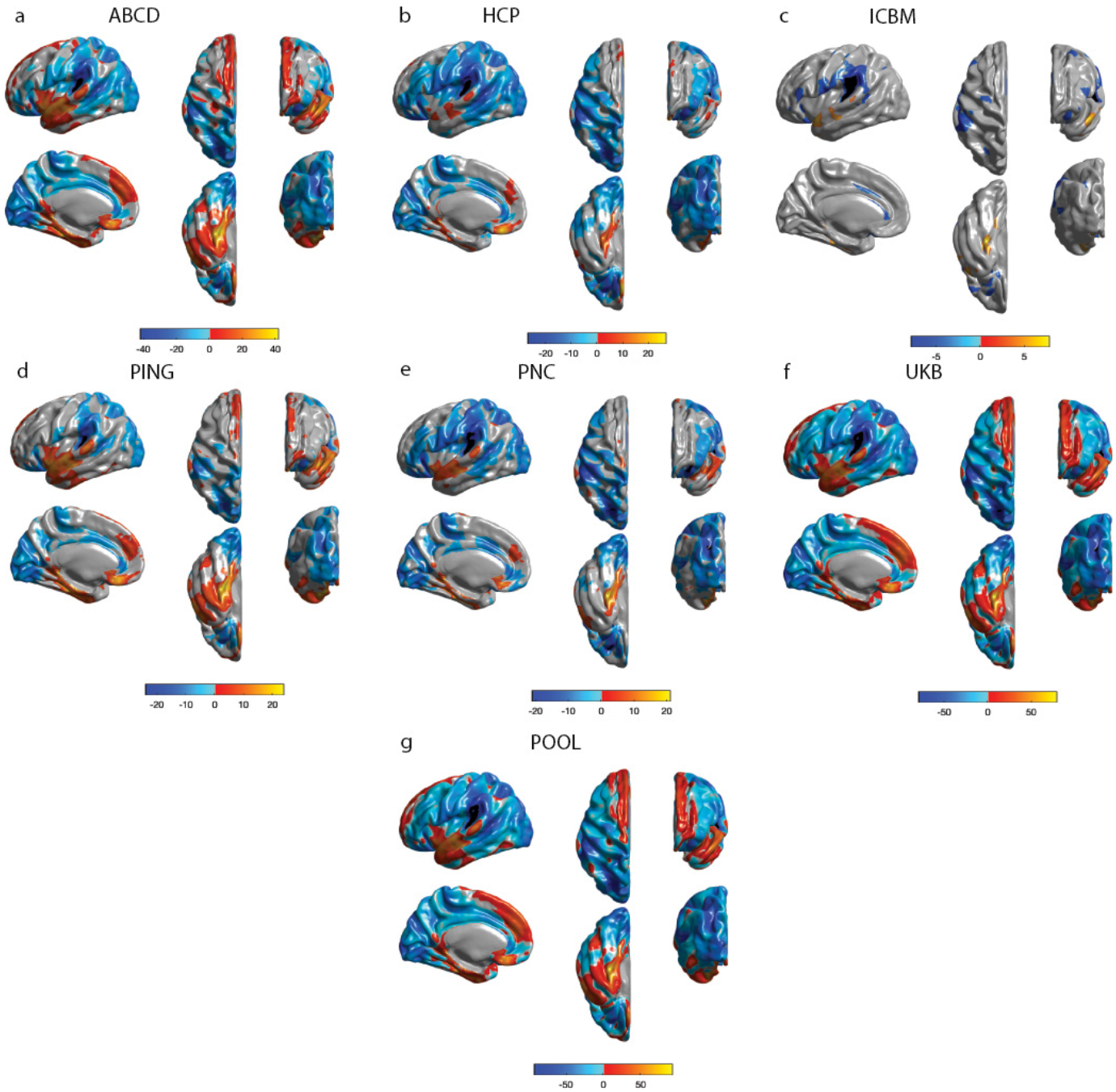

Figure S3-C. Population-level average surface positional asymmetry along the dorso-ventral axis in the individual and pooled datasets. Color bars represent T statistics (thresholded at random field theory corrected $P < 0.05/3$). Red-yellow and blue-cyan show upward and downward displacements of the left hemisphere relative to the right respectively.

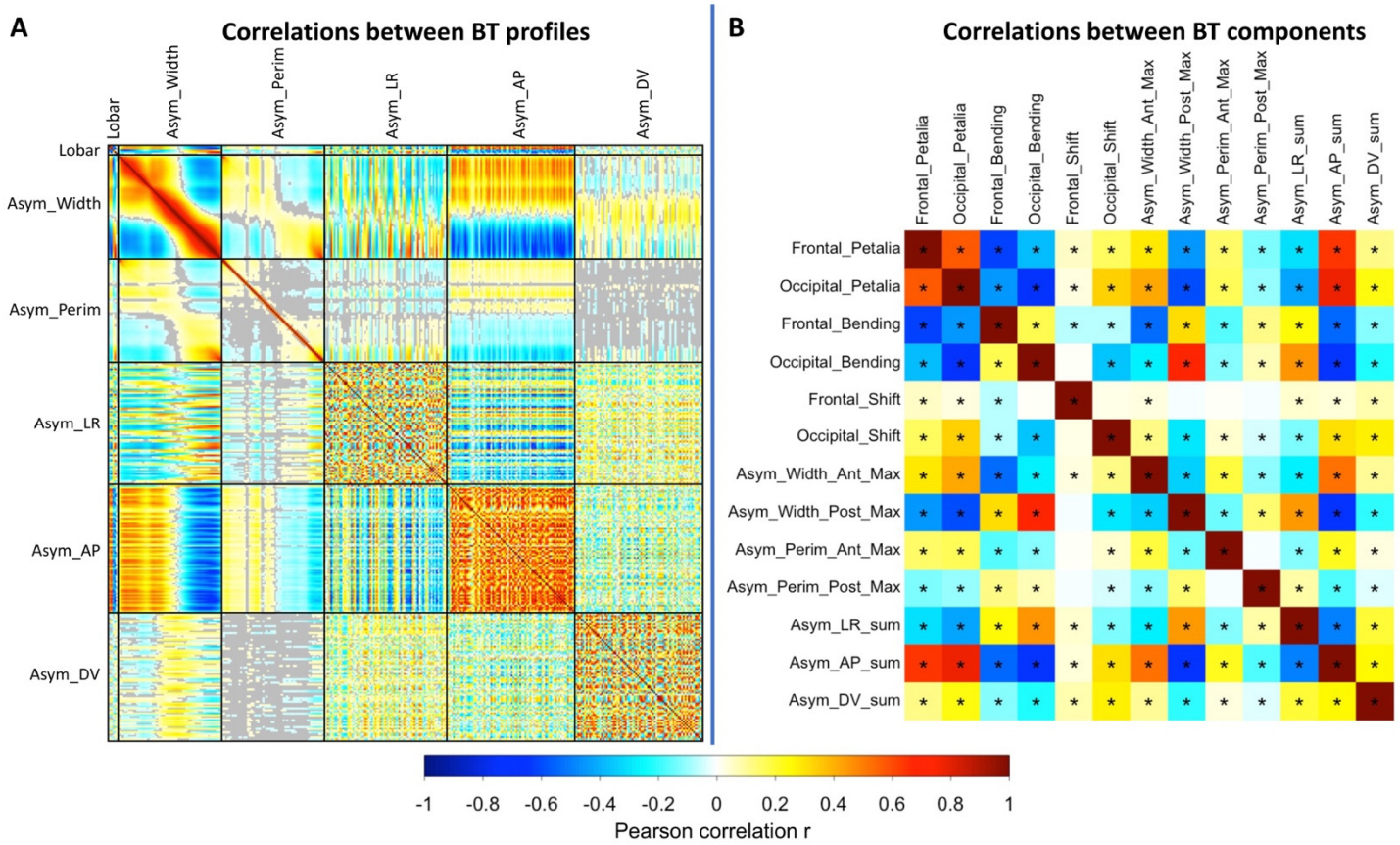

Figure S4: Correlations between brain torque (BT) profiles estimated in the pooled sample. A: heat map for correlations between 348 BT features, including petalia, bending, shift, sectional asymmetries in hemispheric width (Asym_Width) and perimeter (Asym_Perim) and regional mean surface positional asymmetries along the left-right (Asym_LR), anterior-posterior (Asym_AP), and dorsal-ventral (Asym_DV) axes. Non-significant correlations ($P > 0.05/(348\times347/2)$) are shown in grey. B: correlations between 13 primary components of BT, including measures of petalia, bending, shift and summary metrics for sectional tissue distribution asymmetries (Asym_Width_Ant_Max, Asym_Width_Post_Max, Asym_Perim_Ant_Max and Asym_Perim_Post_Max) and surface positional asymmetries (Asym_LR_sum, Asym_AP_sum and Asym_DV_sum). Definitions of these summary metrics are described in Supplementary Methods in detail. Significant correlations ($P < 0.05/(13\times12/2)$) are highlighted with asterisks. Color bar shows the Pearson correlation coefficient r.

A. Age Effects on Width Asymmetries

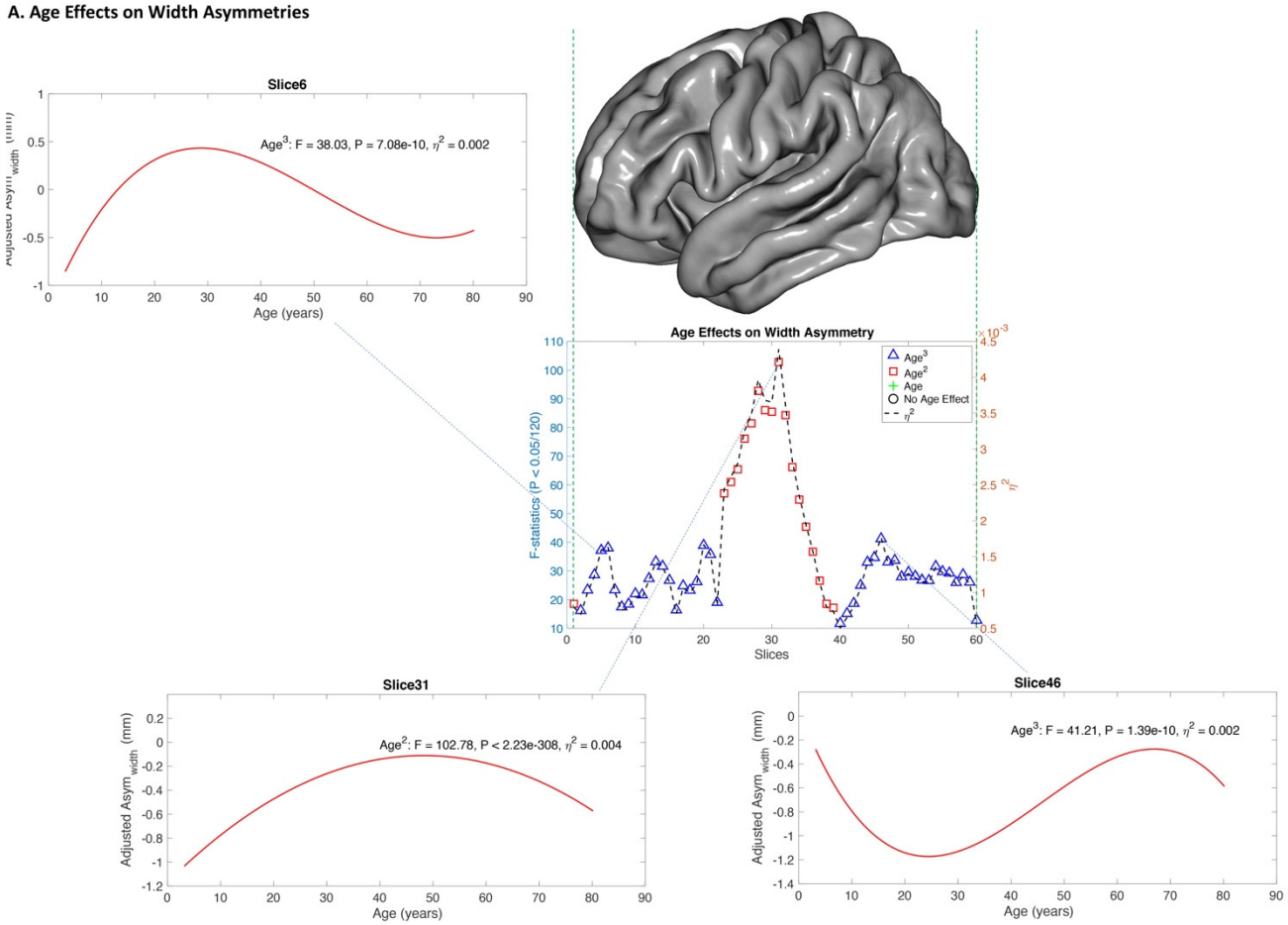

B. Age Effects on Perimeter Asymmetries

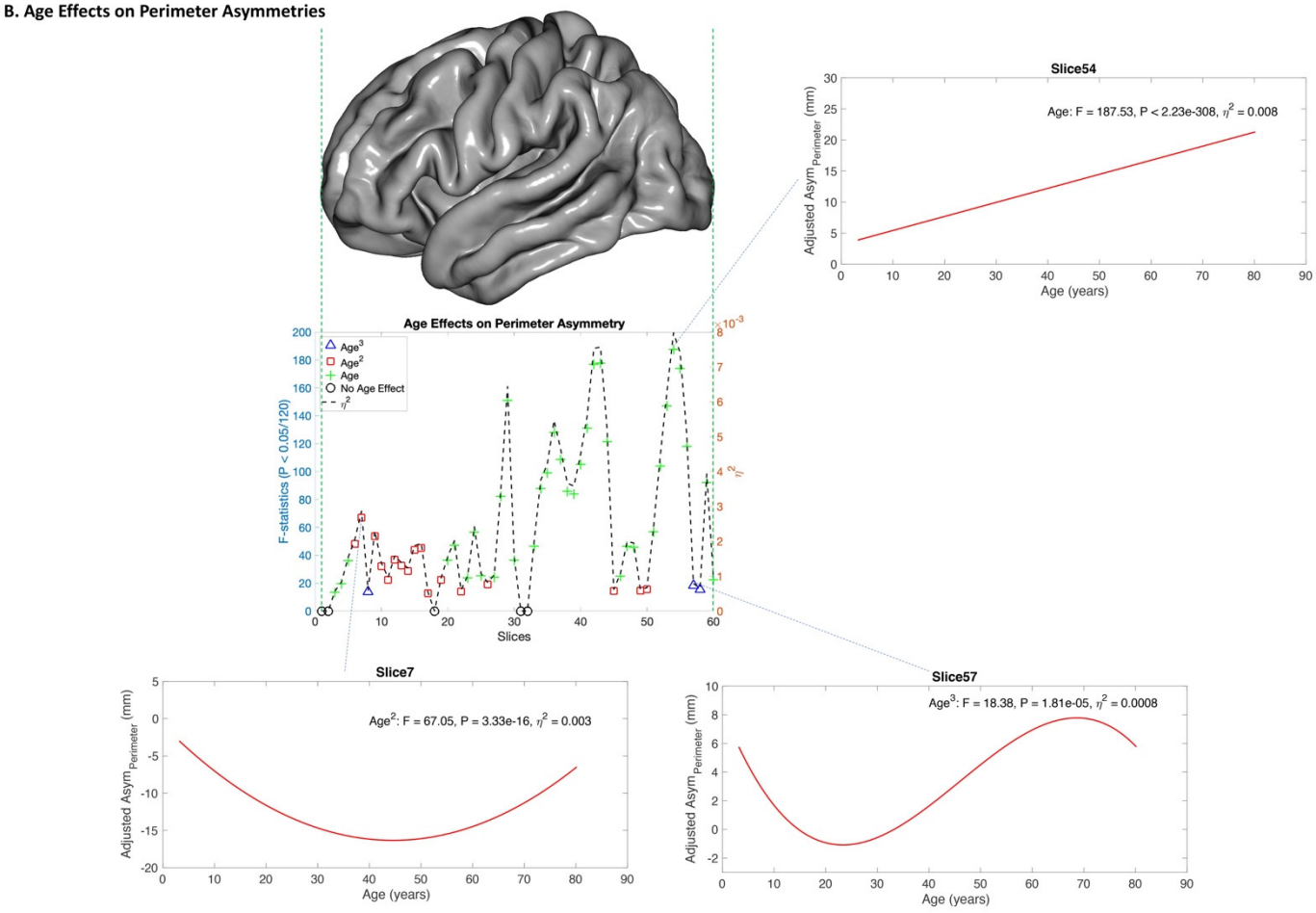

Figure S5. Age effects on asymmetries in hemispheric width (A) and perimeter (B) assessed using the pooled sample. Significant ($P < 0.05/120$) cubic, quadratic and linear age effects are marked with blue triangles, red square and green '+' symbols respectively. Fitted age trajectories are depicted for selected brain slices. The left hemisphere of the FreeSurfer fsaverage cortical surface template is displayed above the plots of age effects as the reference of brain anatomy. $Asym_{width}$ = width asymmetry, $Asym_{perimeter}$ = perimeter asymmetry.

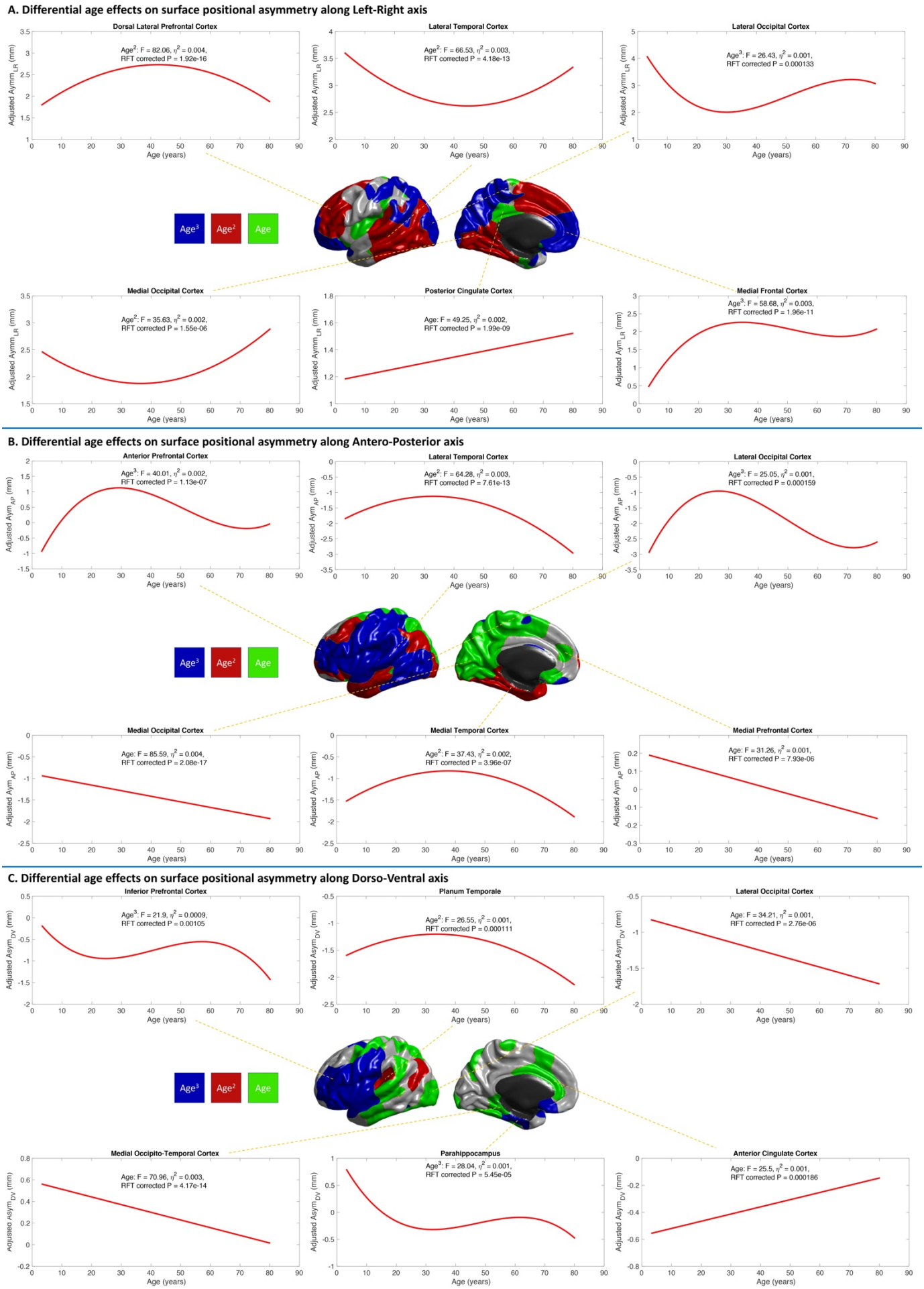
A. Differential age effects on surface positional asymmetry along Left-Right axis
Dorsal Lateral Prefrontal Cortex
Age²: F = 82.06, η² = 0.004,
RFT corrected P = 1.92e-16
Lateral Temporal Cortex
Age²: F = 66.53, η² = 0.003,
RFT corrected P = 4.18e-13
Lateral Occipital Cortex
Age³: F = 26.43, η² = 0.001,
RFT corrected P = 0.000133
Age³
Age²
Age
Medial Occipital Cortex
Age²: F = 35.63, η² = 0.002,
RFT corrected P = 1.55e-06
Posterior Cingulate Cortex
Age: F = 49.25, η² = 0.002,
RFT corrected P = 1.99e-09
Medial Frontal Cortex
Age³: F = 58.68, η² = 0.003,
RFT corrected P = 1.96e-11
Adjusted Aymm_LR (mm)
Adjusted Aym_LR (mm)
Age (years)
B. Differential age effects on surface positional asymmetry along Antero-Posterior axis
Anterior Prefrontal Cortex
Age³: F = 40.01, η² = 0.002,
RFT corrected P = 1.13e-07
Lateral Temporal Cortex
Age²: F = 64.28, η² = 0.003,
RFT corrected P = 7.61e-13
Lateral Occipital Cortex
Age³: F = 25.05, η² = 0.001,
RFT corrected P = 0.000159
Age³
Age²
Age
Medial Occipital Cortex
Age: F = 85.59, η² = 0.004,
RFT corrected P = 2.08e-17
Medial Temporal Cortex
Age²: F = 37.43, η² = 0.002,
RFT corrected P = 3.96e-07
Medial Prefrontal Cortex
Age: F = 31.26, η² = 0.001,
RFT corrected P = 7.93e-06
Adjusted Aym_AP (mm)
Age (years)
C. Differential age effects on surface positional asymmetry along Dorso-Ventral axis
Inferior Prefrontal Cortex
Age³: F = 21.9, η² = 0.0009,
RFT corrected P = 0.00105
Planum Temporale
Age²: F = 26.55, η² = 0.001,
RFT corrected P = 0.000111
Lateral Occipital Cortex
Age: F = 34.21, η² = 0.001,
RFT corrected P = 2.76e-06
Age³
Age²
Age
Medial Occipito-Temporal Cortex
Age: F = 70.96, η² = 0.003,
RFT corrected P = 4.17e-14
Parahippocampus
Age³: F = 28.04, η² = 0.001,
RFT corrected P = 5.45e-05
Anterior Cingulate Cortex
Age: F = 25.5, η² = 0.001,
RFT corrected P = 0.000186
Adjusted Asym_DV (mm)
Age (years)

Figure S6. Distributions of significant (random field theory (RFT) corrected P < 0.05/3) cubic (blue areas), quadratic (red areas) and linear (green areas) age effects on surface positional asymmetries along the Left-Right (A), Antero-Posterior (B) and Dorso-Ventral (C) axes assessed using the pooled sample. Fitted age trajectories are depicted for selected vertices. L-R = Left-Right, A-P = Antero-Posterior, D-V = Dorso-Ventral. $Asym_{LR}$ = asymmetry along left-right axis, $Asym_{AP}$ = asymmetry along Antero-Posterior axis, $Asym_{DV}$ = asymmetry along Dorso-Ventral axis.

A. Age Effects on Width Asymmetries

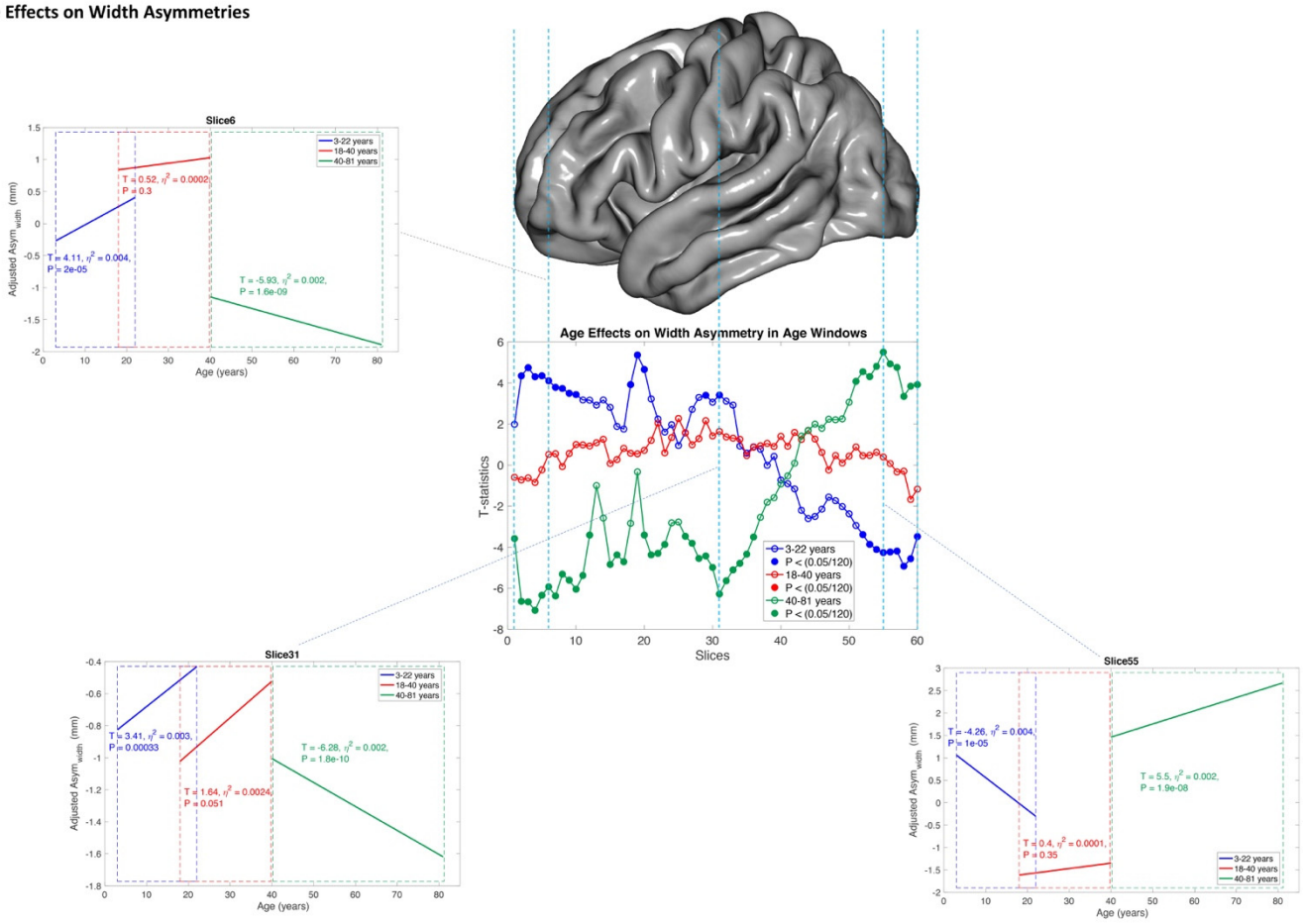

B. Age Effects on Perimeter Asymmetries

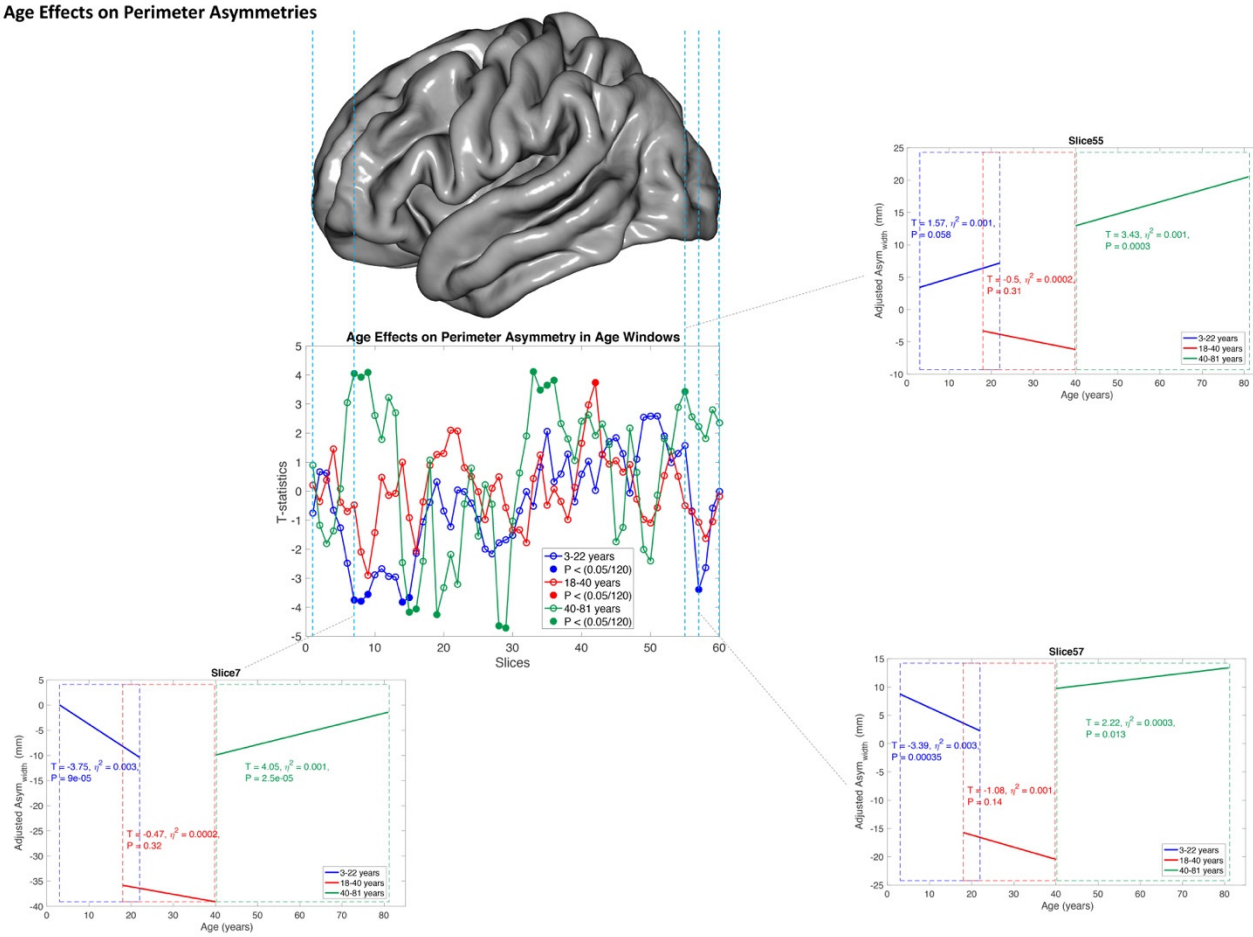

Figure S7: Age effects on asymmetries in hemispheric width (A) and perimeter (B) assessed in separate age windows using subsamples with overlapped age ranges (ABCD, PING and PNC for 3-22 years, HCP and a part of ICBM for 18-40 years, UKB and a part of ICBM for 40-81 years) and adjusting for sites and scanners and other covariates. Significant age effects ($P < 0.05/120$) detected in age windows of 3-22, 18-40 and 40-81 years are marked as blue, red and green dots respectively. Fitted age trajectories are depicted for selected brain slices. Blue, red and green lines represent fitted age trajectories in age windows of 3-22, 18-40 and 40-81 years respectively. Statistics for age effects in each age window are annotated with the same color. Blue, red and green dash rectangles highlight the age windows respectively. The left hemisphere of the FreeSurfer fsaverage cortical surface template is displayed above the plots of age effects as the reference of brain anatomy. $Asym_{width}$ = width asymmetry, $Asym_{perimeter}$ = perimeter asymmetry.

A. age effects on surface positional asymmetry along Left-Right axis in different age windows

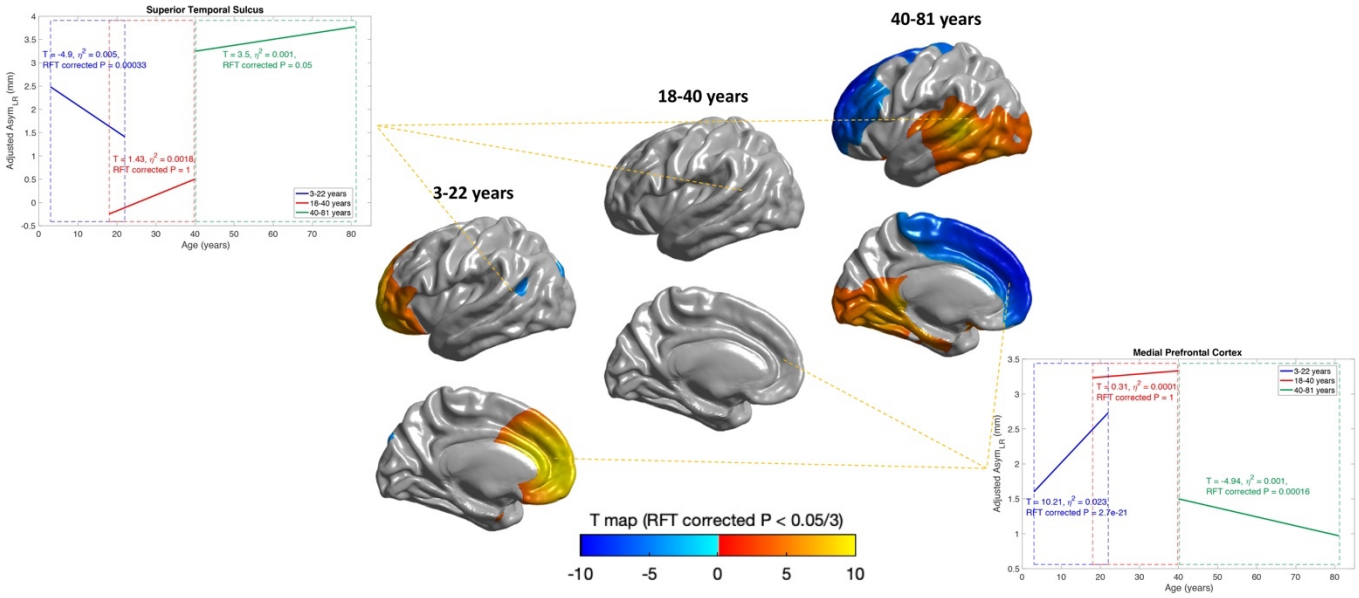

B. age effects on surface positional asymmetry along Antero-Posterior axis in different age windows

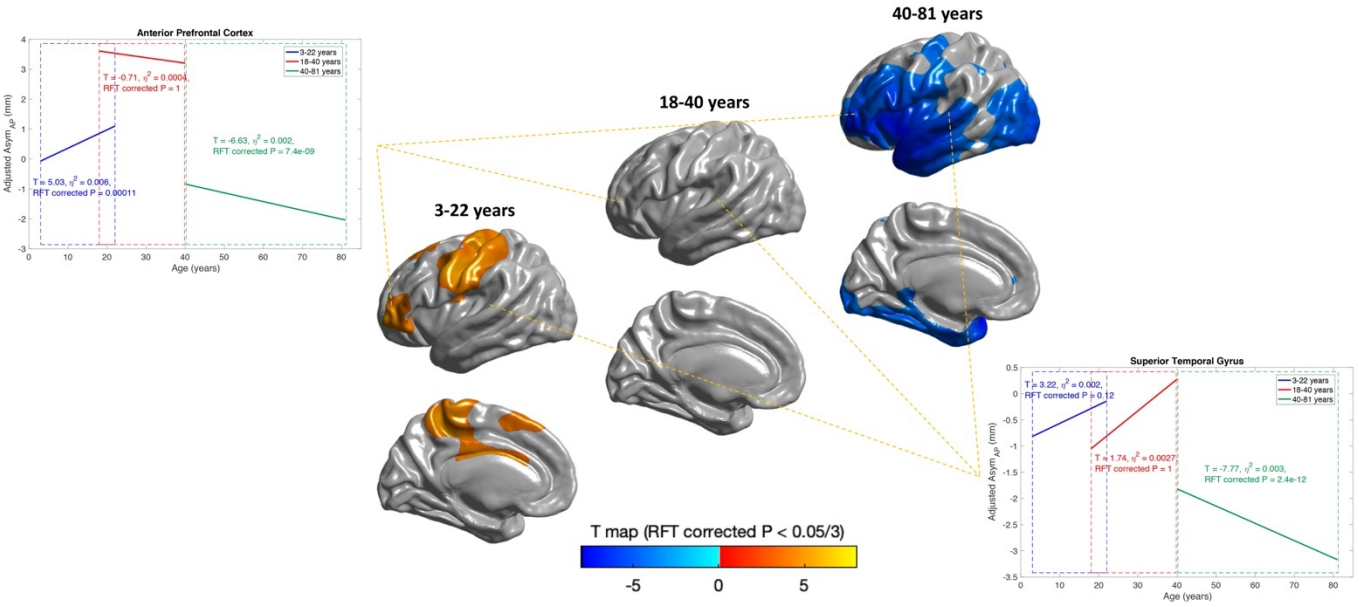

C. age effects on surface positional asymmetry along Dorso-Ventral axis in different age windows

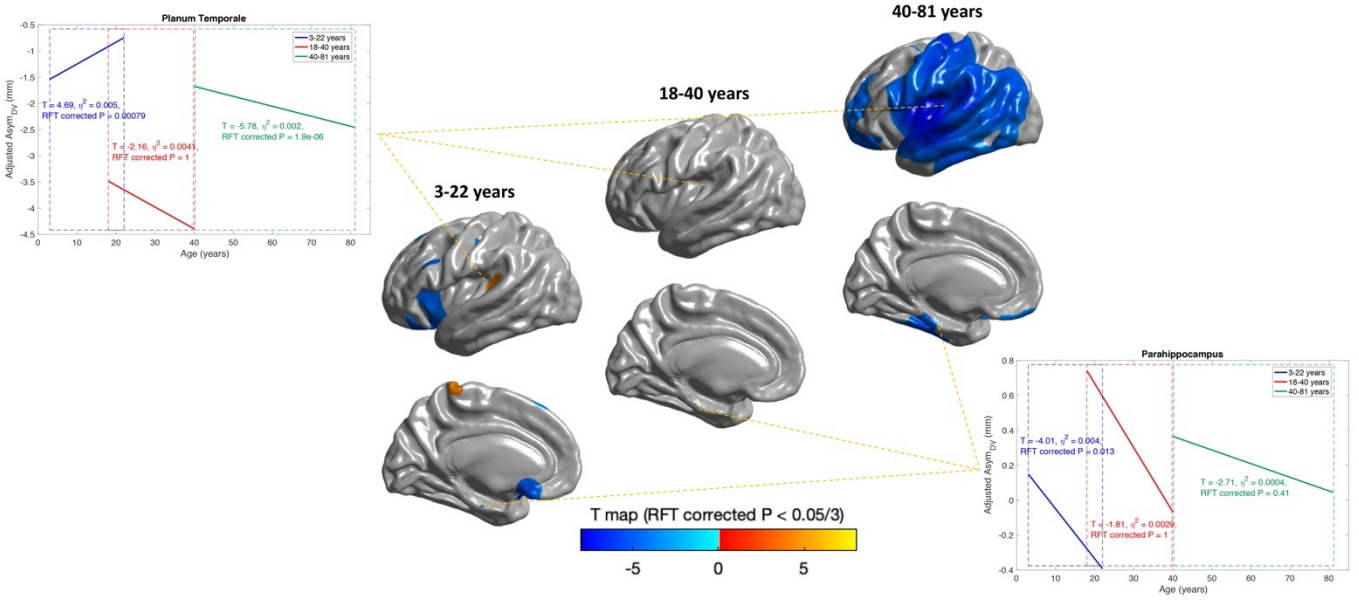

Figure S8: Maps of significant age effects (random field theory (RFT) corrected P < 0.05/3)) on asymmetries in surface positional asymmetries along the left-right (A), anterior-posterior (B) and dorsal-ventral (C), assessed in separate age windows using subsamples with overlapped age ranges (ABCD, PING and PNC for 3-22 years, HCP and a part of ICBM for 18-40 years, UKB and a part of ICBM for 40-81 years) and adjusting for sites and scanners and other covariates. Fitted age trajectories are depicted for selected vertices. Blue, red and green lines represent fitted age trajectories in age windows of 3-22, 18-40 and 40-81 years respectively. Statistics for age effects in each age window are annotated with the same color. Blue, red and green dash rectangles highlight the age windows respectively.

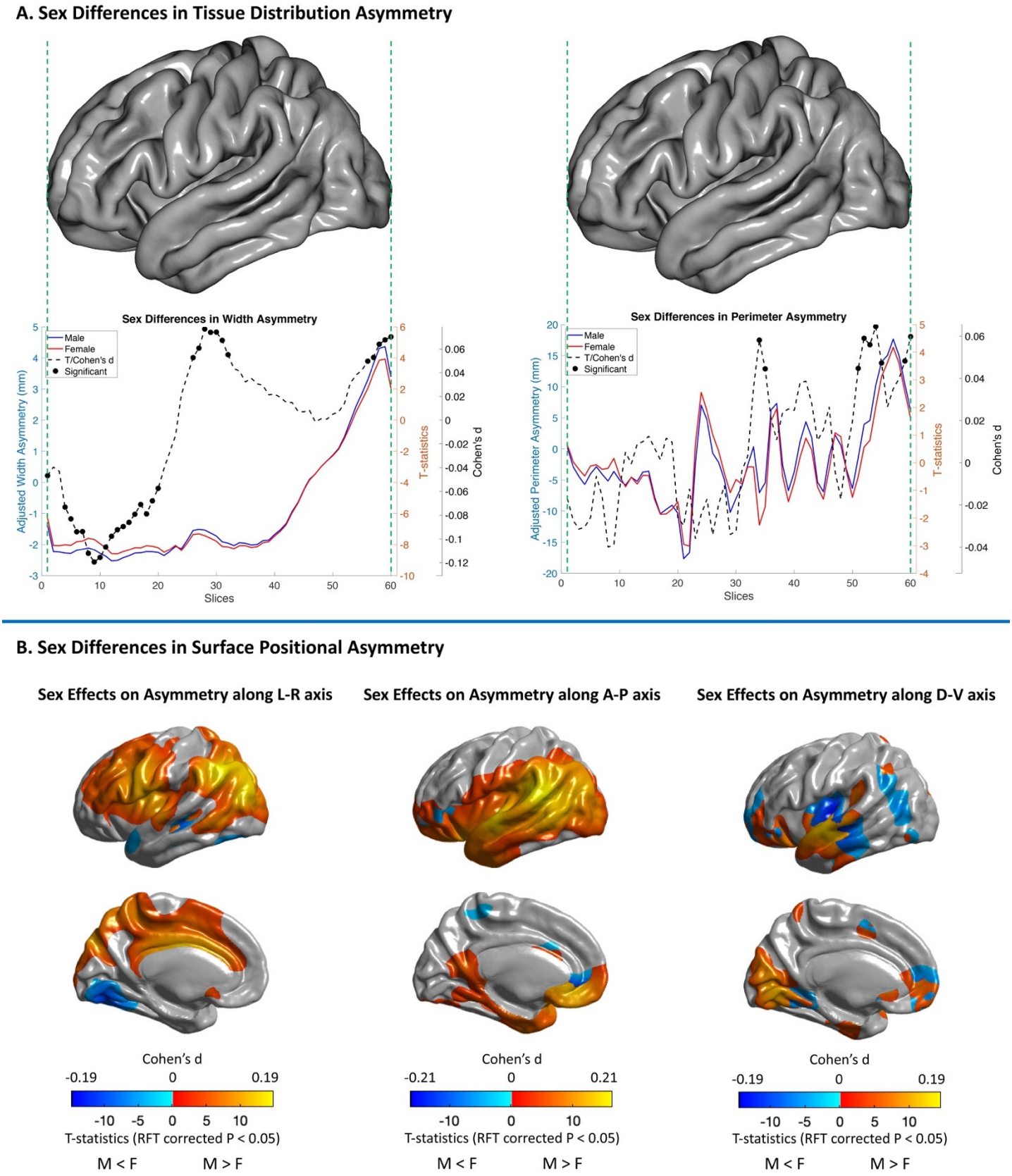

Figure S9: Sex differences in brain tissue asymmetries (A) and surface positional asymmetries (B) assessed using the pooled sample. A. Blue and red lines represent adjusted sectional width (left column) and perimeter asymmetries (right column) for males (M) and females (F), respectively. Dash lines show T-statistics and Cohen's d for sex differences (M vs F). Black dots indicate significant (P < 0.05/120) sex differences. The left hemisphere of the FreeSurfer fsaverage cortical surface template is displayed above the plots of sex differences as the reference of brain anatomy. B. Significant (random field theory (RFT) corrected P < 0.05/3) sex effects on surface positional asymmetries along the Left-Right (left panel), Antero-Posterior (middle panel) and Dorso-Ventral (right panel) axes. Color bars represent T statistics and Cohen's d for sex differences. Red-yellow and blue-cyan indicate enlargement and reduction of asymmetry magnitude in males relative to females, respectively. L-R = Left-Right, A-P = Antero-Posterior, D-V = Dorso-Ventral.

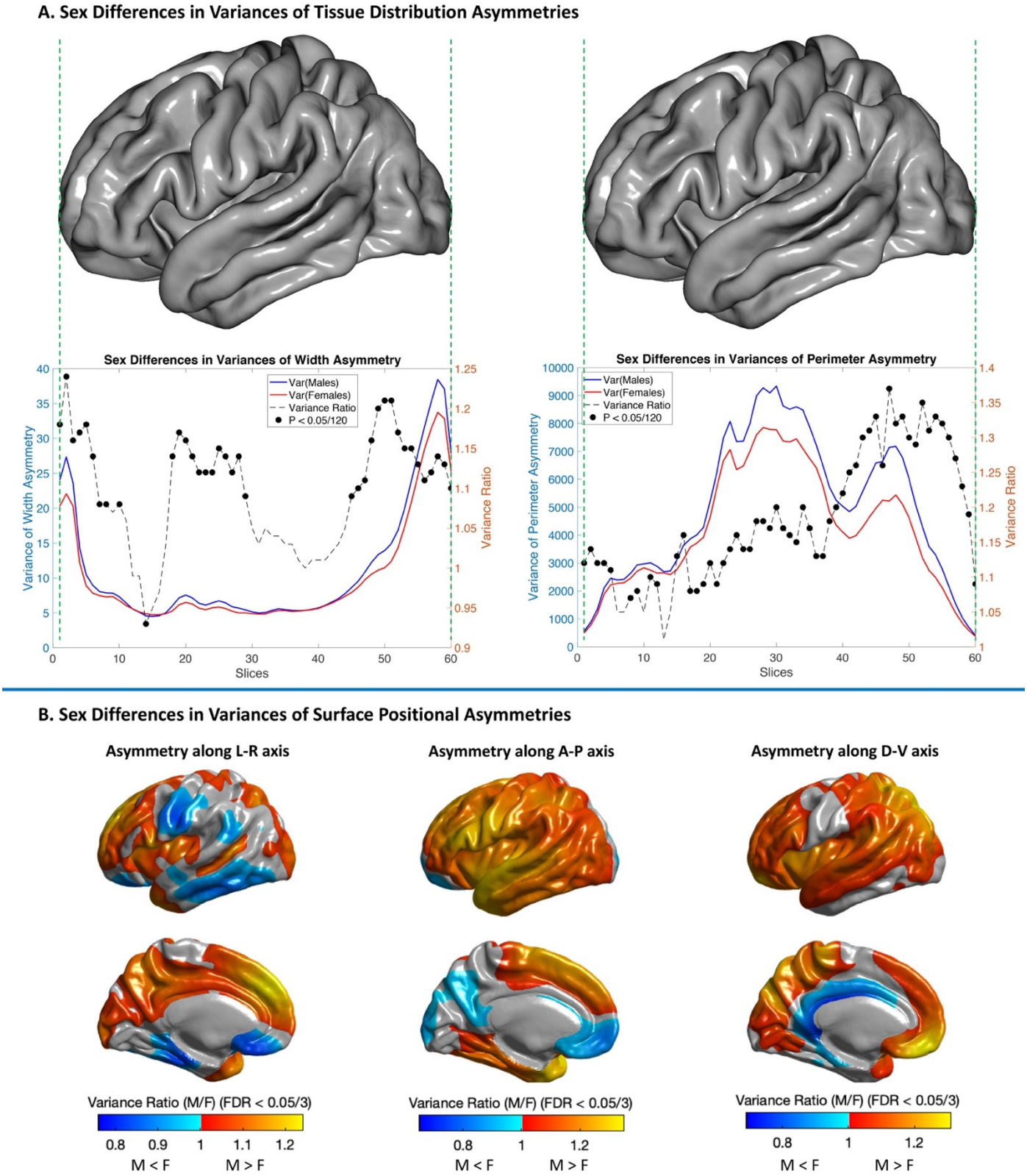

Figure S10: Sex differences in variances of brain tissue asymmetries and surface positional asymmetries assessed using the pooled sample. A. Blue and red lines represent variances of sectional hemispheric width (left column) and perimeter asymmetries (right column) for males (M) and females (F), respectively. Dash lines represent variance ratio (M/F). Black dots indicate significant (P < 0.05/120) sex differences in variances. The left hemisphere of the FreeSurfer fsaverage cortical surface template is displayed above the plots of sex differences as the reference of brain anatomy. B. Significant (false discover rate (FDR) < 0.05/3) sex differences in variances of surface positional asymmetries along the Left-Right (left panel), Antero-Posterior (middle panel) and Dorso-Ventral (right panel) axes. Color bars represent variance ratio of males to females. Red-yellow and blue-cyan indicate greater and smaller variance in males relative to females, respectively. L-R = Left-Right, A-P = Antero-Posterior, D-V = Dorso-Ventral.

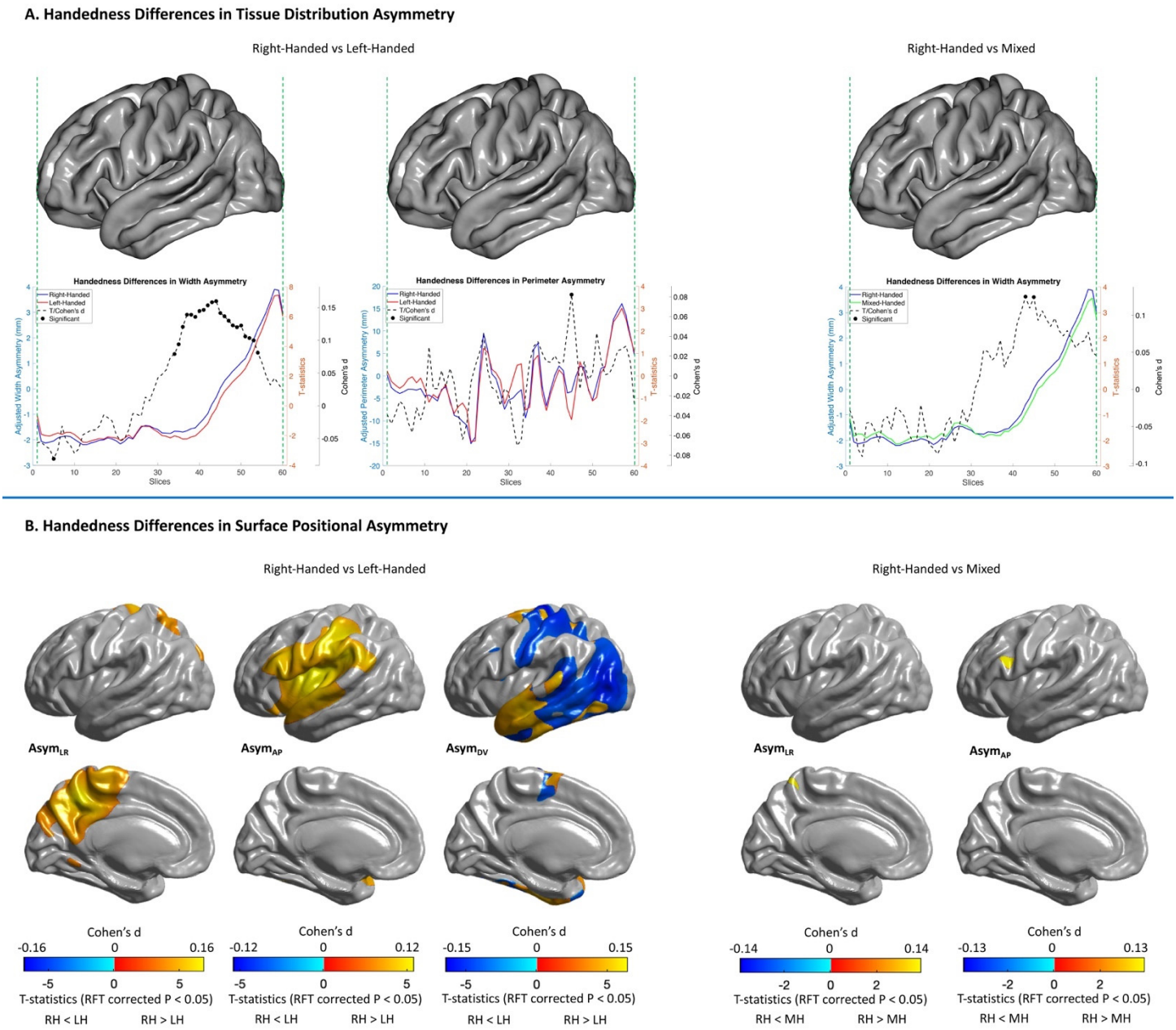

Figure S11: Handedness differences in brain tissue asymmetry (A) and surface positional asymmetry (B) assessed using the pooled sample. A. Left panel shows differences between right-handers (RH) and left-handers (LH) in sectional width and perimeter asymmetries; right panel shows differences between RH and mixed-handers (MH). Blue, red and green lines represent adjusted sectional hemispheric width asymmetries for RH, LH and MH, respectively. Dash lines show T-statistics and Cohen's d for handedness differences. Significant ($P < 0.05/120$) handedness differences were highlighted with black dots. The left hemisphere of the FreeSurfer fsaverage cortical surface template is displayed as the reference of brain anatomy. No significant differences between RH and MH in perimeter asymmetries and between LH and MH in width and perimeter asymmetries were found. Thus, the results are not shown here. B. The left panel shows significant (random field theory (RFT) corrected $P < 0.05/3$) differences between RH and LH in surface positional asymmetries along the Left-Right ($Asym_{LR}$), Antero-Posterior ($Asym_{AP}$) and Dorso-Ventral ($Asym_{DV}$) axes; the right panel shows significant differences between RH and MH in $Asym_{LR}$ and $Asym_{AP}$. Color bars represent T statistics and Cohen's d for handedness differences. No significant differences between RH and MH in $Asym_{DV}$ and between LH and MH in all surface positional asymmetry measures were found. Thus, the results are not shown here.

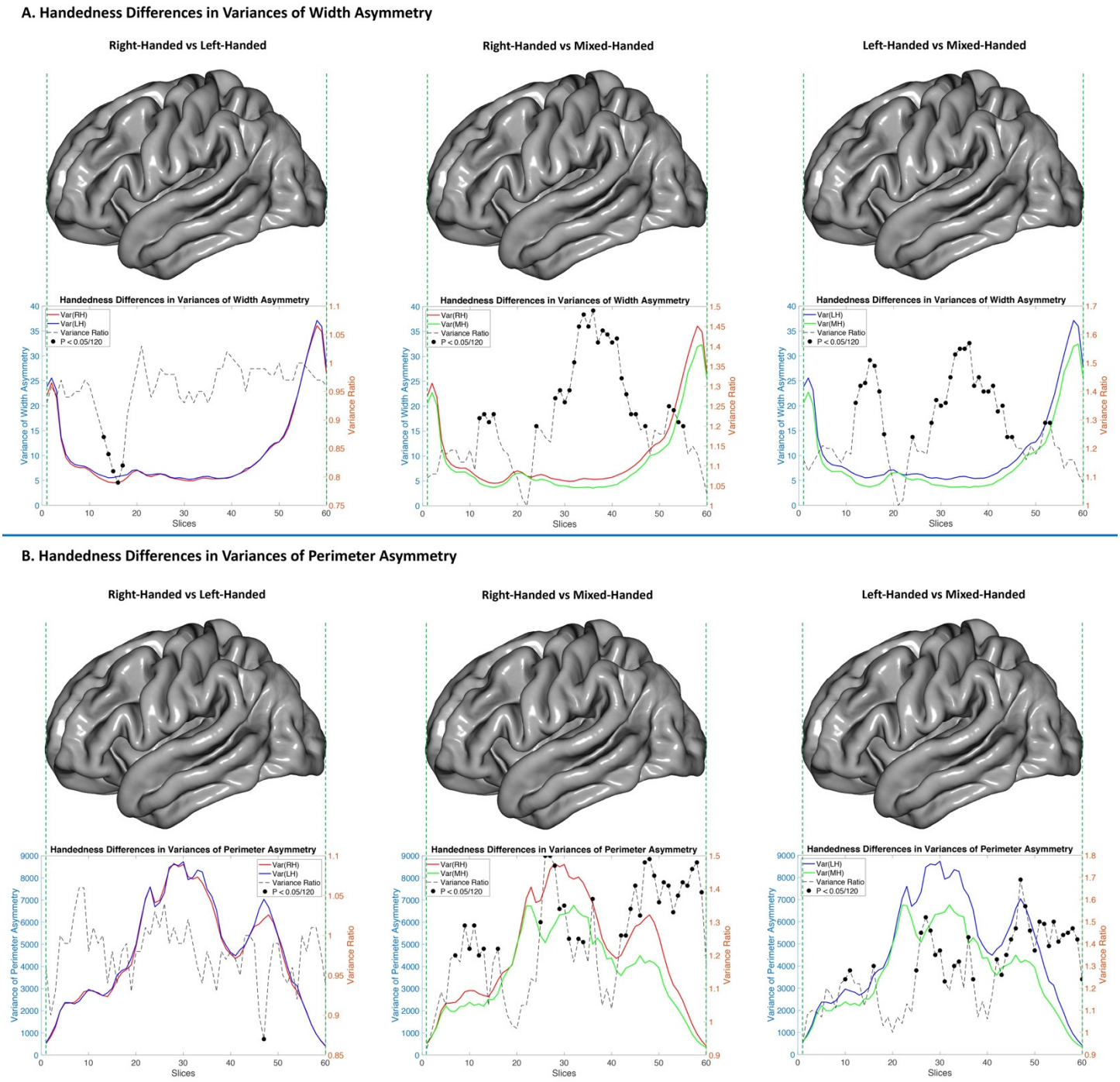

Figure S12: Handedness differences in variances of asymmetries in hemispheric width (A) and perimeter (B) assessed using the pooled sample. Blue, red and green lines represent variances of sectional hemispheric width/perimeter asymmetries for right-handers (RH), left-handers (LH) and mixed-handers (MH), respectively. Dash lines represent variance ratio. Black dots indicate significant ($P < 0.05/120$) handedness differences in variances. The left hemisphere of the FreeSurfer fsaverage cortical surface template is displayed above the plots of handedness differences as the reference of brain anatomy.

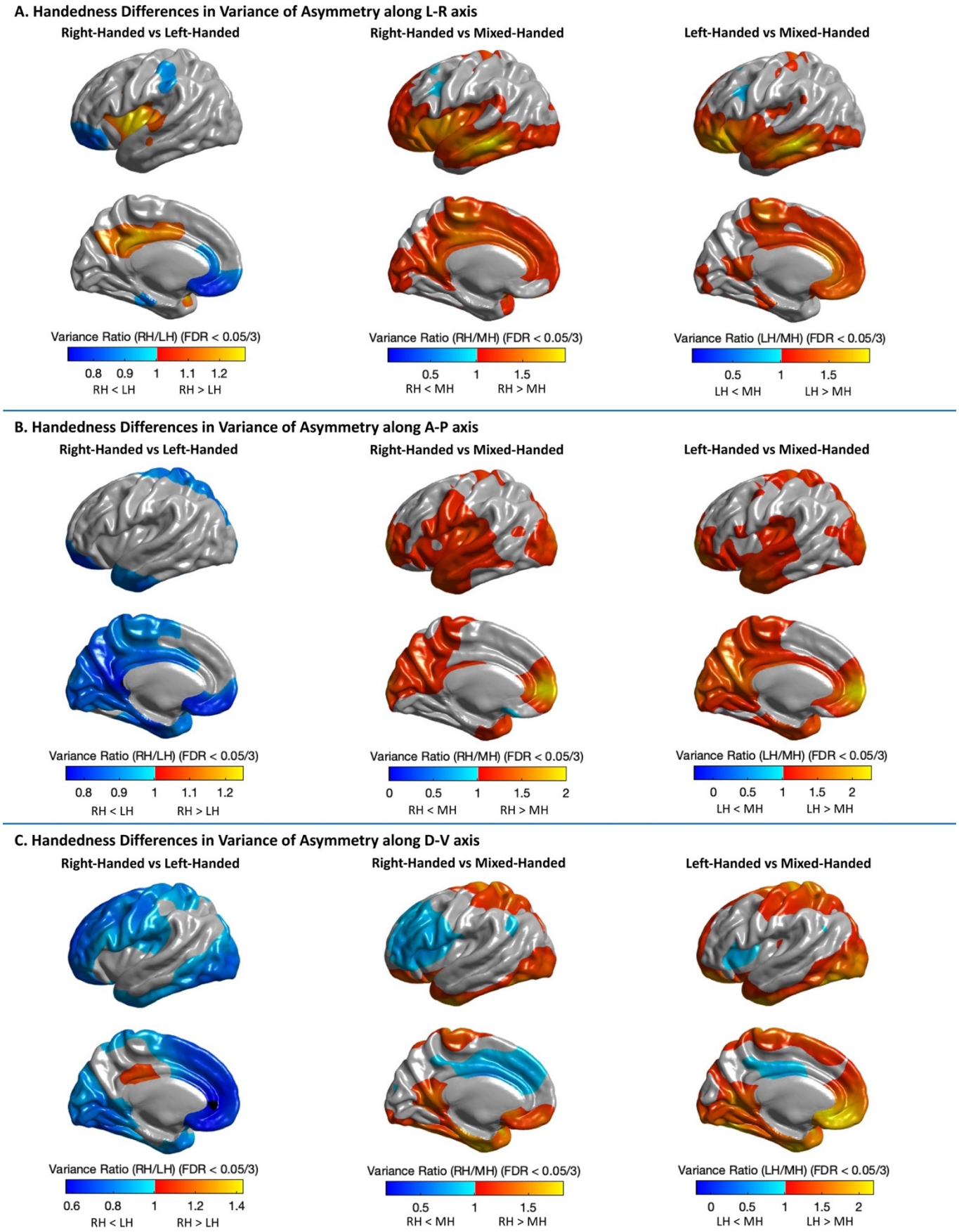

Figure S13: Handedness differences in variances of surface positional asymmetries along the Left-Right (A), Antero-Posterior (B), and Dorso-Ventral (C) axes assessed using the pooled sample. Color bars represent variance ratio. The maps are thresholded at false discover rate (FDR) < 0.05/3. L-R = Left-Right, A-P = Antero-Posterior, D-V = Dorso-Ventral. RH = right-handers, LH = left-handers, MH = mixed-handers.

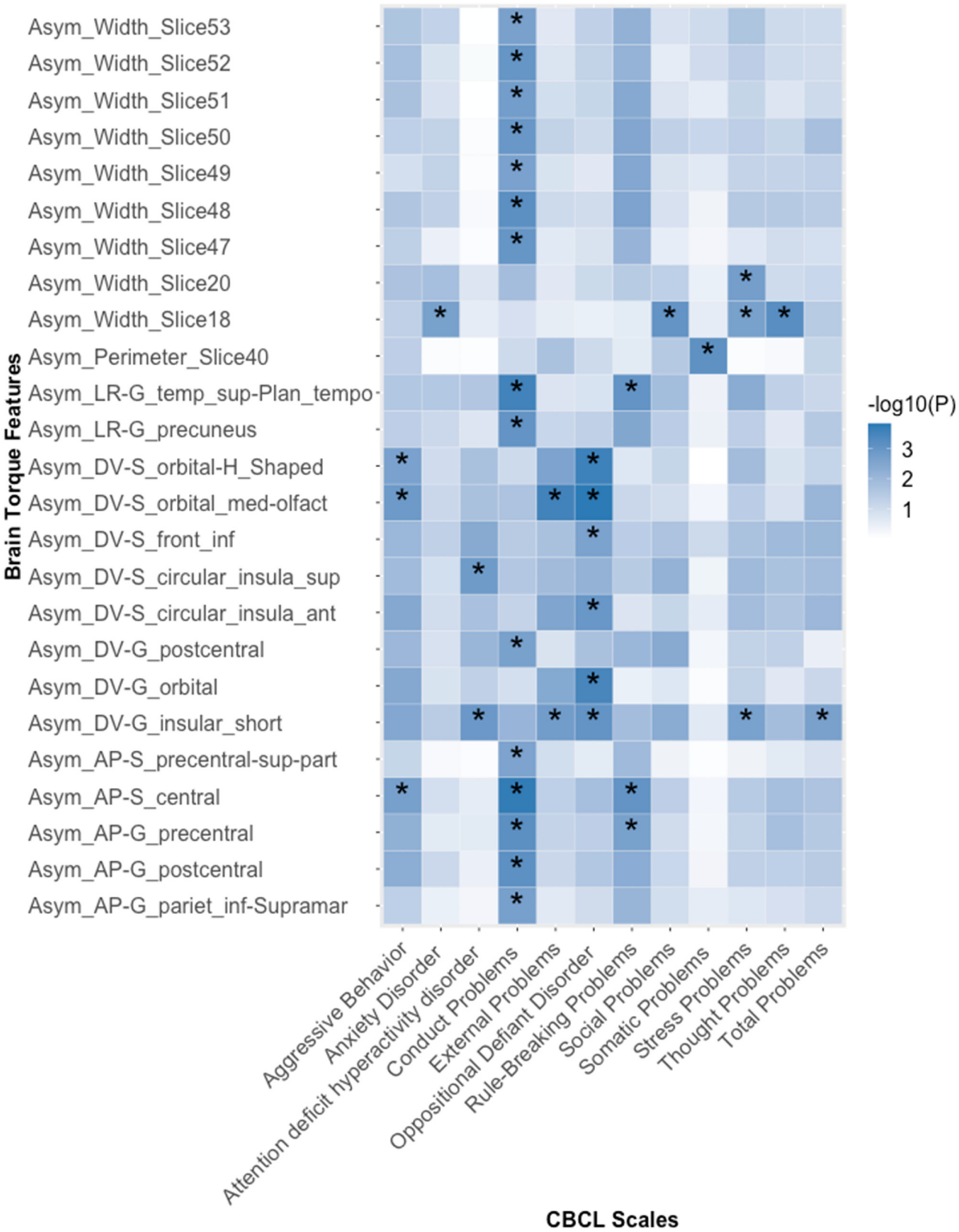

Figure S14: Heat map showing associations between brain torque (BT) features and child psychopathological symptoms assessed using the ABCD dataset. Only BT features and psychopathological measures showing at least one association at the significance level of $P < 0.05/20$ (highlighted with asterisks) are included here. For the abbreviations of brain surface regions, see Table S14. Detailed statistics of these associations are summarized in Table S15.

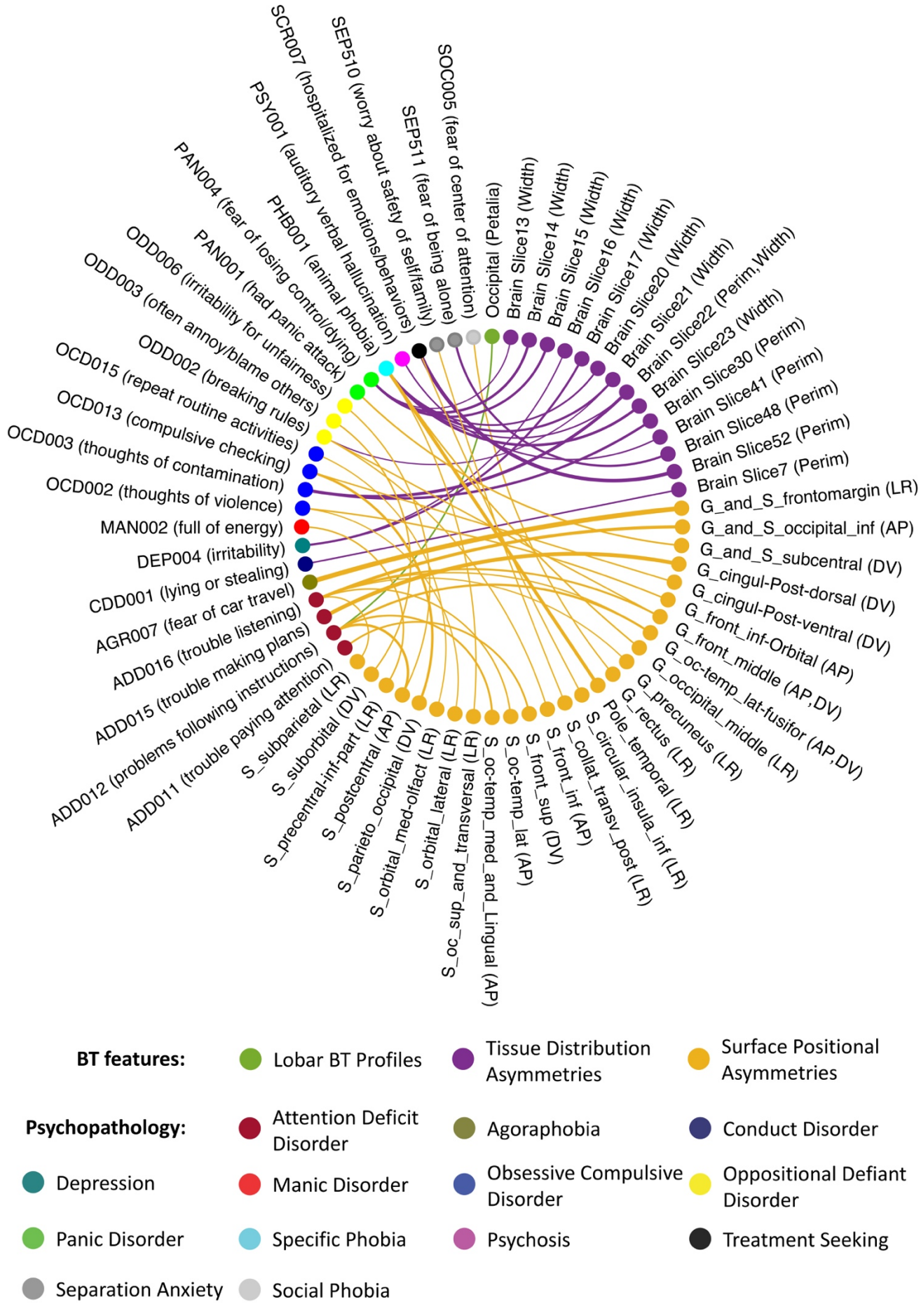
SCR007 (hospitalized for emotions/behaviors)
SEP510 (worry about safety of self/family)
SEP511 (fear of being alone)
SOC005 (fear of center of attention)
PSY001 (auditory verbal hallucination)
PHB001 (animal phobia)
PAN004 (fear of losing control/dying)
PAN001 (had panic attack)
ODD006 (irritability for unfairness)
ODD003 (often annoy/blame others)
ODD002 (breaking rules)
OCD015 (repeat routine activities)
OCD013 (compulsive checking)
OCD003 (thoughts of contamination)
OCD002 (thoughts of violence)
MAN002 (full of energy)
DEP004 (irritability)
CDD001 (lying or stealing)
AGR007 (fear of car travel)
ADD016 (trouble listening)
ADD015 (trouble making plans)
ADD012 (problems following instructions)
ADD011 (trouble paying attention)
S_subparietal (LR)
S_suborbital (DV)
S_precentral-inf-part (LR)
S_postcentral (AP)
S_parieto_occipital (DV)
S_orbital_med-olfact (LR)
S_orbital_lateral (LR)
S_oc_sup_and_transversal (LR)
S_oc-temp_med_and_Lingual (AP)
S_oc-temp_lat (AP)
S_front_sup (DV)
S_front_inf (AP)
S_collat_transv_post (LR)
S_circular_insula_inf (LR)
Pole_temporal (LR)
G_rectus (LR)
G_precuneus (LR)
G_occipital_middle (LR)
G_oc-temp_lat-fusifor (AP,DV)
G_front_middle (AP,DV)
G_front_inf-Orbital (AP)
G_cingul-Post-ventral (DV)
G_cingul-Post-dorsal (DV)
G_and_S_subcentral (DV)
G_and_S_occipital_inf (AP)
G_and_S_frontomargin (LR)
Brain Slice7 (Perim)
Brain Slice52 (Perim)
Brain Slice48 (Perim)
Brain Slice41 (Perim)
Brain Slice30 (Perim)
Brain Slice23 (Width)
Brain Slice22 (Perim,Width)
Brain Slice21 (Width)
Brain Slice20 (Width)
Brain Slice17 (Width)
Brain Slice16 (Width)
Brain Slice15 (Width)
Brain Slice14 (Width)
Brain Slice13 (Width)
Occipital (Petalia)
BT features:
Lobar BT Profiles
Tissue Distribution Asymmetries
Surface Positional Asymmetries
Psychopathology:
Attention Deficit Disorder
Agoraphobia
Conduct Disorder
Depression
Manic Disorder
Obsessive Compulsive Disorder
Oppositional Defiant Disorder
Panic Disorder
Specific Phobia
Psychosis
Treatment Seeking
Separation Anxiety
Social Phobia

Figure S15: Connectogram showing associations between brain torque (BT) features and child psychopathological symptoms assessed using the PNC dataset. Ribbons are colored with the colors of linked BT profiles. Ribbon thickness represents the -log(P) value of the corresponding association. The psychopathological measures are annotated with the PNC GOASSESS items and brief descriptions. Only BT features and psychopathological measures showing at least one association at the significance level of $P < 0.05/112$ are included here. ADD = Attention Deficit Disorder, AGR = Agoraphobia, CDD = Conduct Disorder, DEP = Depression, MAN = Manic Disorder, OCD = Obsessive Compulsive Disorder, ODD = Oppositional Defiant Disorder, PAN = Panic Disorder, PHB = Specific Phobia, PSY = Psychosis, SCR = Treatment Seeking, SEP = Separation Anxiety, SOC = Social Phobia, Width = Width Asymmetry, Perim = Perimeter Asymmetry, LR = asymmetry along left-right axis, AP = asymmetry along Antero-Posterior axis, DV = asymmetry along Dorso-Ventral axis. For the abbreviations of brain surface regions, see Table S14. Detailed statistics of these associations are summarized in Table S16.

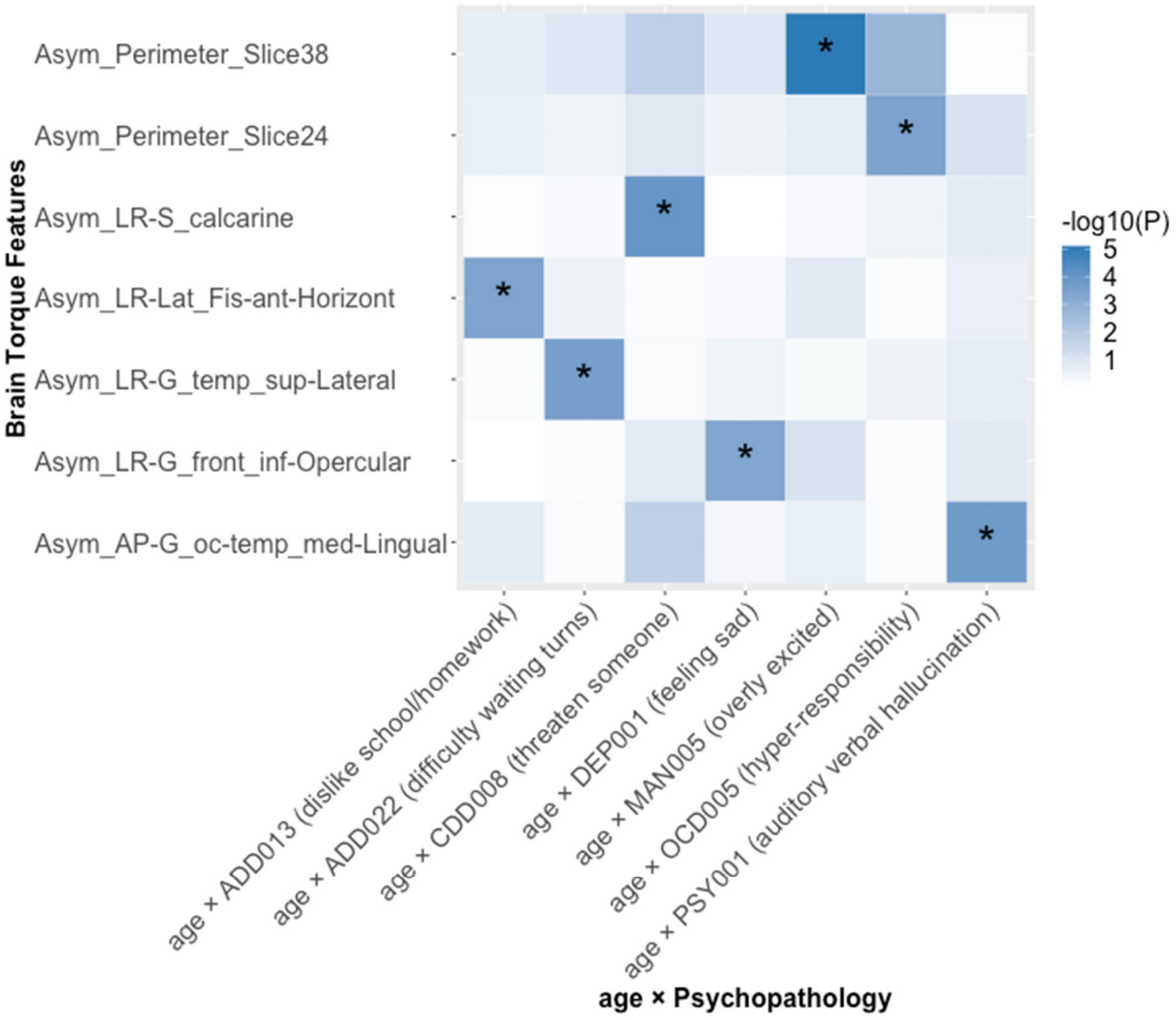

Figure S16: Heat map showing associations between brain torque (BT) features and age-by-psychopathology interactions assessed using the PNC dataset. Only BT features and psychopathological measures showing at least one association at the significance level of $P < 0.05/112$ (highlighted with asterisks) are included here. ADD = Attention Deficit Disorder, CDD = Conduct Disorder, DEP = Depression, MAN = Manic Disorder, OCD = Obsessive Compulsive Disorder, PSY = Psychosis. For the abbreviations of brain surface regions, see Table S14. Detailed statistics of these associations are summarized in Table S17.

A. LDSC

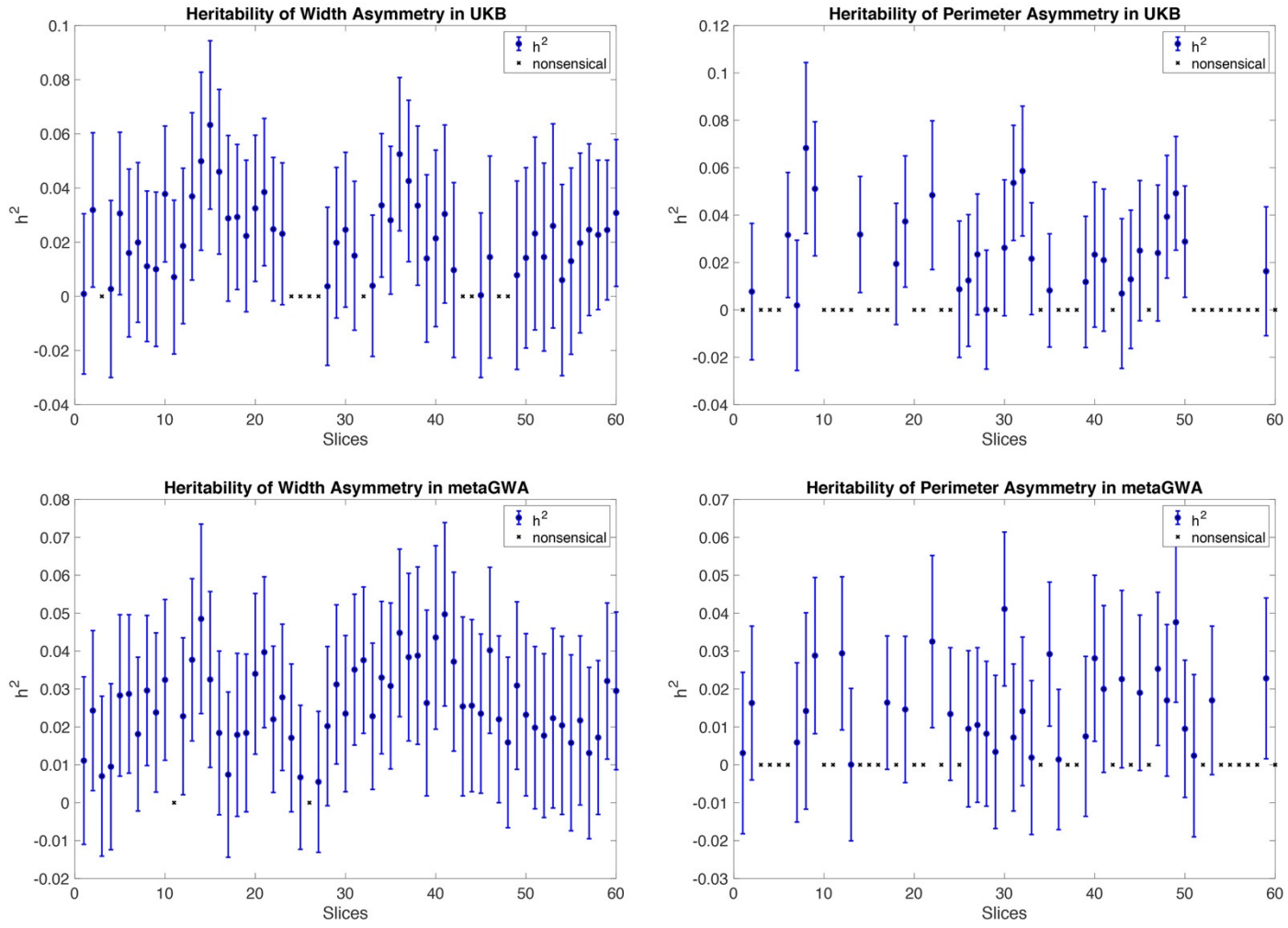

B. GCTA-GREML

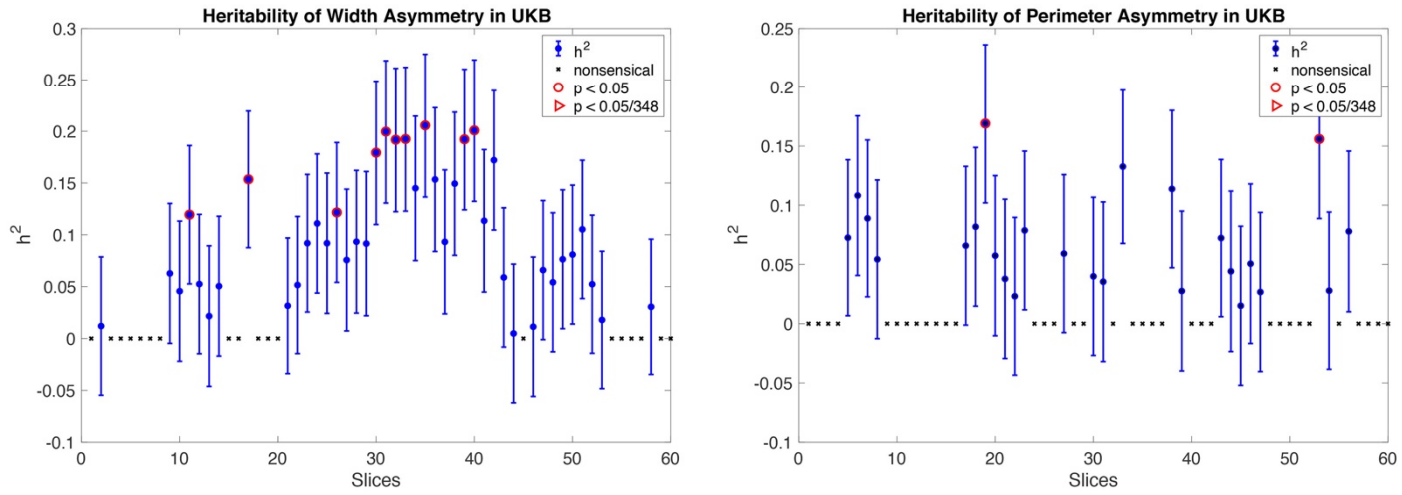

Figure S17. SNP-based heritability of sectional asymmetries of hemispheric width (A) and perimeter (B) estimated using the LDSC and GCTA-GREML methods. LDSC was applied to the GWAS summary statistics for the UK biobank (UKB) cohort and the meta-GWAS summary statistics. GCTA-GREML was applied to the UKB genomic data. Blue dots represent the heritability estimates; error bars show the standard errors; symbol 'x' presents nonsensical estimates of $h^2 < 0$.

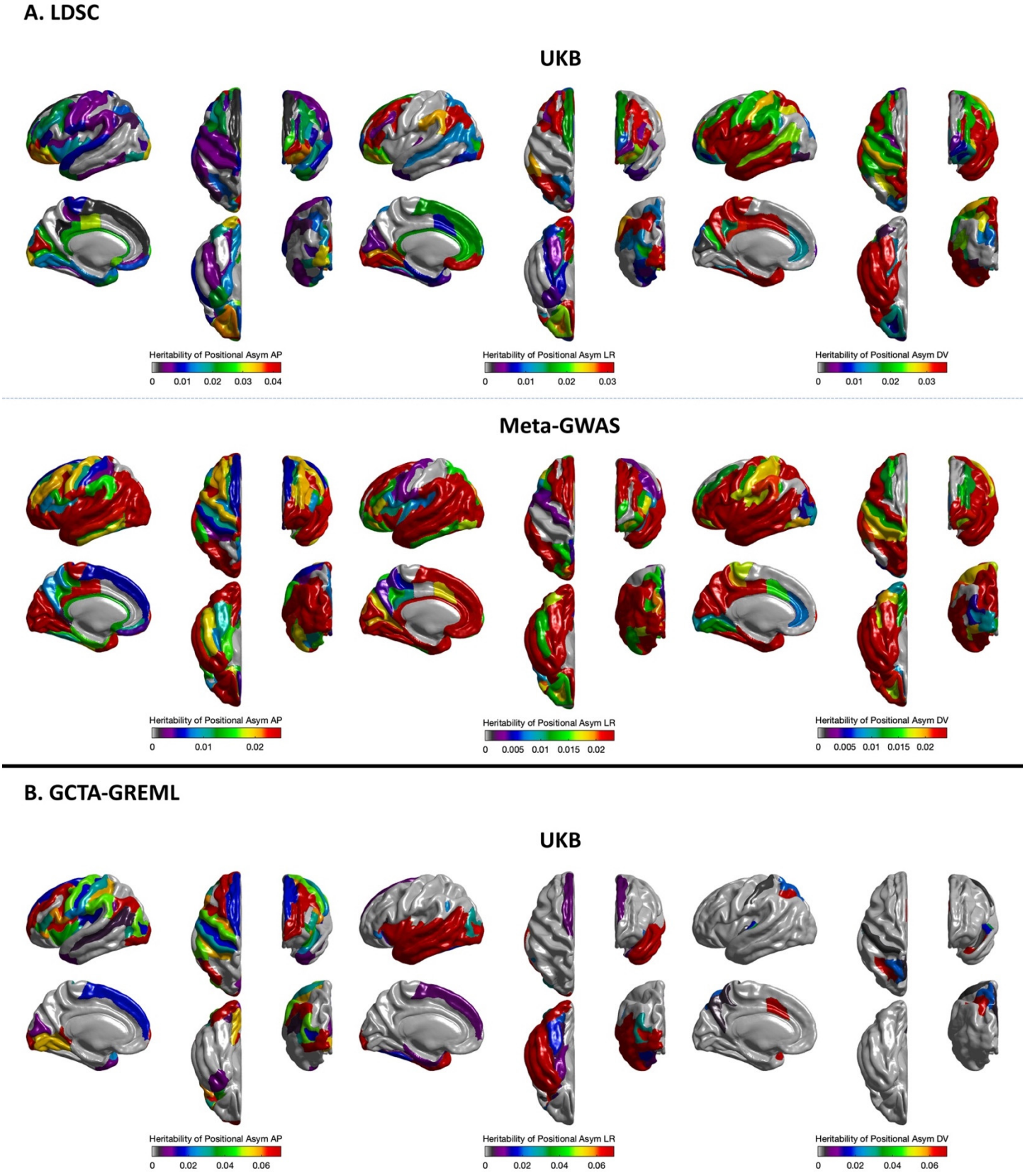

Figure S18. SNP-based heritability of regional mean surface positional asymmetries along the left-right ($Asym_{LR}$), antero-posterior ($Asym_{AP}$) and dorsal-ventral ($Asym_{DV}$) axes estimated using the LDSC (A) and GCTA-GREML (B) methods. LDSC was applied to the GWAS summary statistics for the UK biobank (UKB) cohort and the meta-GWAS summary statistics. GCTA-GREML was applied to the UKB genomic data.

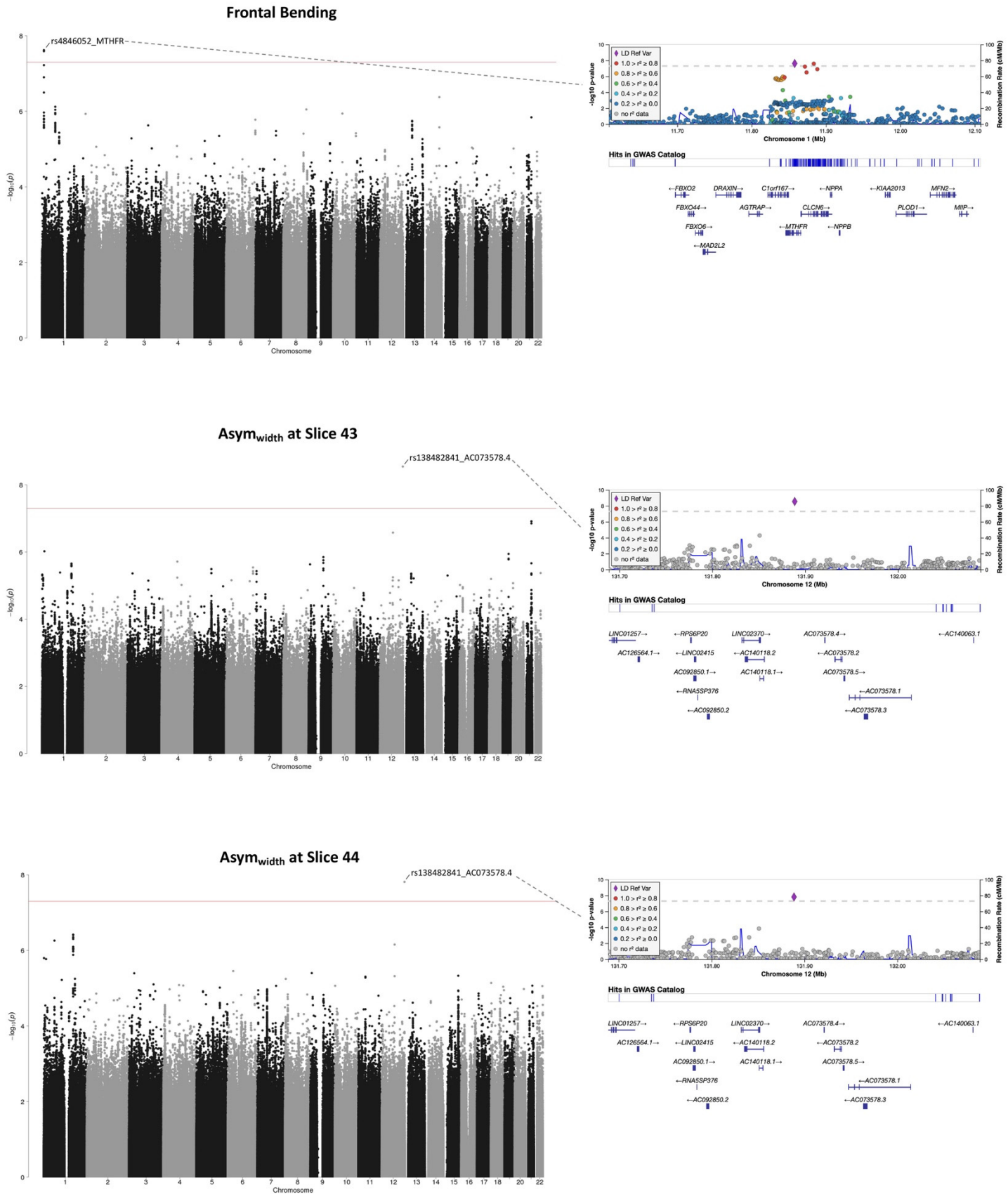

Figure S19 - Part 1. Manhattan plots of meta-GWAS summary statistics for the brain torque profiles showing significant genetic associations. Red and blue lines represent the significance levels of P < 5e-8 and P < 5e-8/348 = 1.44e-10 respectively. Independent lead variants are annotated with their SNP IDs and the closest genes. LocusZoom plots (purple diamond symbols indicate lead SNPs) are attached to show regional associations. For the abbreviations of brain regions, see Table S14.

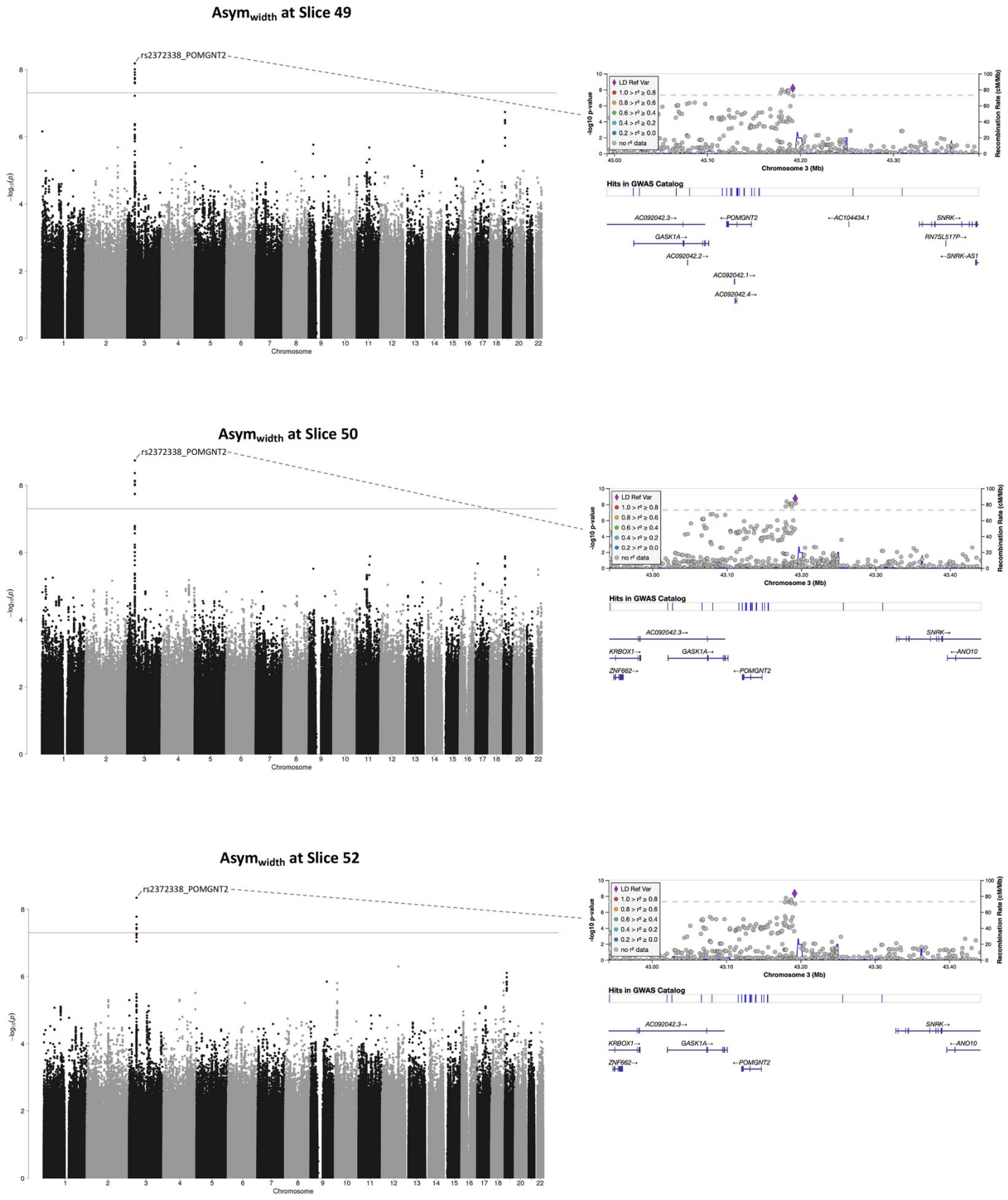

Figure S19 - Part 2. Manhattan plots of meta-GWAS summary statistics for the brain torque profiles showing significant genetic associations. Red and blue lines represent the significance levels of P < 5e-8 and P < 5e-8/348 = 1.44e-10 respectively. Independent lead variants are annotated with their SNP IDs and the closest genes. LocusZoom plots (purple diamond symbols indicate lead SNPs) are attached to show regional associations. For the abbreviations of brain regions, see Table S14.

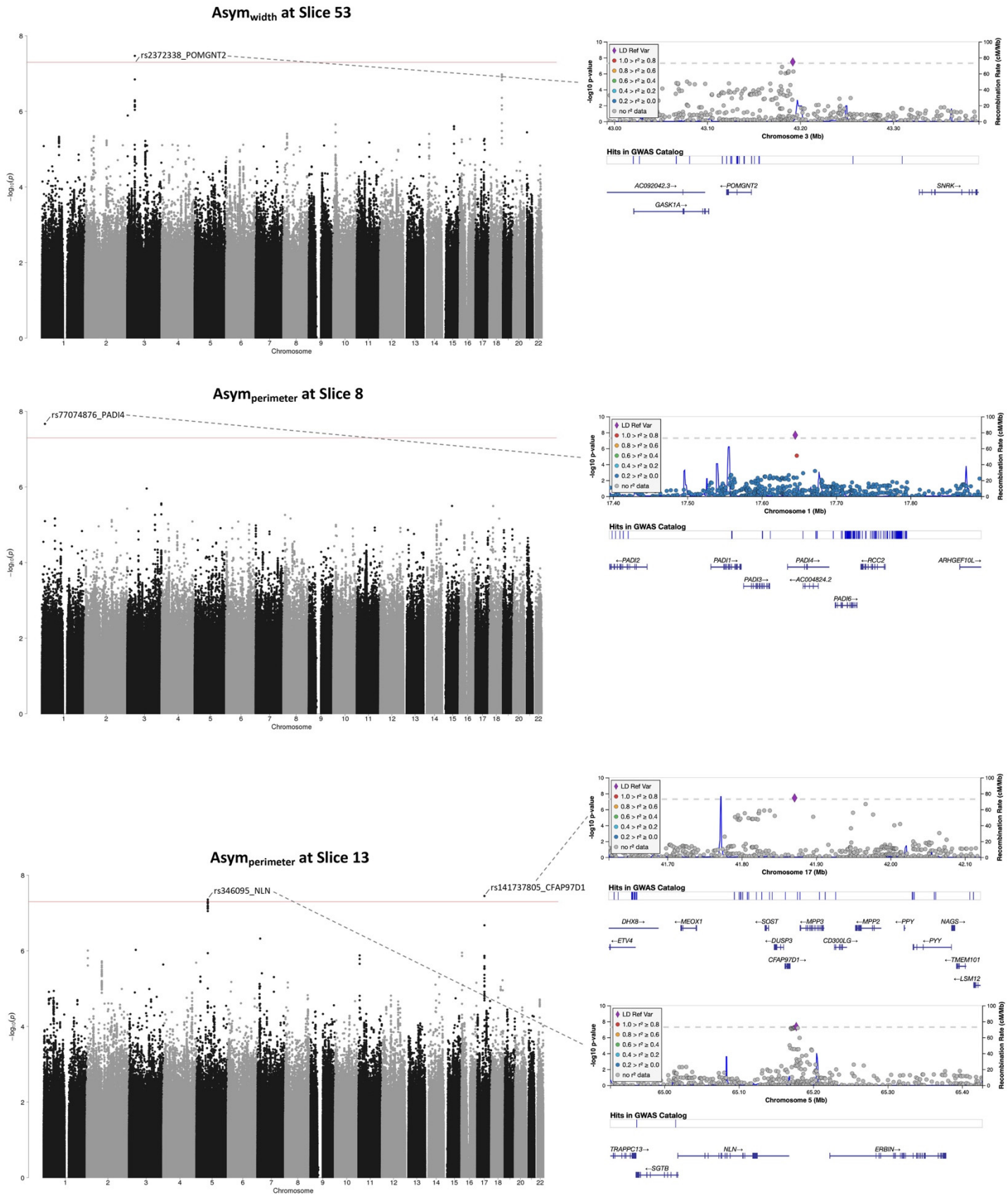

Figure S19 - Part 3. Manhattan plots of meta-GWAS summary statistics for the brain torque profiles showing significant genetic associations. Red and blue lines represent the significance levels of P < 5e-8 and P < 5e-8/348 = 1.44e-10 respectively. Independent lead variants are annotated with their SNP IDs and the closest genes. LocusZoom plots (purple diamond symbols indicate lead SNPs) are attached to show regional associations. For the abbreviations of brain regions, see Table S14.

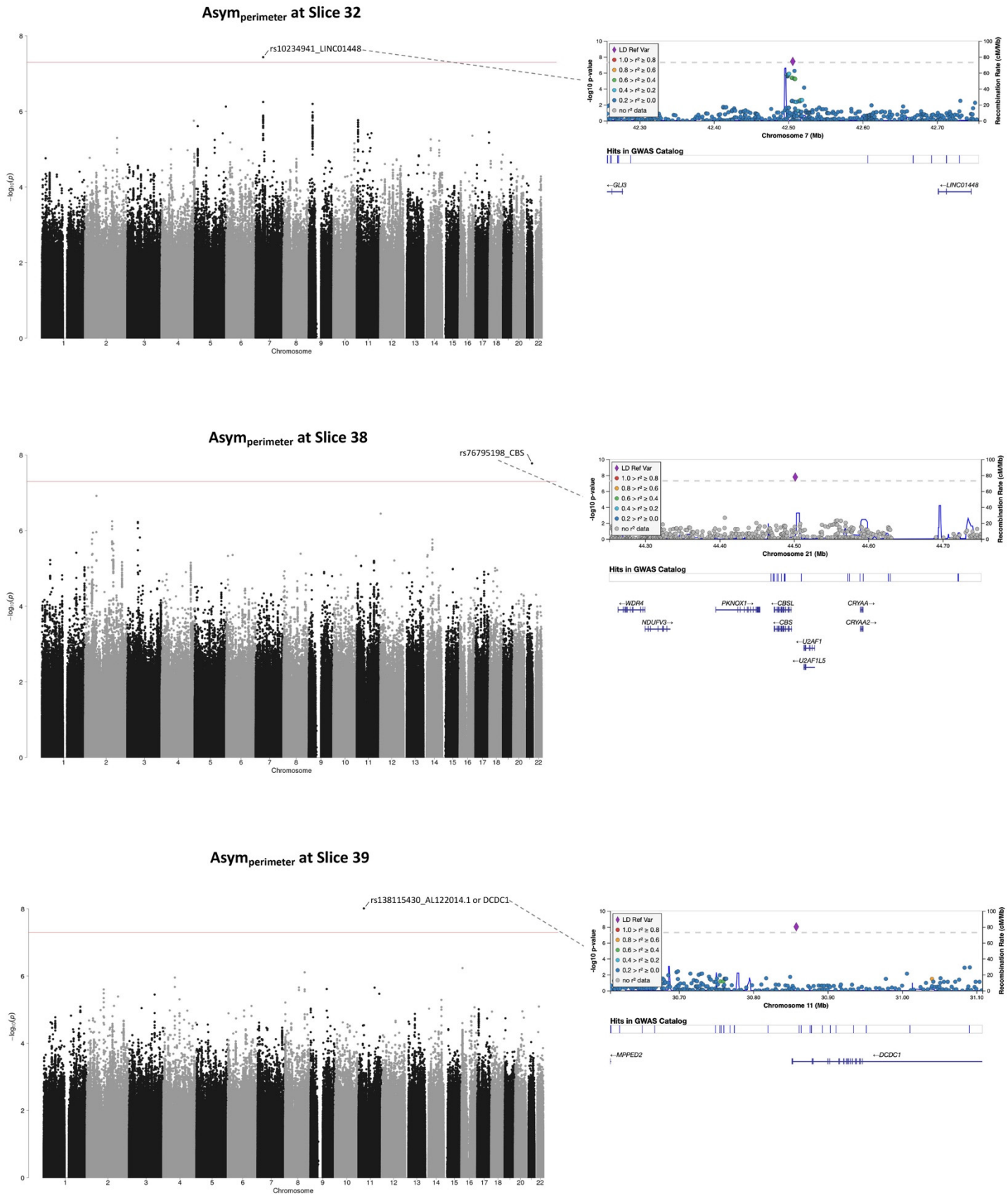

Figure S19 - Part 4. Manhattan plots of meta-GWAS summary statistics for the brain torque profiles showing significant genetic associations. Red and blue lines represent the significance levels of P < 5e-8 and P < 5e-8/348 = 1.44e-10 respectively. Independent lead variants are annotated with their SNP IDs and the closest genes. LocusZoom plots (purple diamond symbols indicate lead SNPs) are attached to show regional associations. For the abbreviations of brain regions, see Table S14.

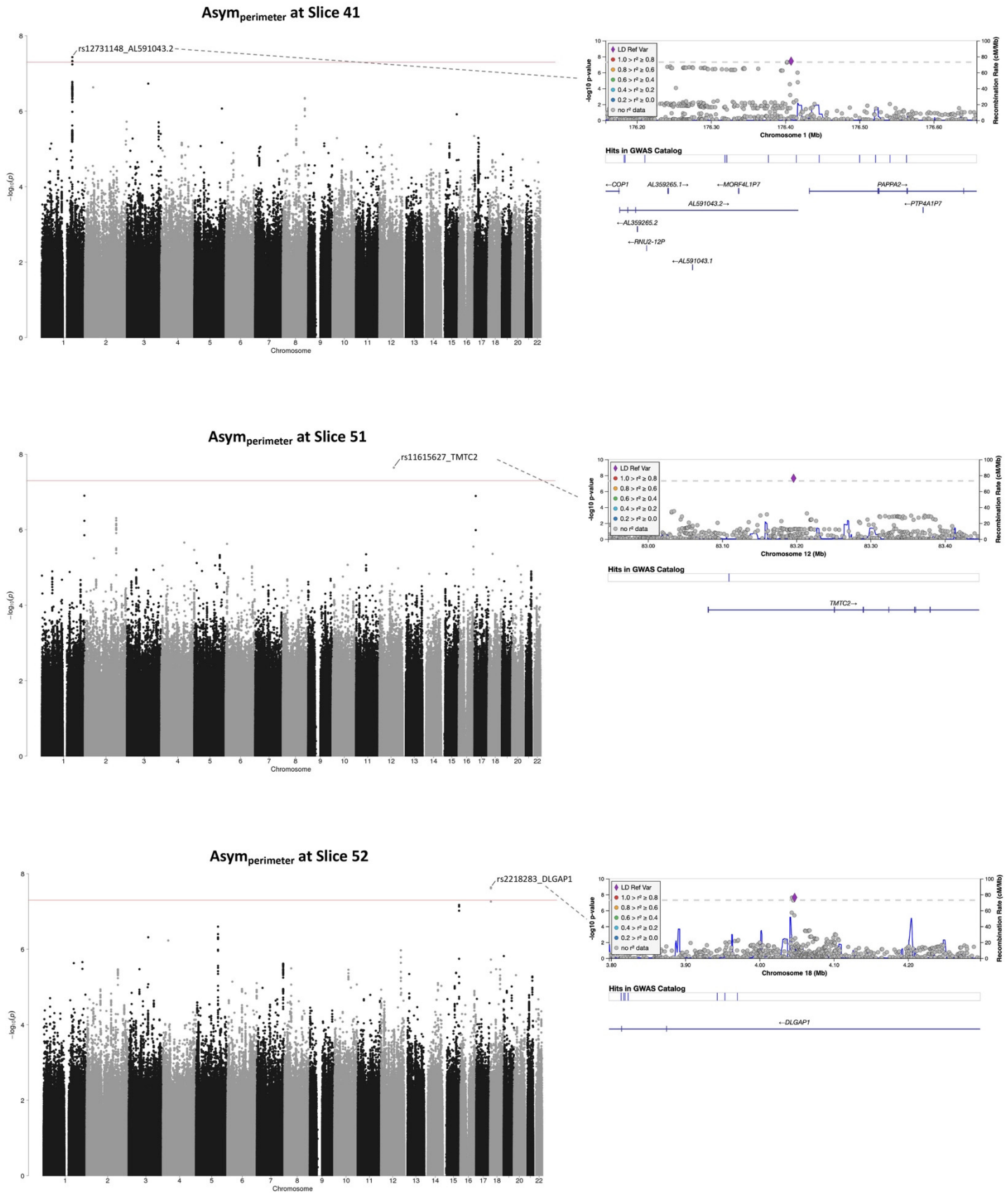

Figure S19 - Part 5. Manhattan plots of meta-GWAS summary statistics for the brain torque profiles showing significant genetic associations. Red and blue lines represent the significance levels of P < 5e-8 and P < 5e-8/348 = 1.44e-10 respectively. Independent lead variants are annotated with their SNP IDs and the closest genes. LocusZoom plots (purple diamond symbols indicate lead SNPs) are attached to show regional associations. For the abbreviations of brain regions, see Table S14.

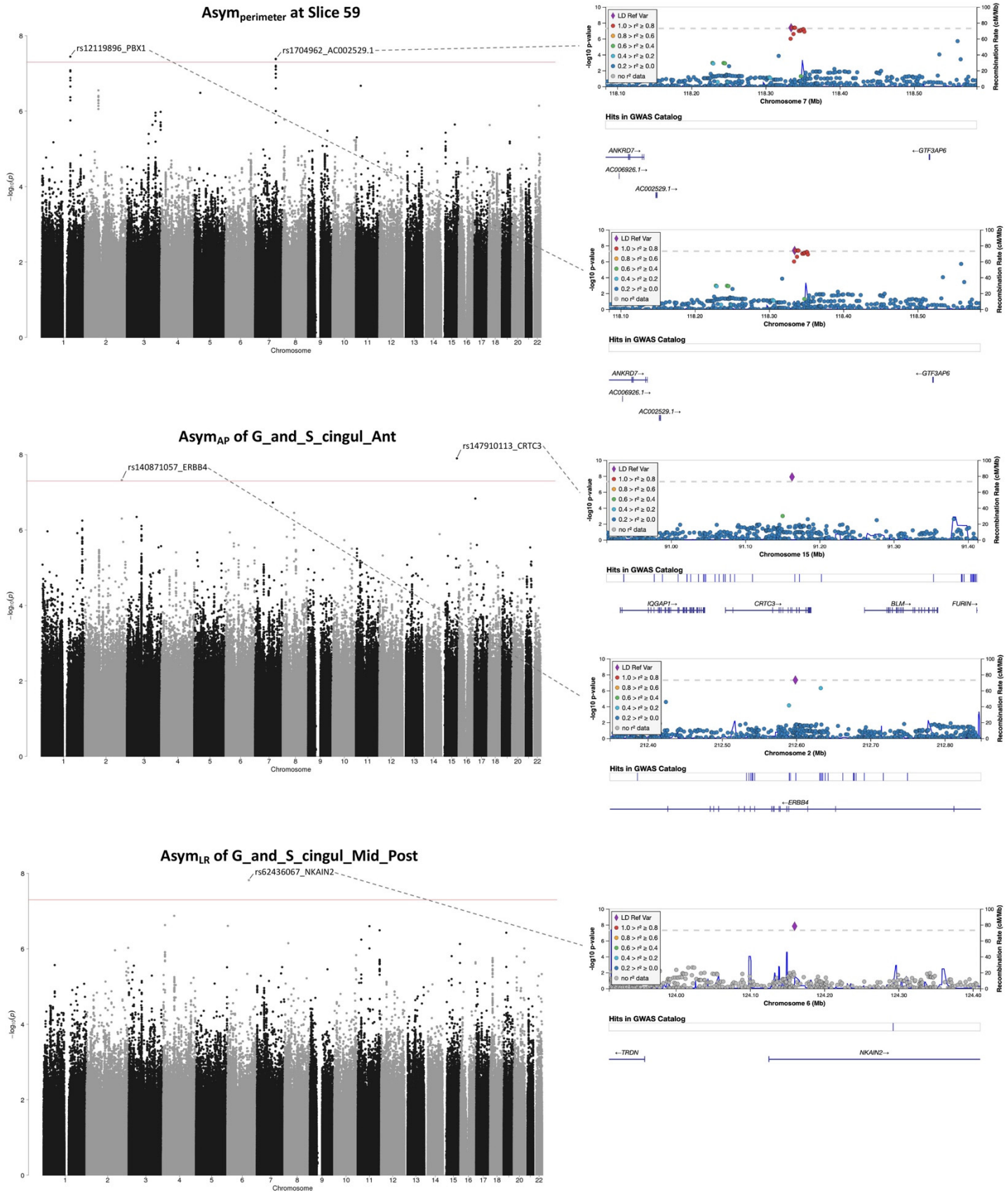

Figure S19 - Part 6. Manhattan plots of meta-GWAS summary statistics for the brain torque profiles showing significant genetic associations. Red and blue lines represent the significance levels of P < 5e-8 and P < 5e-8/348 = 1.44e-10 respectively. Independent lead variants are annotated with their SNP IDs and the closest genes. LocusZoom plots (purple diamond symbols indicate lead SNPs) are attached to show regional associations. For the abbreviations of brain regions, see Table S14.

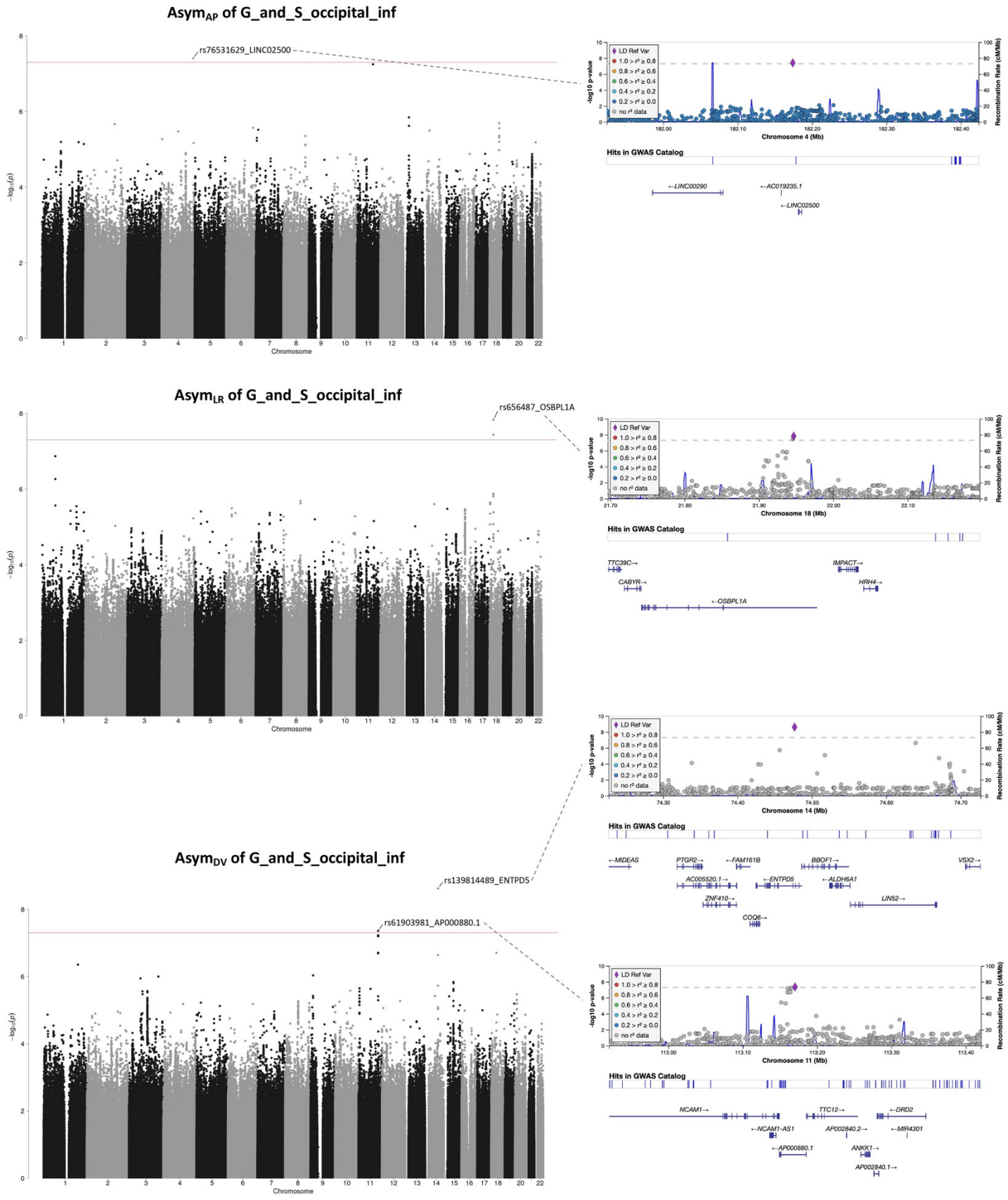

Figure S19 - Part 7. Manhattan plots of meta-GWAS summary statistics for the brain torque profiles showing significant genetic associations. Red and blue lines represent the significance levels of P < 5e-8 and P < 5e-8/348 = 1.44e-10 respectively. Independent lead variants are annotated with their SNP IDs and the closest genes. LocusZoom plots (purple diamond symbols indicate lead SNPs) are attached to show regional associations. For the abbreviations of brain regions, see Table S14.

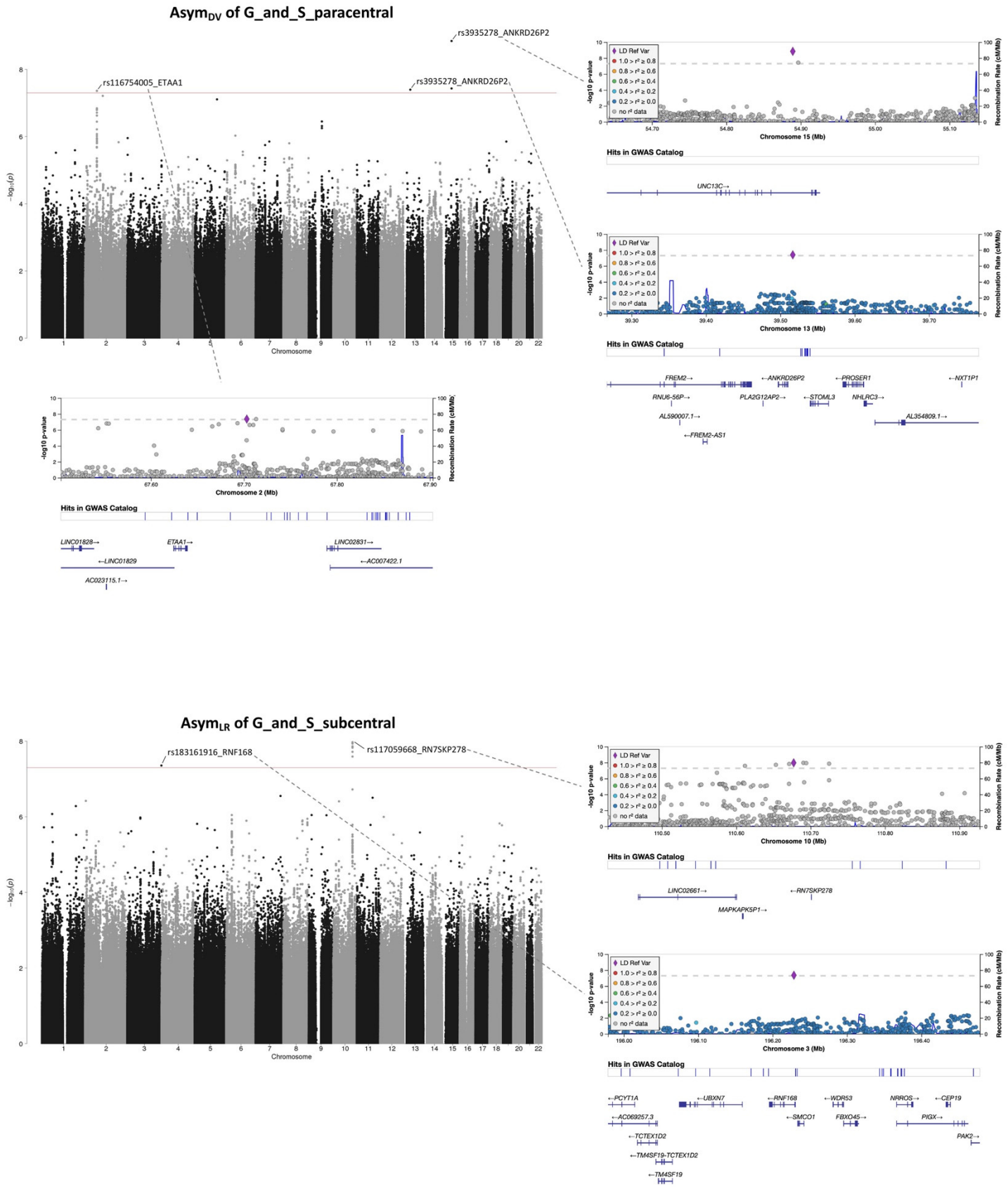

Figure S19 - Part 8. Manhattan plots of meta-GWAS summary statistics for the brain torque profiles showing significant genetic associations. Red and blue lines represent the significance levels of P < 5e-8 and P < 5e-8/348 = 1.44e-10 respectively. Independent lead variants are annotated with their SNP IDs and the closest genes. LocusZoom plots (purple diamond symbols indicate lead SNPs) are attached to show regional associations. For the abbreviations of brain regions, see Table S14.

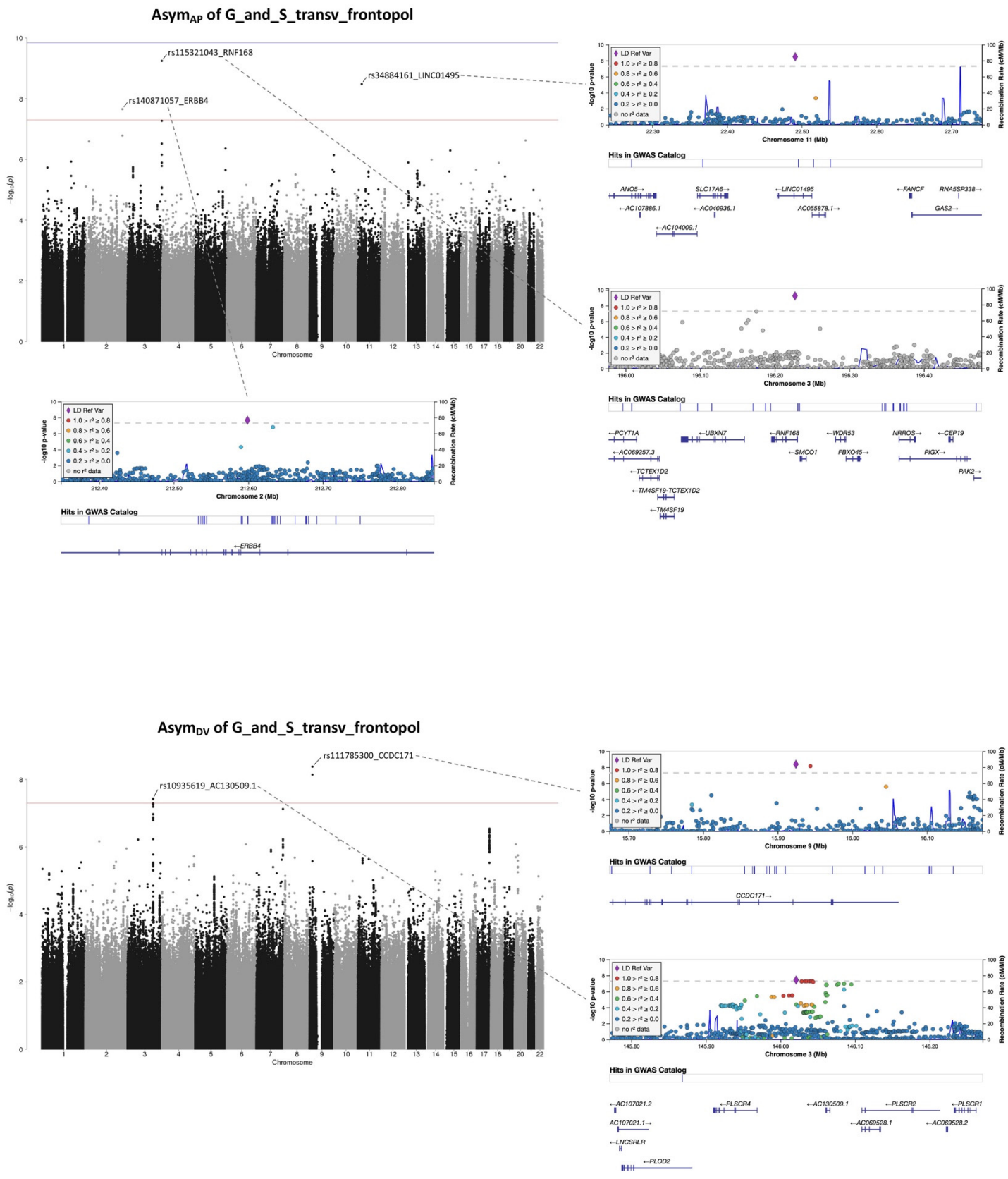

Figure S19 - Part 9. Manhattan plots of meta-GWAS summary statistics for the brain torque profiles showing significant genetic associations. Red and blue lines represent the significance levels of P < 5e-8 and P < 5e-8/348 = 1.44e-10 respectively. Independent lead variants are annotated with their SNP IDs and the closest genes. LocusZoom plots (purple diamond symbols indicate lead SNPs) are attached to show regional associations. For the abbreviations of brain regions, see Table S14.

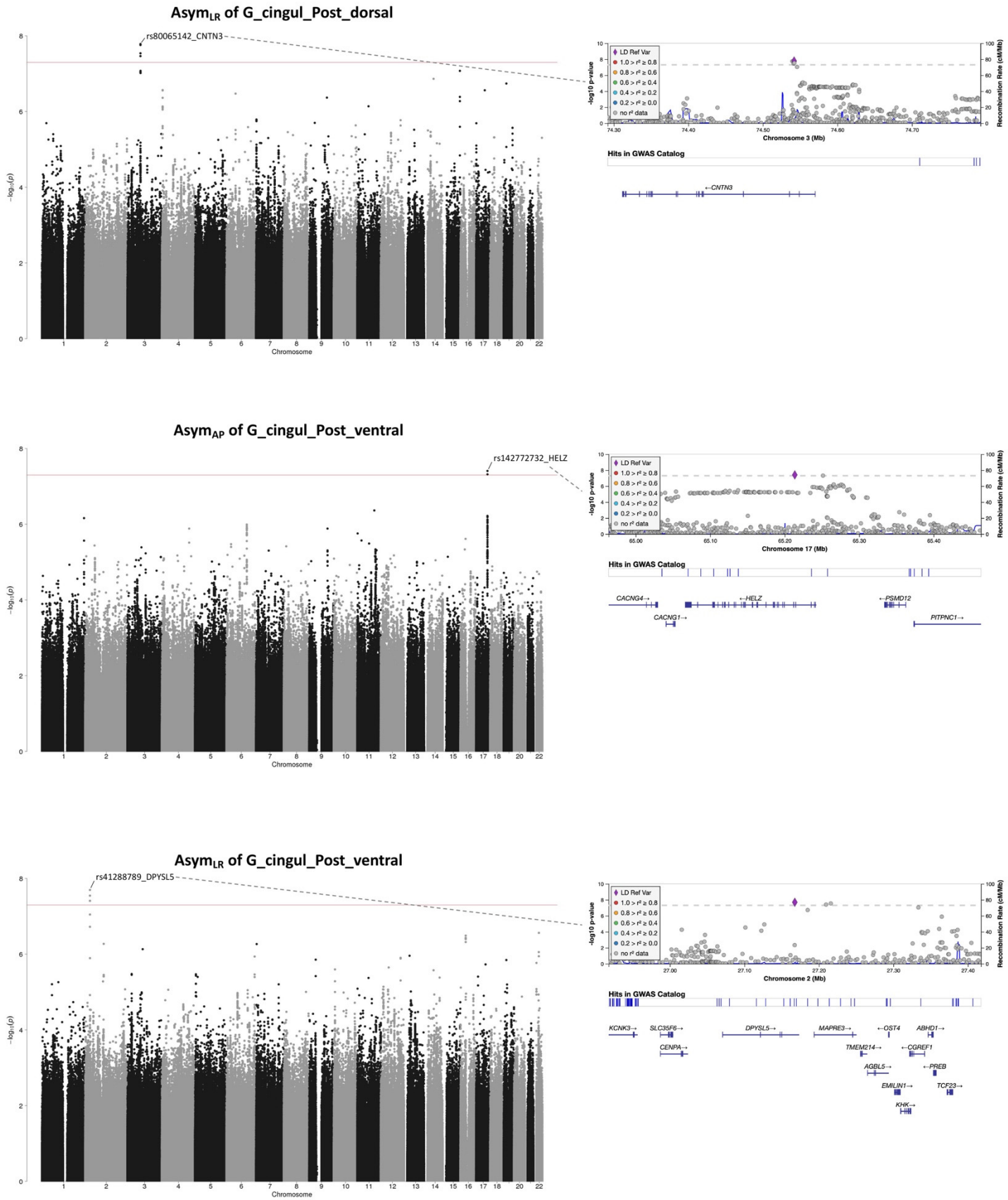

Figure S19 - Part 10. Manhattan plots of meta-GWAS summary statistics for the brain torque profiles showing significant genetic associations. Red and blue lines represent the significance levels of P < 5e-8 and P < 5e-8/348 = 1.44e-10 respectively. Independent lead variants are annotated with their SNP IDs and the closest genes. LocusZoom plots (purple diamond symbols indicate lead SNPs) are attached to show regional associations. For the abbreviations of brain regions, see Table S14.

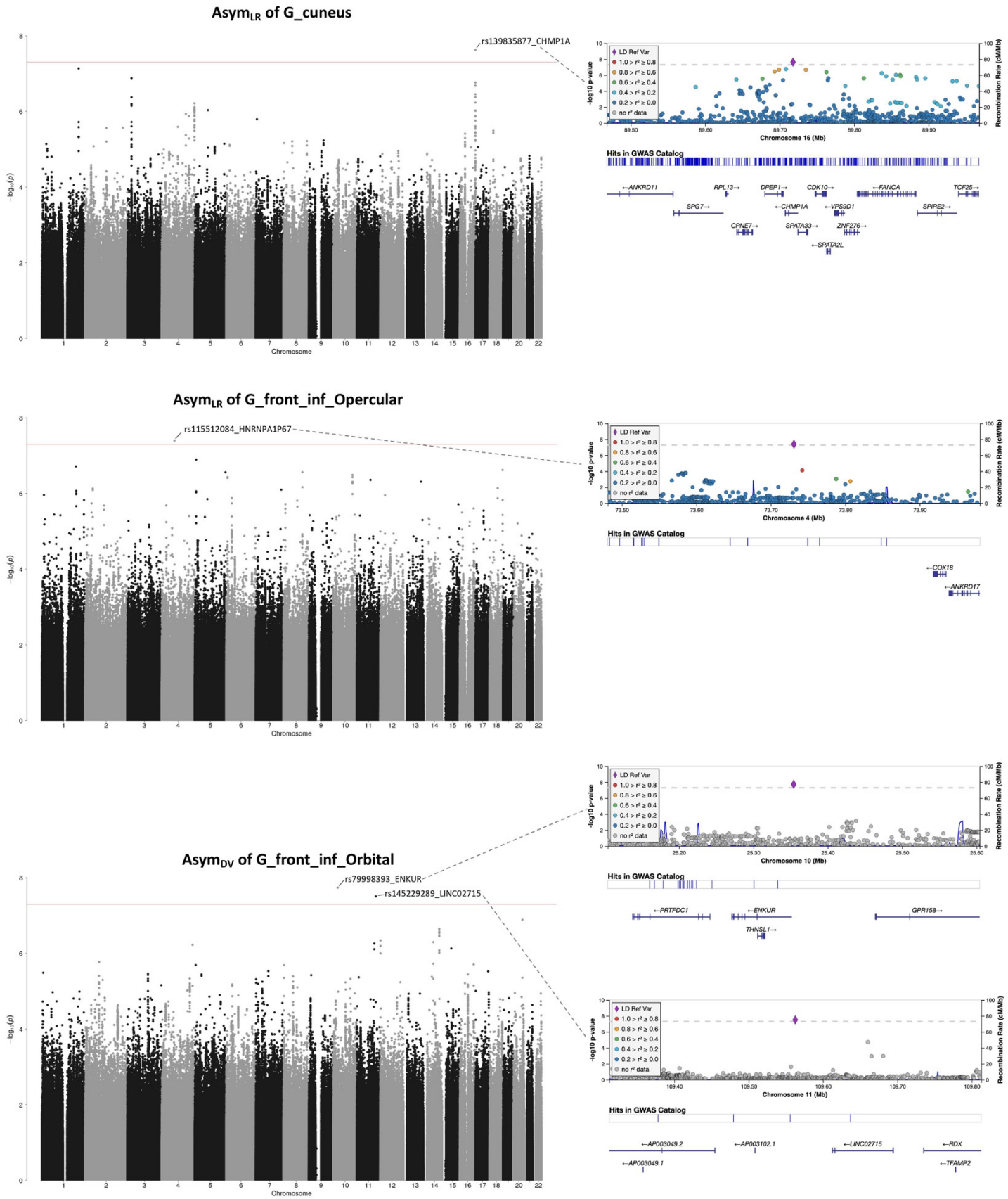

Figure S19 - Part 11. Manhattan plots of meta-GWAS summary statistics for the brain torque profiles showing significant genetic associations. Red and blue lines represent the significance levels of P < 5e-8 and P < 5e-8/348 = 1.44e-10 respectively. Independent lead variants are annotated with their SNP IDs and the closest genes. LocusZoom plots (purple diamond symbols indicate lead SNPs) are attached to show regional associations. For the abbreviations of brain regions, see Table S14.

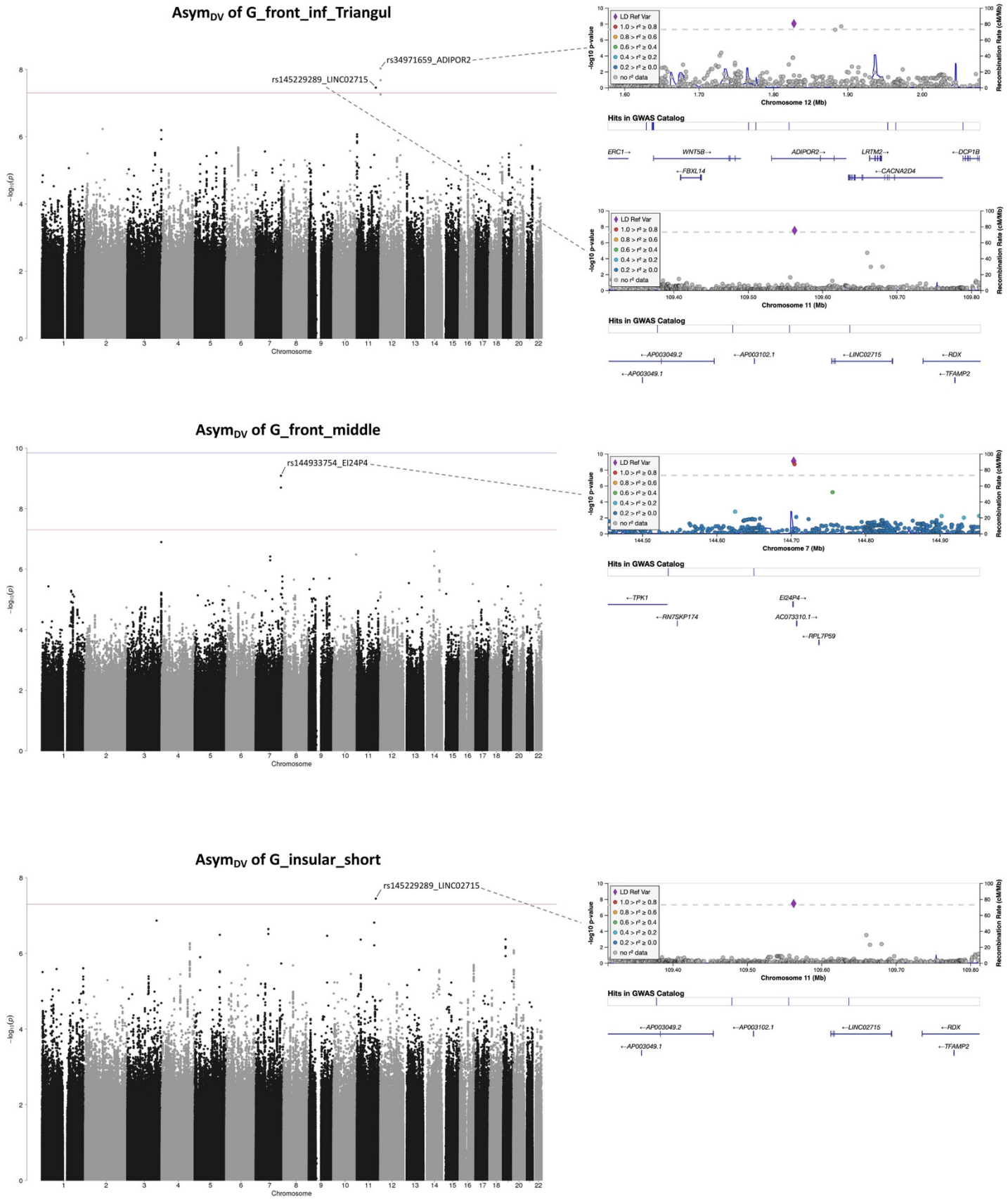

Figure S19 - Part 12. Manhattan plots of meta-GWAS summary statistics for the brain torque profiles showing significant genetic associations. Red and blue lines represent the significance levels of P < 5e-8 and P < 5e-8/348 = 1.44e-10 respectively. Independent lead variants are annotated with their SNP IDs and the closest genes. LocusZoom plots (purple diamond symbols indicate lead SNPs) are attached to show regional associations. For the abbreviations of brain regions, see Table S14.

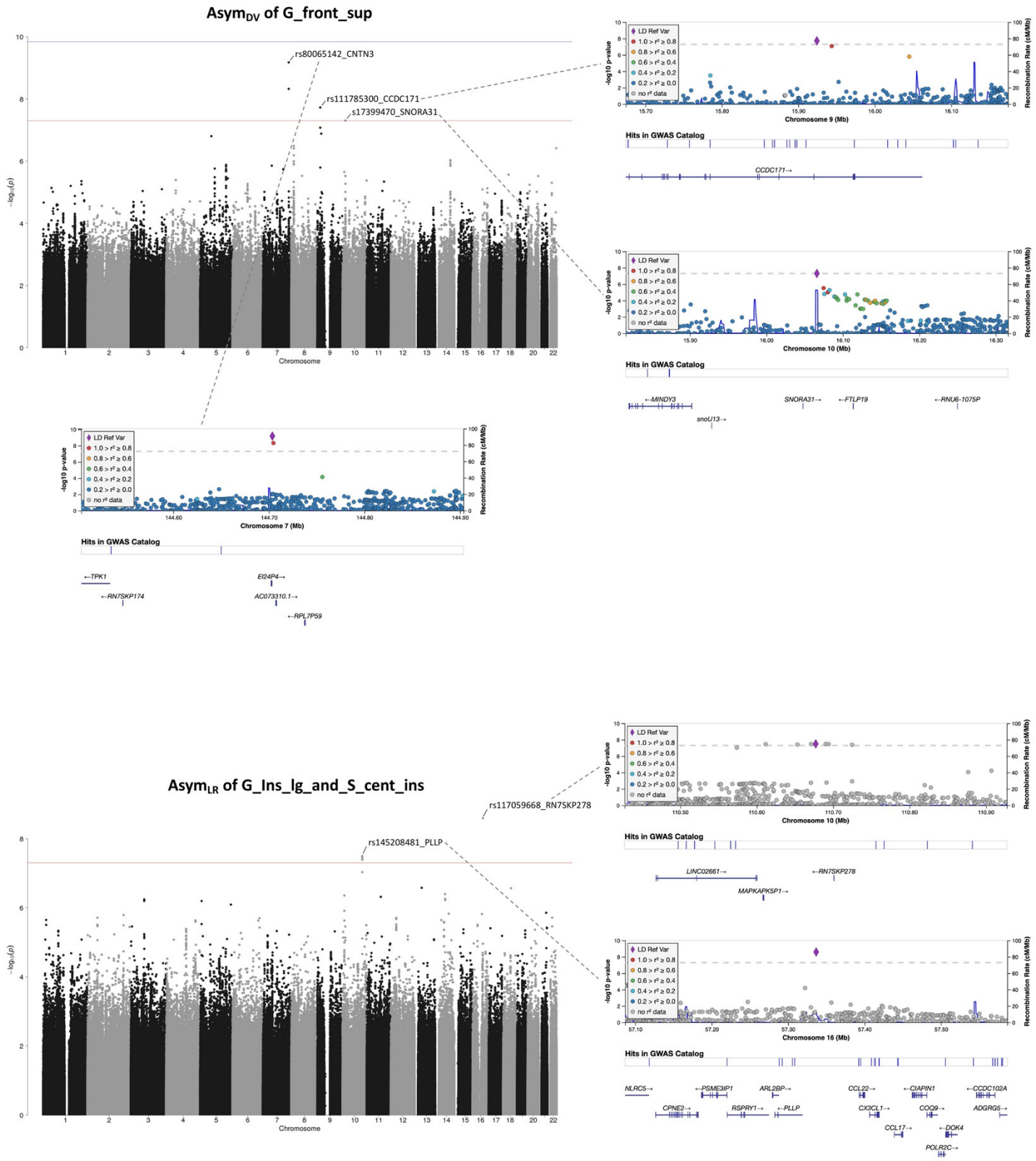

Figure S19 - Part 13. Manhattan plots of meta-GWAS summary statistics for the brain torque profiles showing significant genetic associations. Red and blue lines represent the significance levels of P < 5e-8 and P < 5e-8/348 = 1.44e-10 respectively. Independent lead variants are annotated with their SNP IDs and the closest genes. LocusZoom plots (purple diamond symbols indicate lead SNPs) are attached to show regional associations. For the abbreviations of brain regions, see Table S14.

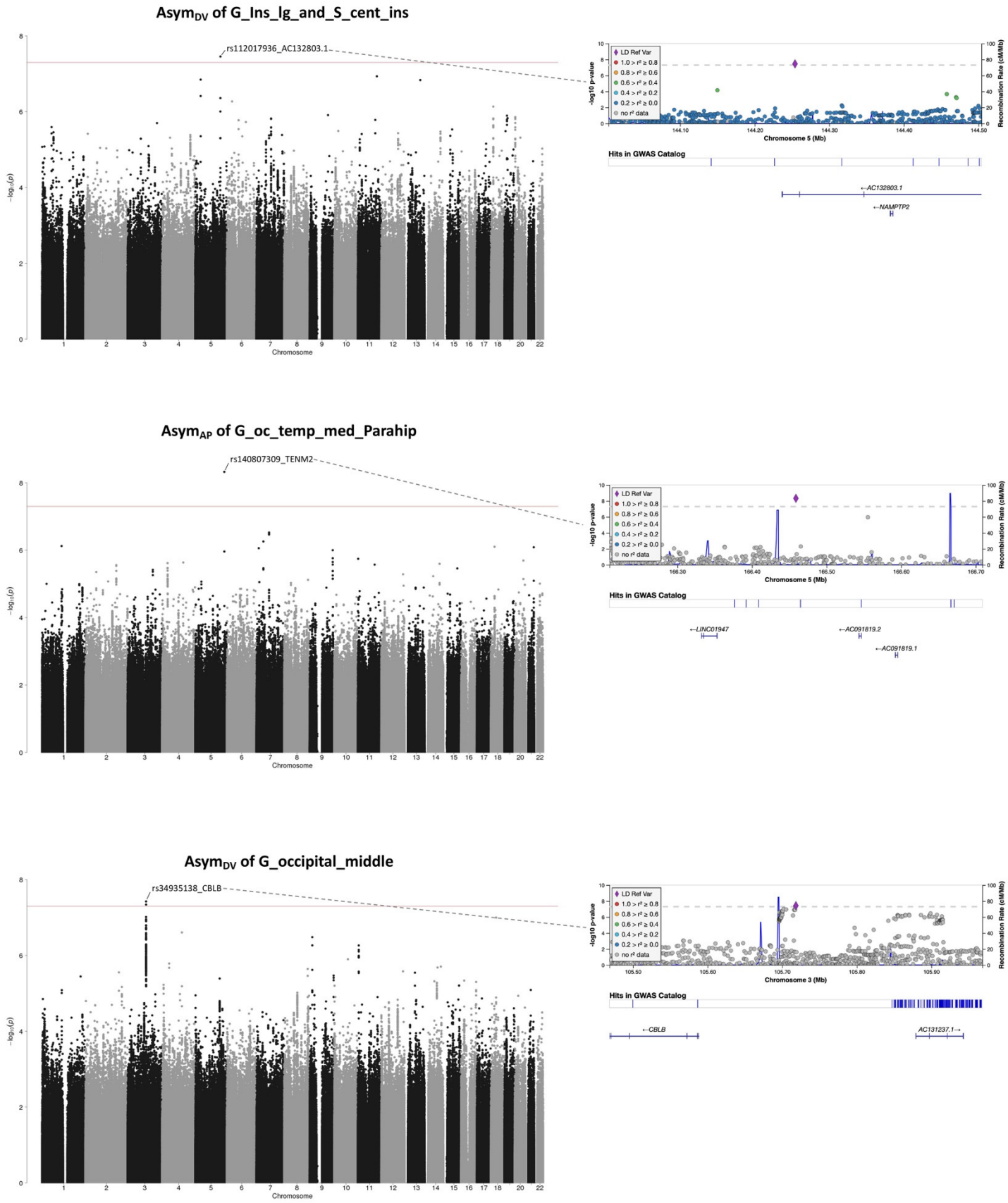

Figure S19 - Part 14. Manhattan plots of meta-GWAS summary statistics for the brain torque profiles showing significant genetic associations. Red and blue lines represent the significance levels of P < 5e-8 and P < 5e-8/348 = 1.44e-10 respectively. Independent lead variants are annotated with their SNP IDs and the closest genes. LocusZoom plots (purple diamond symbols indicate lead SNPs) are attached to show regional associations. For the abbreviations of brain regions, see Table S14.

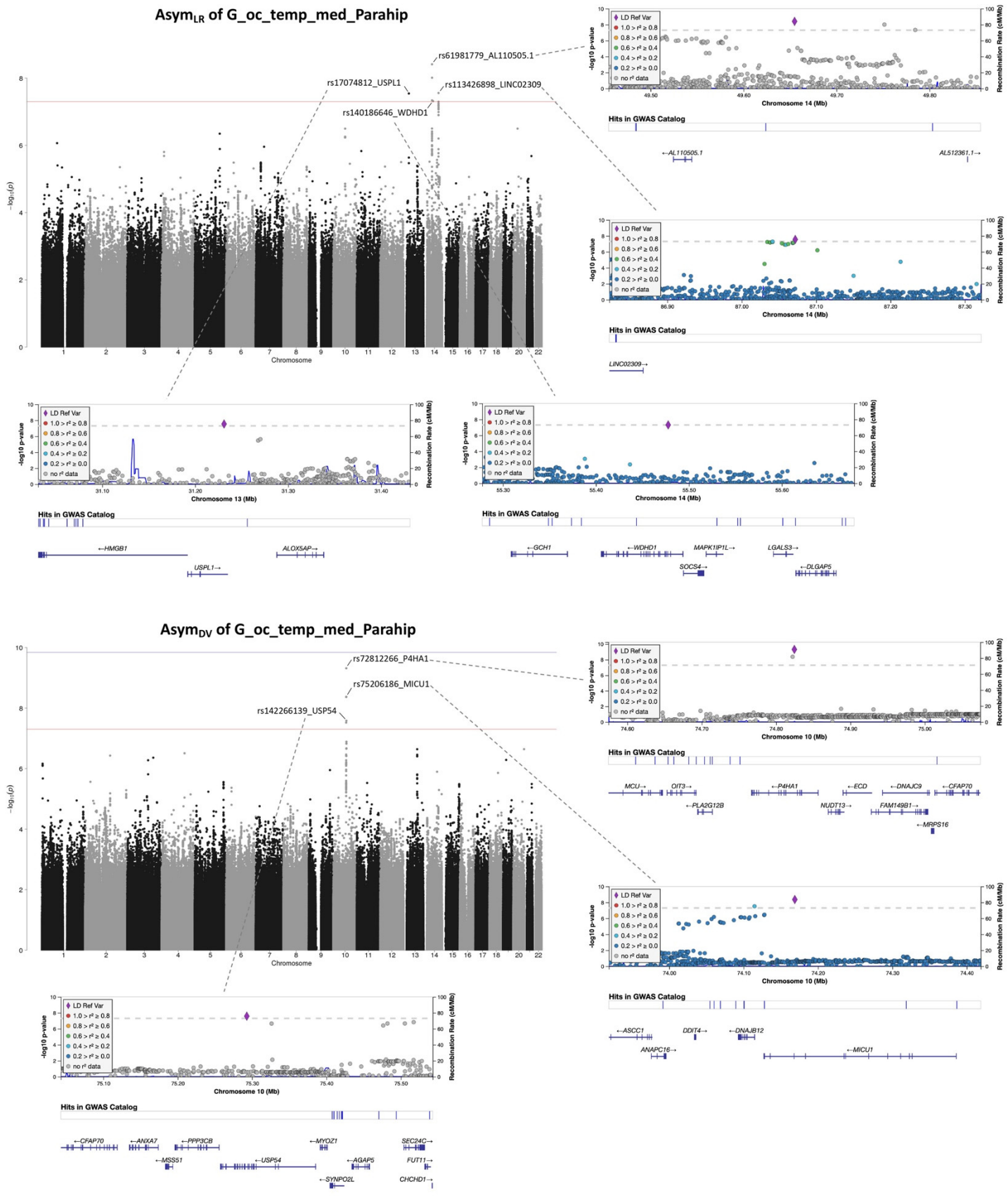

Figure S19 - Part 15. Manhattan plots of meta-GWAS summary statistics for the brain torque profiles showing significant genetic associations. Red and blue lines represent the significance levels of P < 5e-8 and P < 5e-8/348 = 1.44e-10 respectively. Independent lead variants are annotated with their SNP IDs and the closest genes. LocusZoom plots (purple diamond symbols indicate lead SNPs) are attached to show regional associations. For the abbreviations of brain regions, see Table S14.

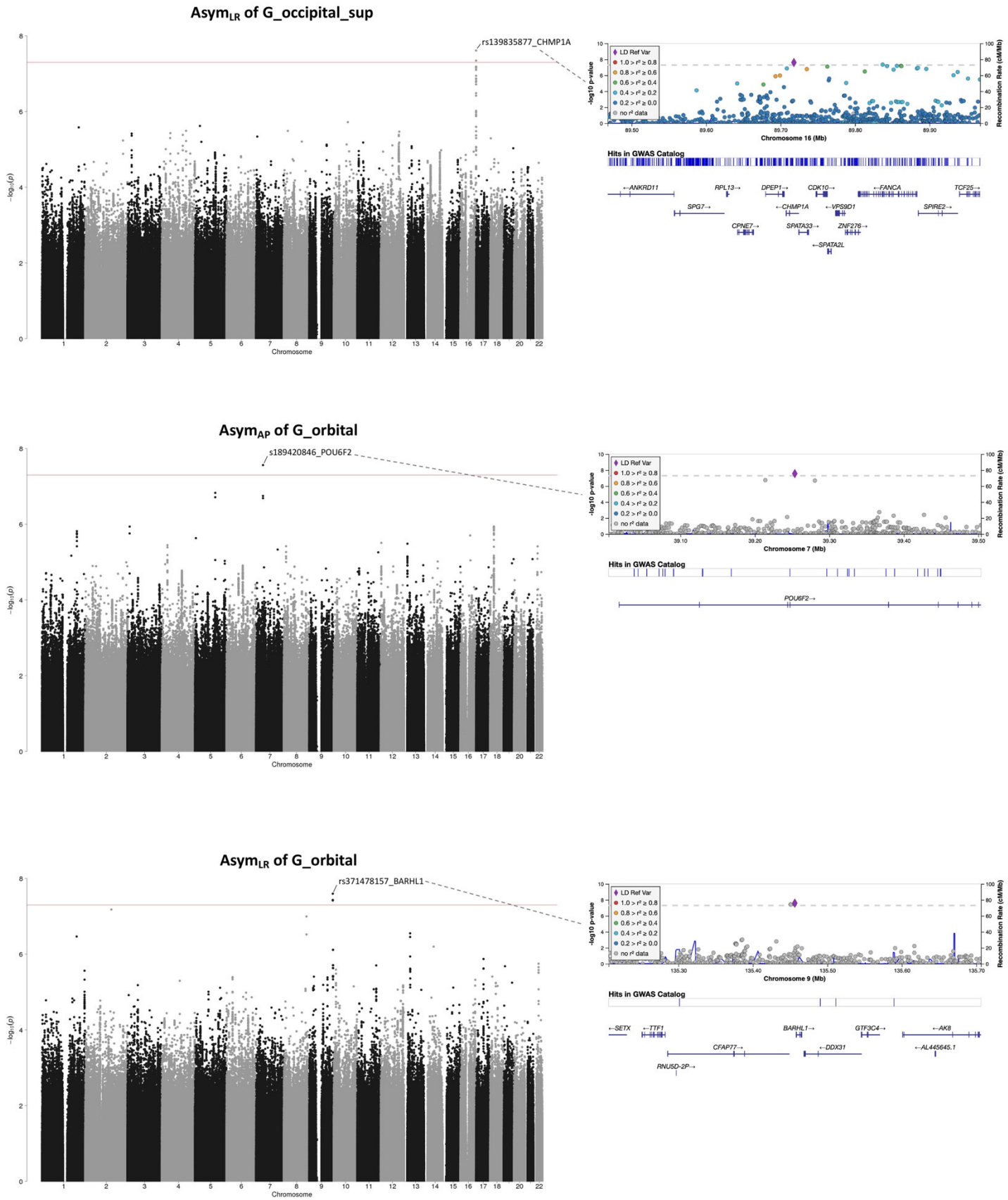

Figure S19 - Part 16. Manhattan plots of meta-GWAS summary statistics for the brain torque profiles showing significant genetic associations. Red and blue lines represent the significance levels of P < 5e-8 and P < 5e-8/348 = 1.44e-10 respectively. Independent lead variants are annotated with their SNP IDs and the closest genes. LocusZoom plots (purple diamond symbols indicate lead SNPs) are attached to show regional associations. For the abbreviations of brain regions, see Table S14.

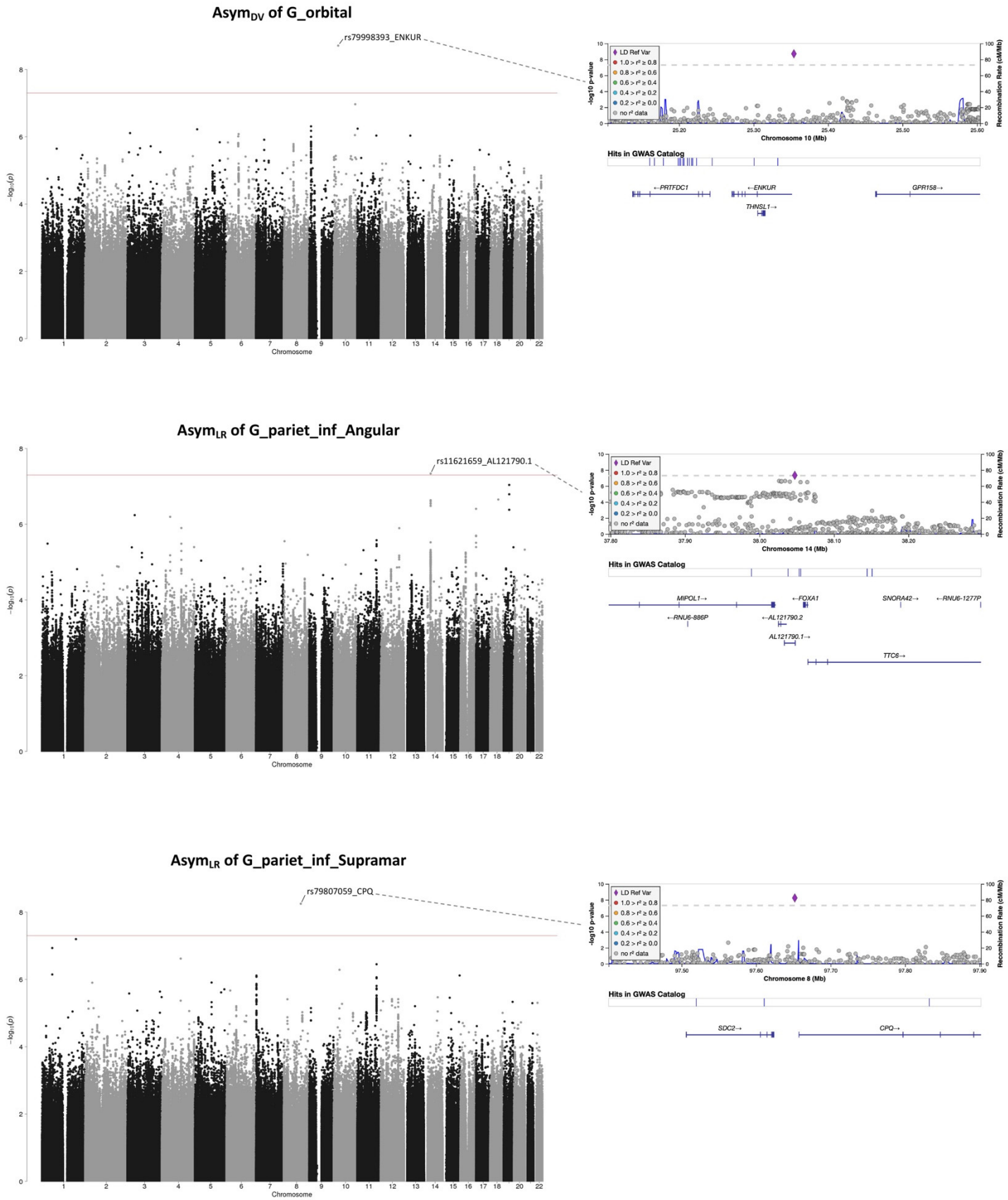

Figure S19 - Part 17. Manhattan plots of meta-GWAS summary statistics for the brain torque profiles showing significant genetic associations. Red and blue lines represent the significance levels of P < 5e-8 and P < 5e-8/348 = 1.44e-10 respectively. Independent lead variants are annotated with their SNP IDs and the closest genes. LocusZoom plots (purple diamond symbols indicate lead SNPs) are attached to show regional associations. For the abbreviations of brain regions, see Table S14.

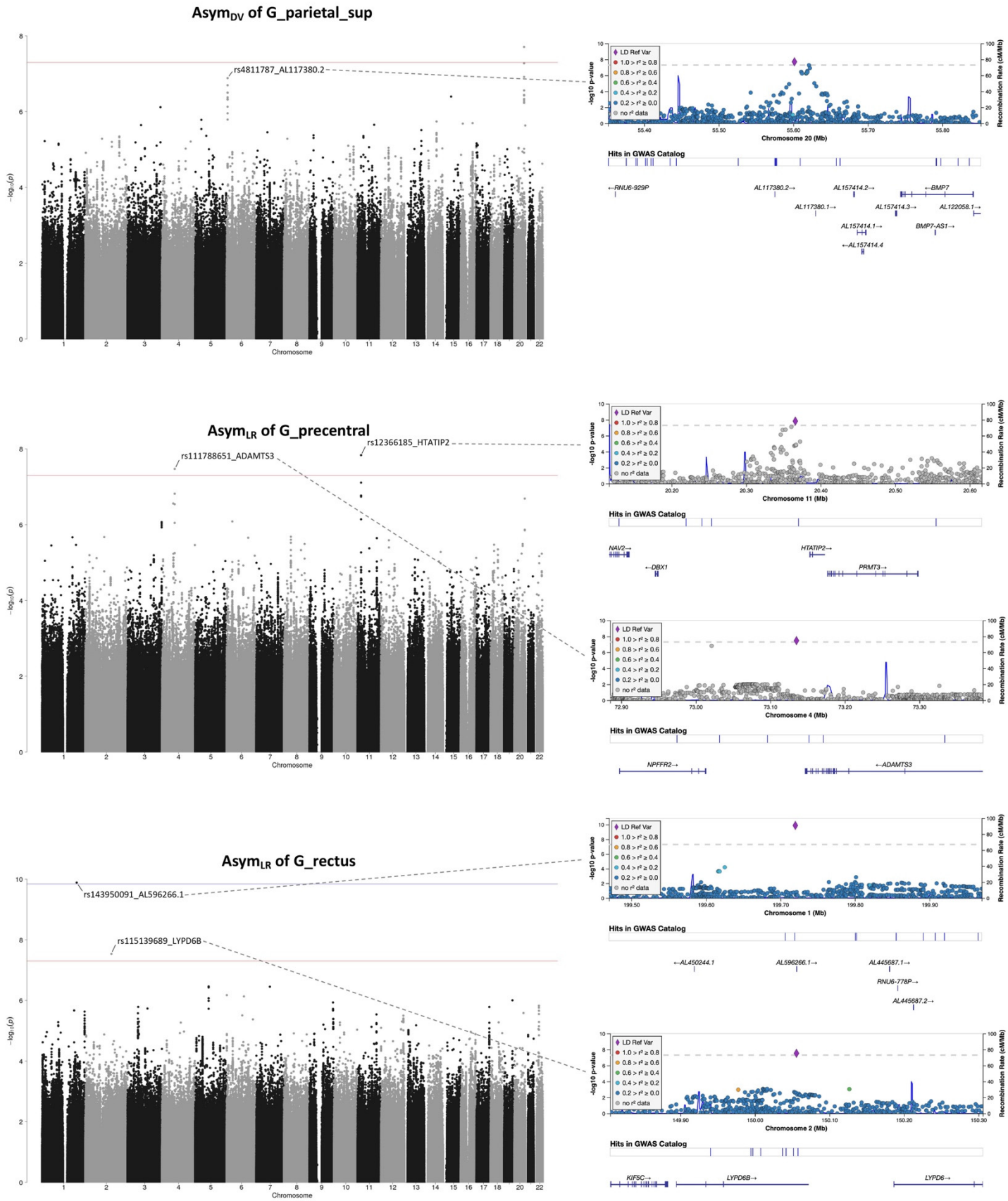

Figure S19 - Part 18. Manhattan plots of meta-GWAS summary statistics for the brain torque profiles showing significant genetic associations. Red and blue lines represent the significance levels of P < 5e-8 and P < 5e-8/348 = 1.44e-10 respectively. Independent lead variants are annotated with their SNP IDs and the closest genes. LocusZoom plots (purple diamond symbols indicate lead SNPs) are attached to show regional associations. For the abbreviations of brain regions, see Table S14.

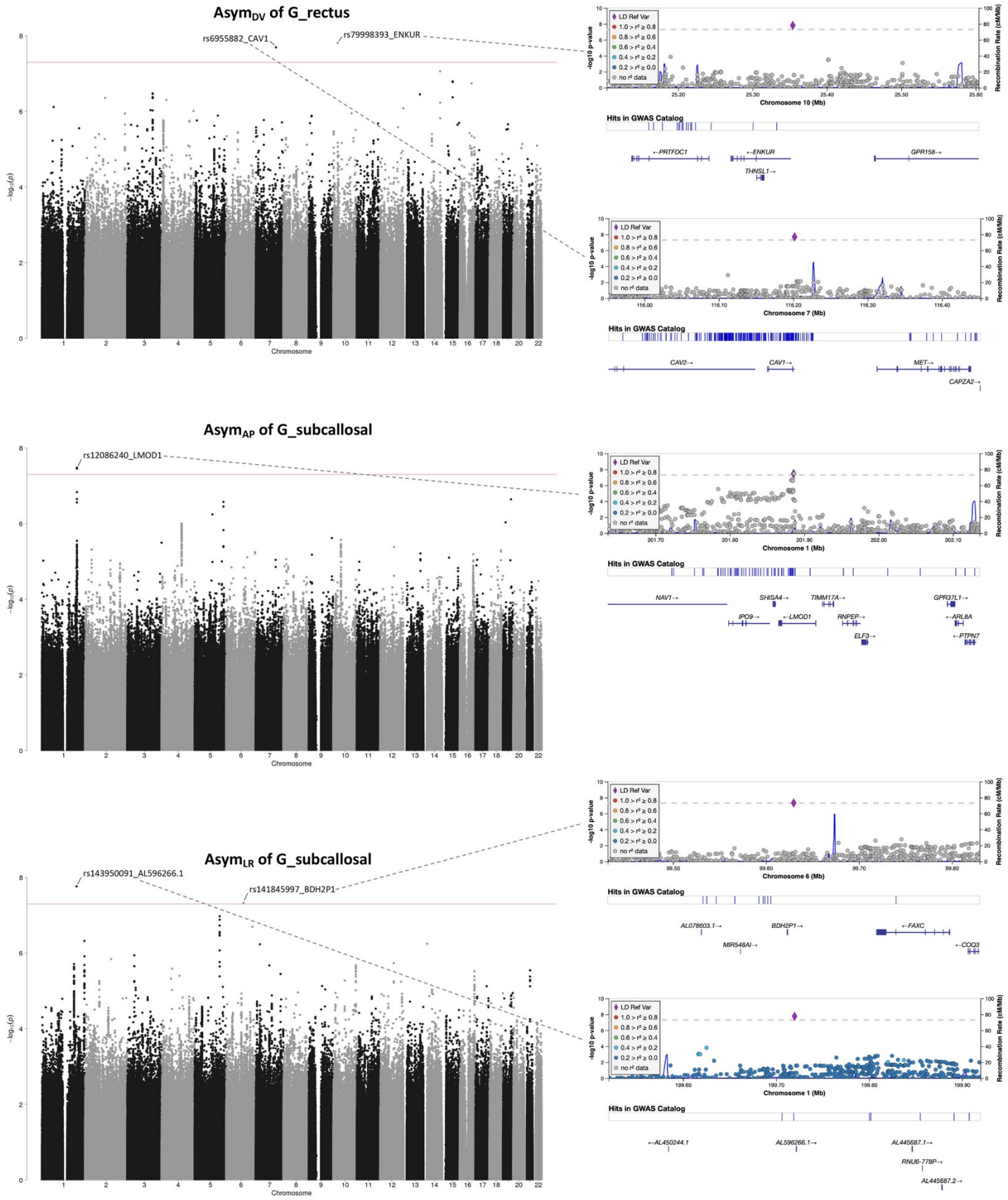

Figure S19 - Part 19. Manhattan plots of meta-GWAS summary statistics for the brain torque profiles showing significant genetic associations. Red and blue lines represent the significance levels of P < 5e-8 and P < 5e-8/348 = 1.44e-10 respectively. Independent lead variants are annotated with their SNP IDs and the closest genes. LocusZoom plots (purple diamond symbols indicate lead SNPs) are attached to show regional associations. For the abbreviations of brain regions, see Table S14.

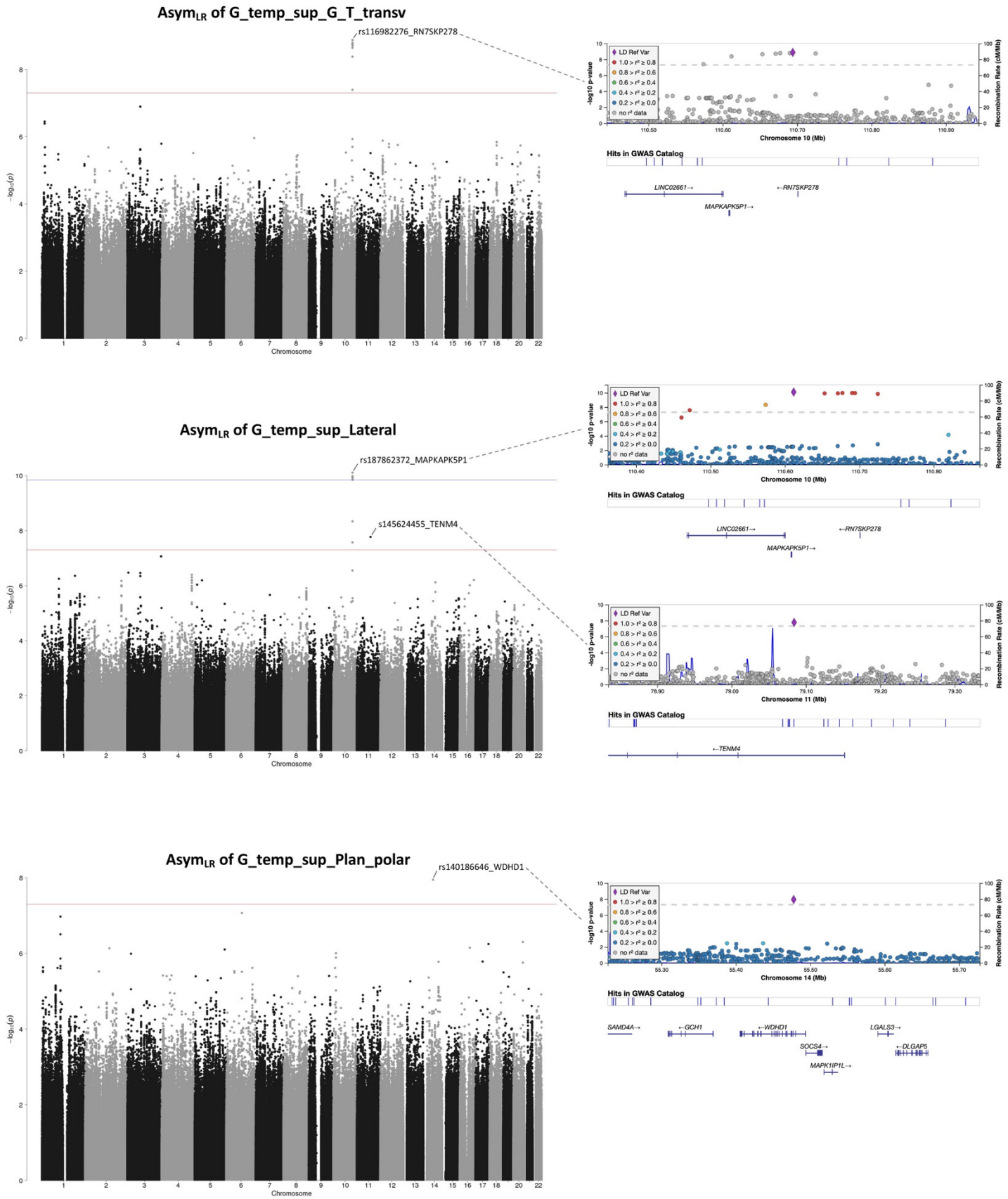

Figure S19 - Part 20. Manhattan plots of meta-GWAS summary statistics for the brain torque profiles showing significant genetic associations. Red and blue lines represent the significance levels of P < 5e-8 and P < 5e-8/348 = 1.44e-10 respectively. Independent lead variants are annotated with their SNP IDs and the closest genes. LocusZoom plots (purple diamond symbols indicate lead SNPs) are attached to show regional associations. For the abbreviations of brain regions, see Table S14.

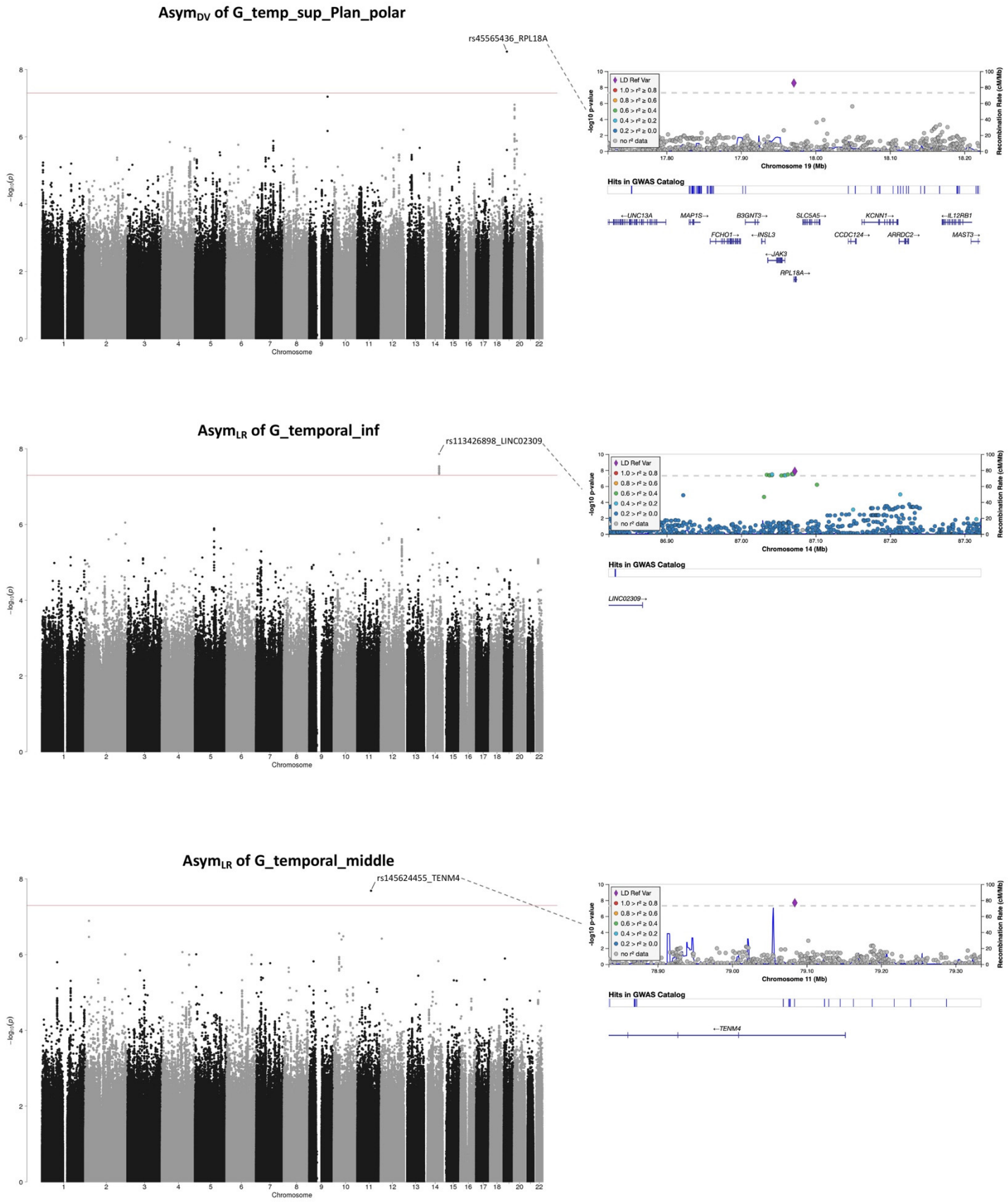

Figure S19 - Part 21. Manhattan plots of meta-GWAS summary statistics for the brain torque profiles showing significant genetic associations. Red and blue lines represent the significance levels of P < 5e-8 and P < 5e-8/348 = 1.44e-10 respectively. Independent lead variants are annotated with their SNP IDs and the closest genes. LocusZoom plots (purple diamond symbols indicate lead SNPs) are attached to show regional associations. For the abbreviations of brain regions, see Table S14.

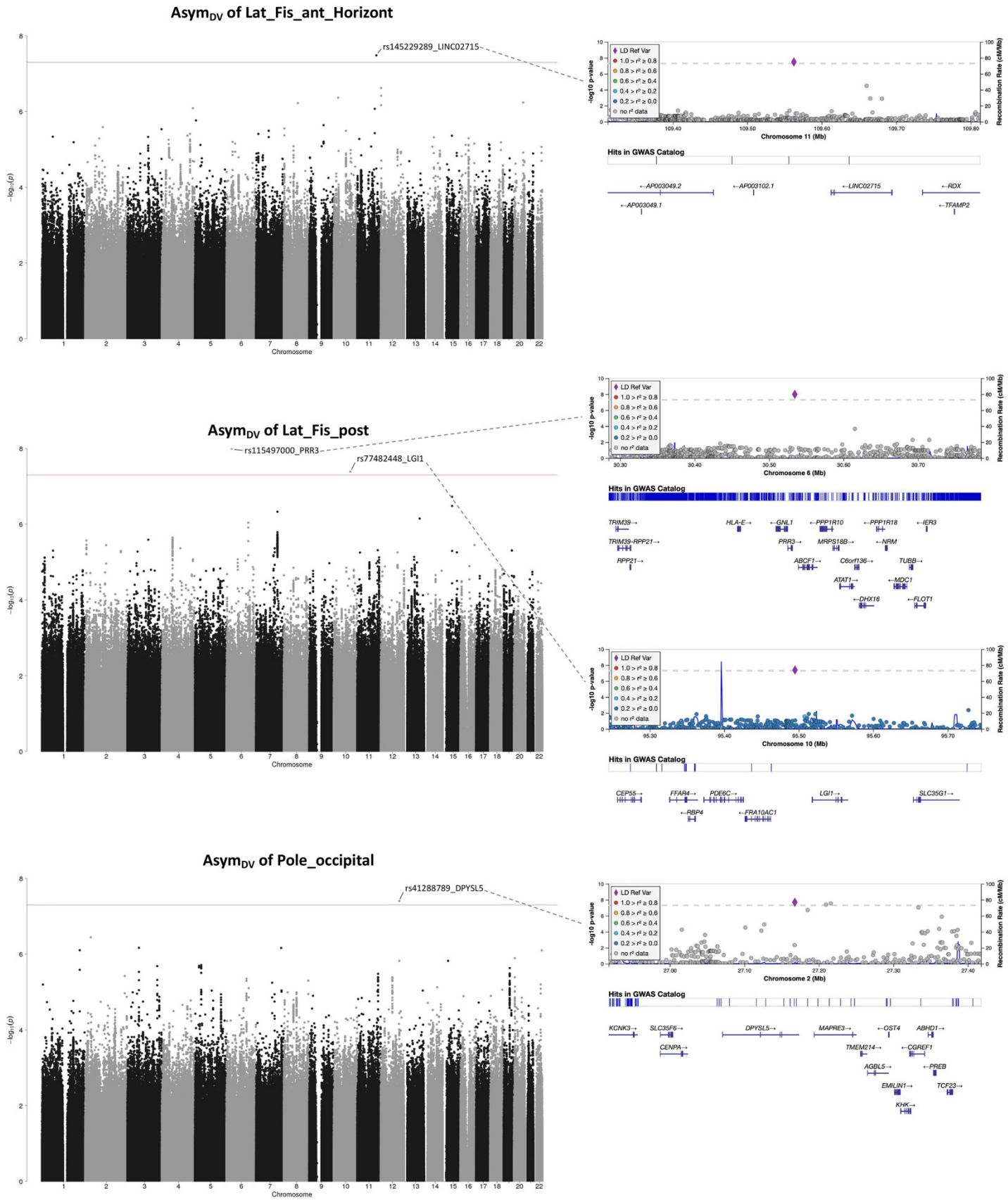

Figure S19 - Part 22. Manhattan plots of meta-GWAS summary statistics for the brain torque profiles showing significant genetic associations. Red and blue lines represent the significance levels of P < 5e-8 and P < 5e-8/348 = 1.44e-10 respectively. Independent lead variants are annotated with their SNP IDs and the closest genes. LocusZoom plots (purple diamond symbols indicate lead SNPs) are attached to show regional associations. For the abbreviations of brain regions, see Table S14.

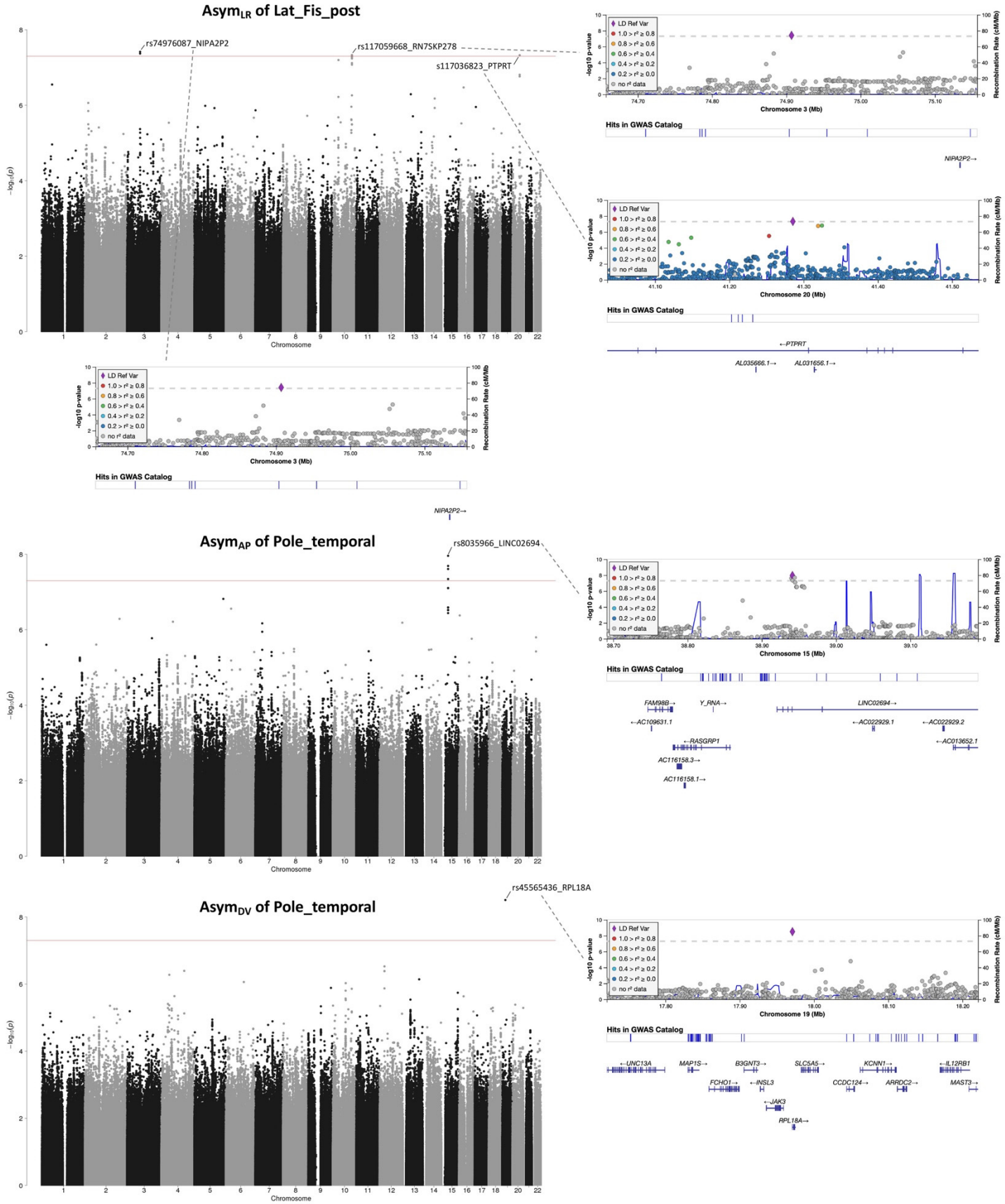

Figure S19 - Part 23. Manhattan plots of meta-GWAS summary statistics for the brain torque profiles showing significant genetic associations. Red and blue lines represent the significance levels of P < 5e-8 and P < 5e-8/348 = 1.44e-10 respectively. Independent lead variants are annotated with their SNP IDs and the closest genes. LocusZoom plots (purple diamond symbols indicate lead SNPs) are attached to show regional associations. For the abbreviations of brain regions, see Table S14.

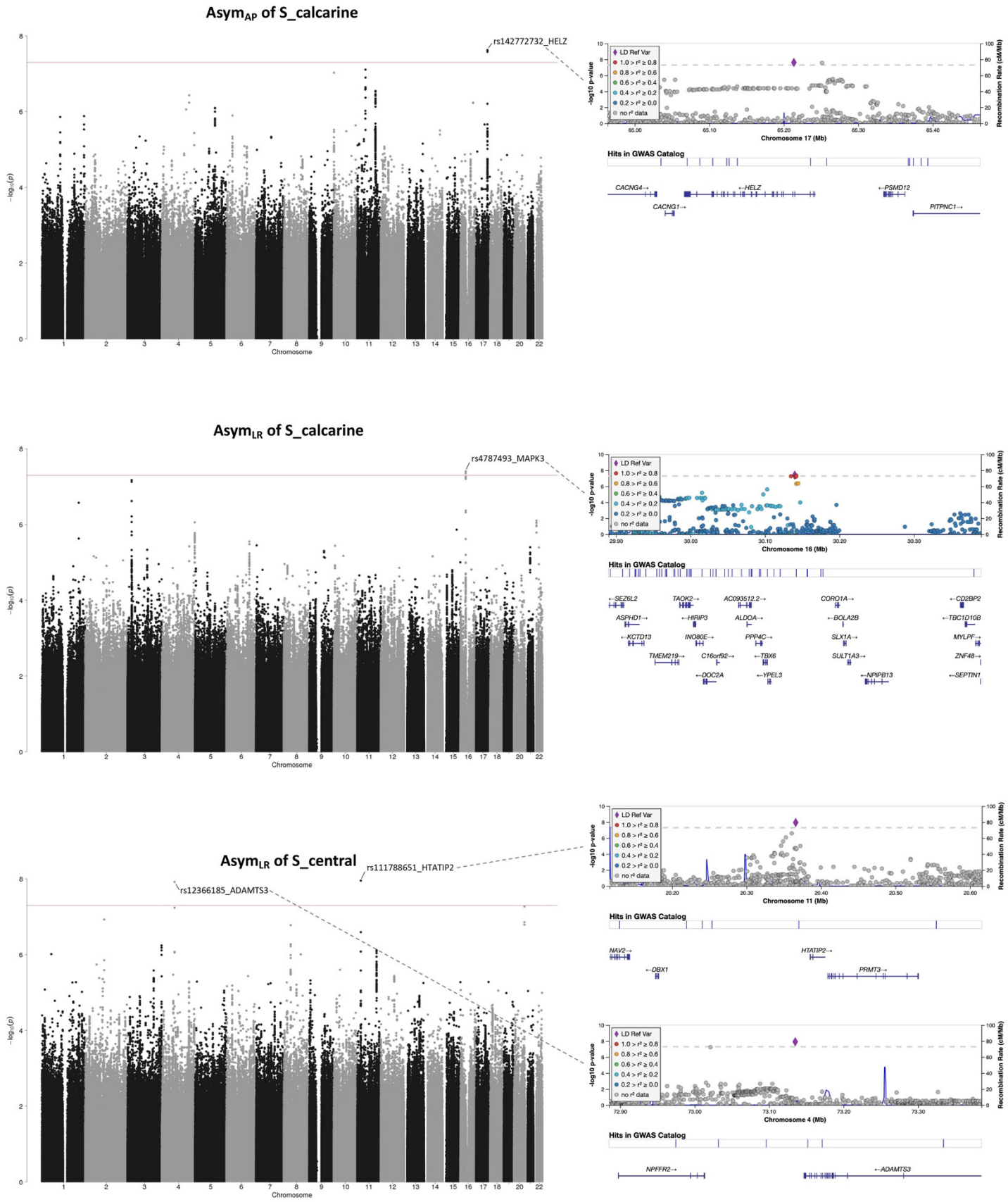

Figure S19 - Part 24. Manhattan plots of meta-GWAS summary statistics for the brain torque profiles showing significant genetic associations. Red and blue lines represent the significance levels of P < 5e-8 and P < 5e-8/348 = 1.44e-10 respectively. Independent lead variants are annotated with their SNP IDs and the closest genes. LocusZoom plots (purple diamond symbols indicate lead SNPs) are attached to show regional associations. For the abbreviations of brain regions, see Table S14.

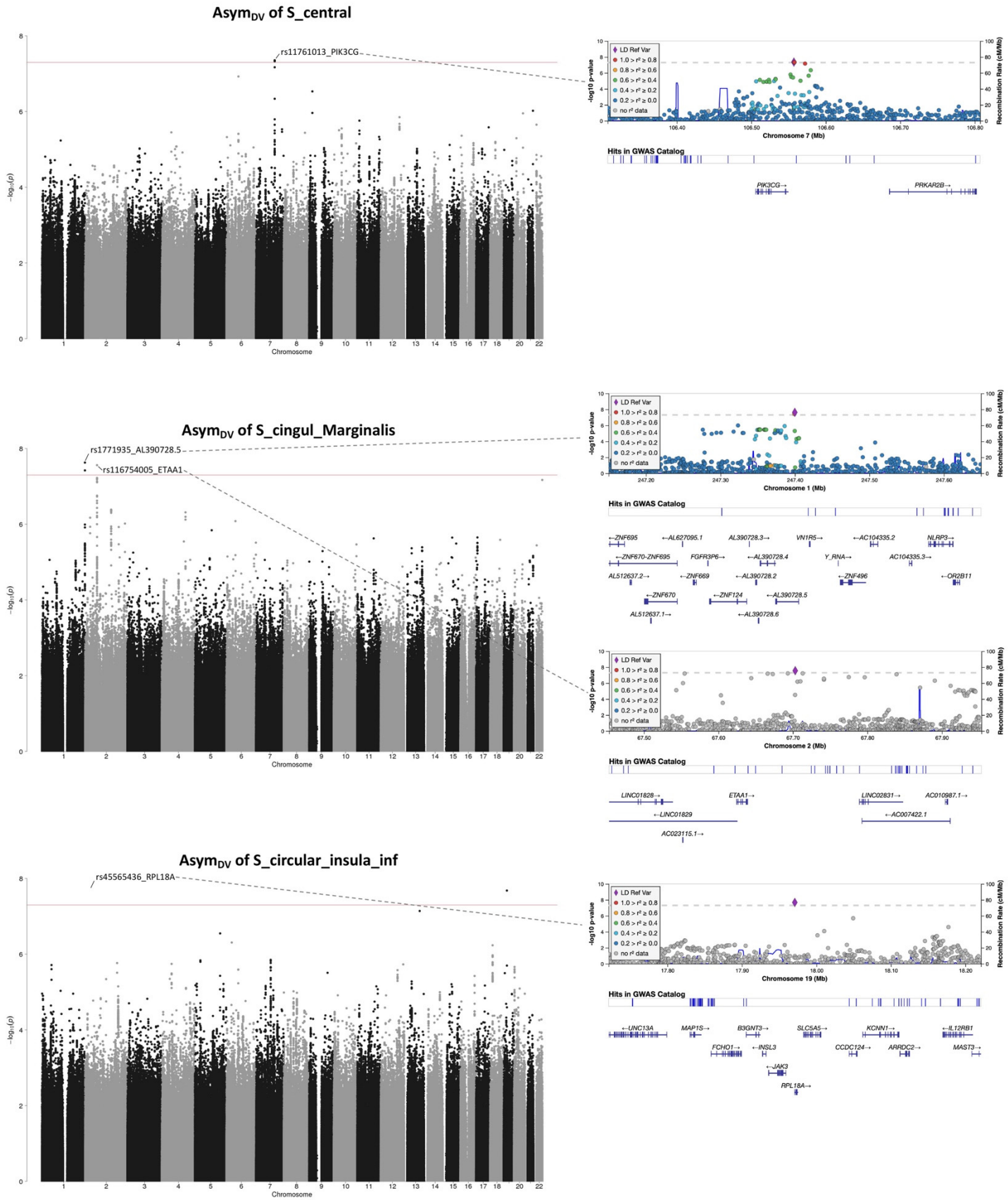

Figure S19 - Part 25. Manhattan plots of meta-GWAS summary statistics for the brain torque profiles showing significant genetic associations. Red and blue lines represent the significance levels of P < 5e-8 and P < 5e-8/348 = 1.44e-10 respectively. Independent lead variants are annotated with their SNP IDs and the closest genes. LocusZoom plots (purple diamond symbols indicate lead SNPs) are attached to show regional associations. For the abbreviations of brain regions, see Table S14.

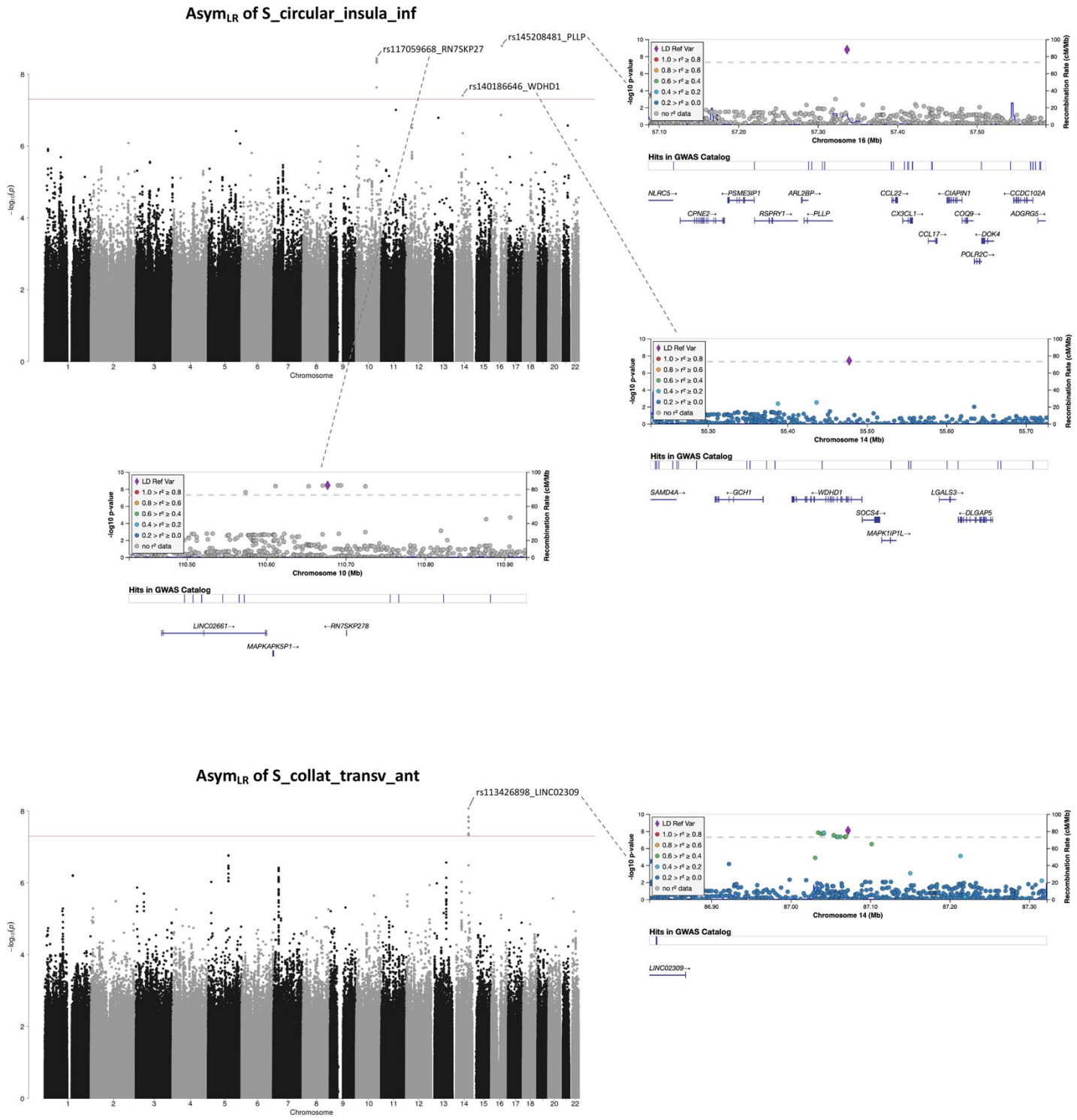

Figure S19 - Part 26. Manhattan plots of meta-GWAS summary statistics for the brain torque profiles showing significant genetic associations. Red and blue lines represent the significance levels of P < 5e-8 and P < 5e-8/348 = 1.44e-10 respectively. Independent lead variants are annotated with their SNP IDs and the closest genes. LocusZoom plots (purple diamond symbols indicate lead SNPs) are attached to show regional associations. For the abbreviations of brain regions, see Table S14.

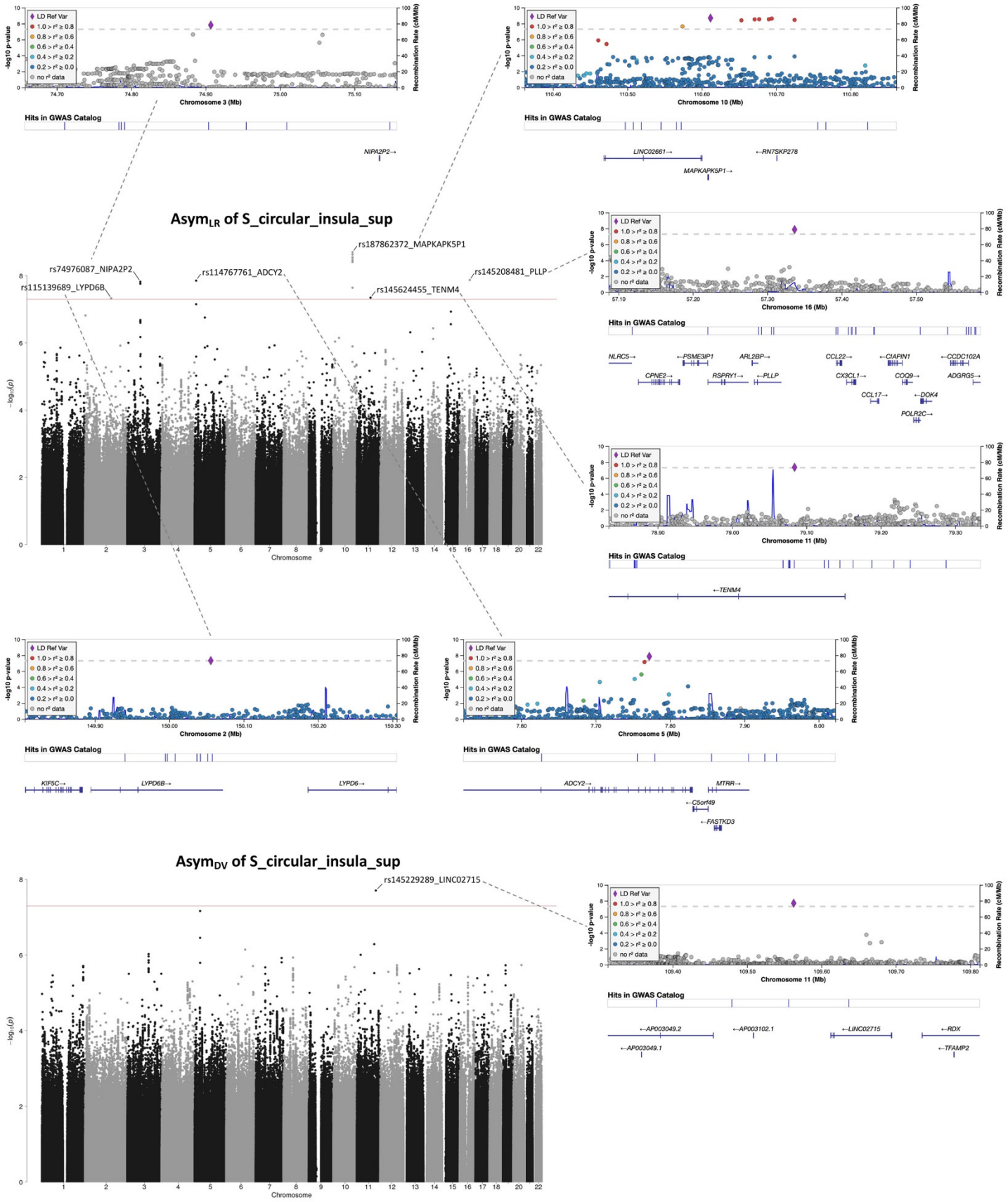

Figure S19 - Part 27. Manhattan plots of meta-GWAS summary statistics for the brain torque profiles showing significant genetic associations. Red and blue lines represent the significance levels of P < 5e-8 and P < 5e-8/348 = 1.44e-10 respectively. Independent lead variants are annotated with their SNP IDs and the closest genes. LocusZoom plots (purple diamond symbols indicate lead SNPs) are attached to show regional associations. For the abbreviations of brain regions, see Table S14.

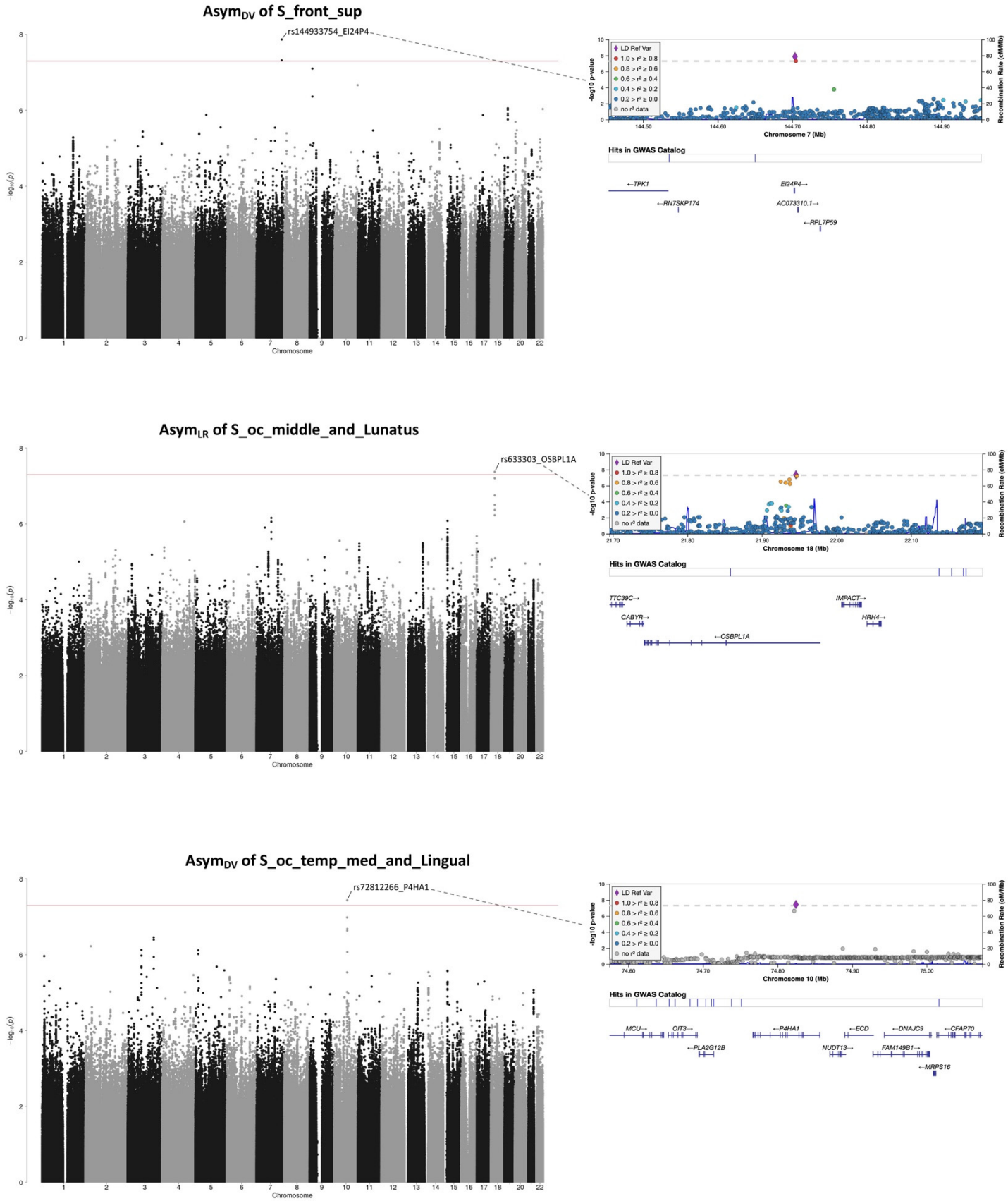

Figure S19 - Part 28. Manhattan plots of meta-GWAS summary statistics for the brain torque profiles showing significant genetic associations. Red and blue lines represent the significance levels of P < 5e-8 and P < 5e-8/348 = 1.44e-10 respectively. Independent lead variants are annotated with their SNP IDs and the closest genes. LocusZoom plots (purple diamond symbols indicate lead SNPs) are attached to show regional associations. For the abbreviations of brain regions, see Table S14.

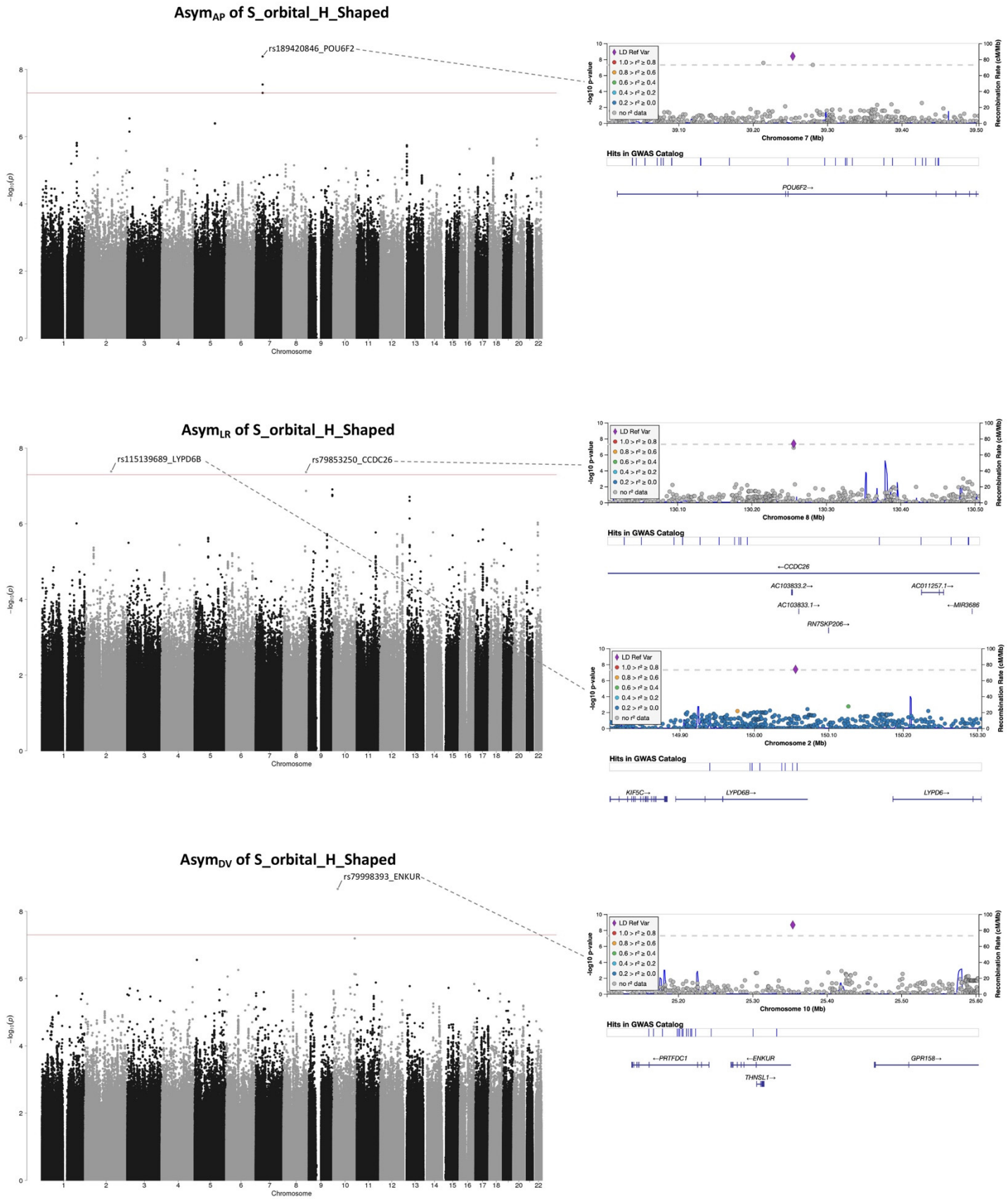

Figure S19 - Part 29. Manhattan plots of meta-GWAS summary statistics for the brain torque profiles showing significant genetic associations. Red and blue lines represent the significance levels of P < 5e-8 and P < 5e-8/348 = 1.44e-10 respectively. Independent lead variants are annotated with their SNP IDs and the closest genes. LocusZoom plots (purple diamond symbols indicate lead SNPs) are attached to show regional associations. For the abbreviations of brain regions, see Table S14.

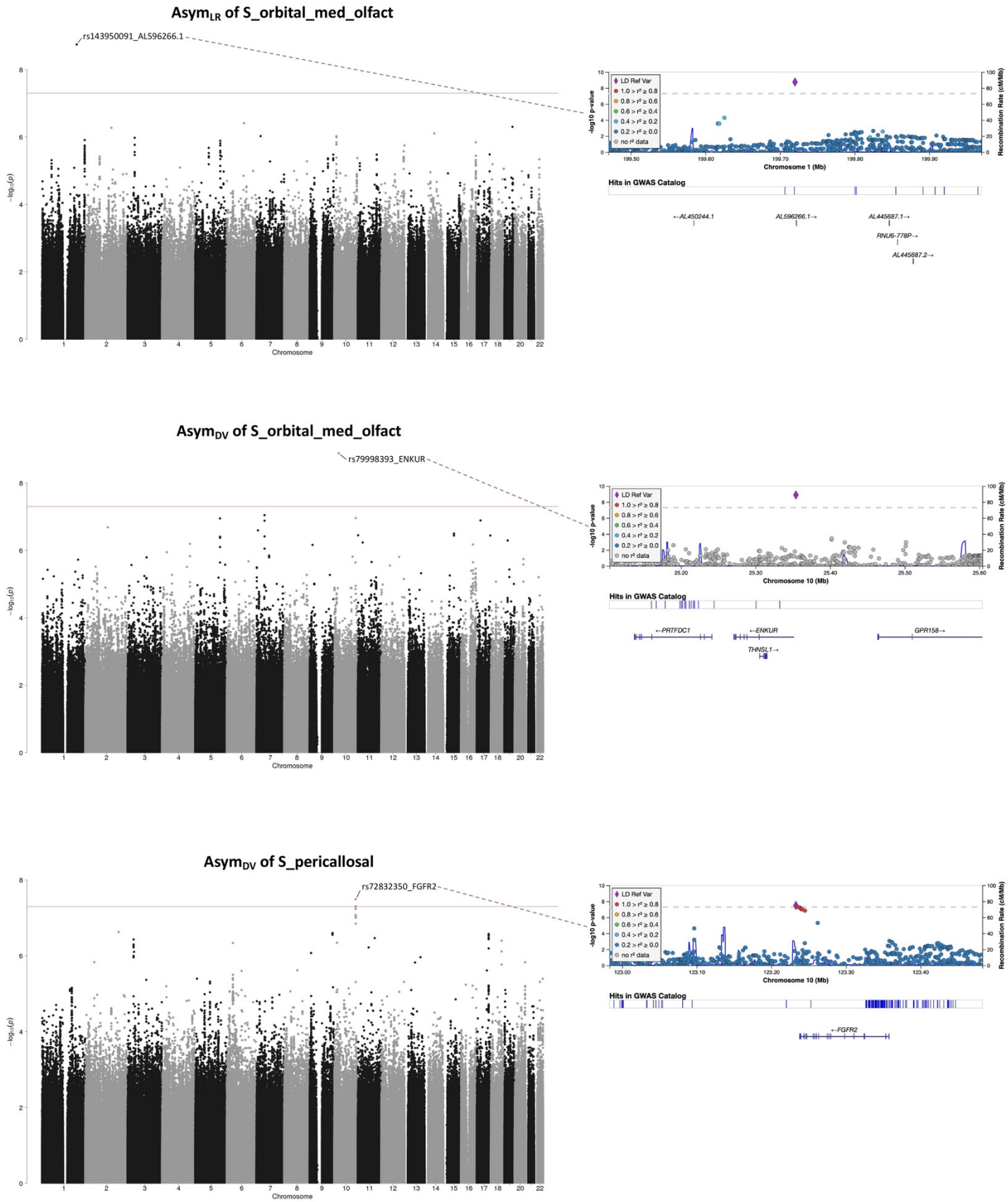

Figure S19 - Part 30. Manhattan plots of meta-GWAS summary statistics for the brain torque profiles showing significant genetic associations. Red and blue lines represent the significance levels of P < 5e-8 and P < 5e-8/348 = 1.44e-10 respectively. Independent lead variants are annotated with their SNP IDs and the closest genes. LocusZoom plots (purple diamond symbols indicate lead SNPs) are attached to show regional associations. For the abbreviations of brain regions, see Table S14.

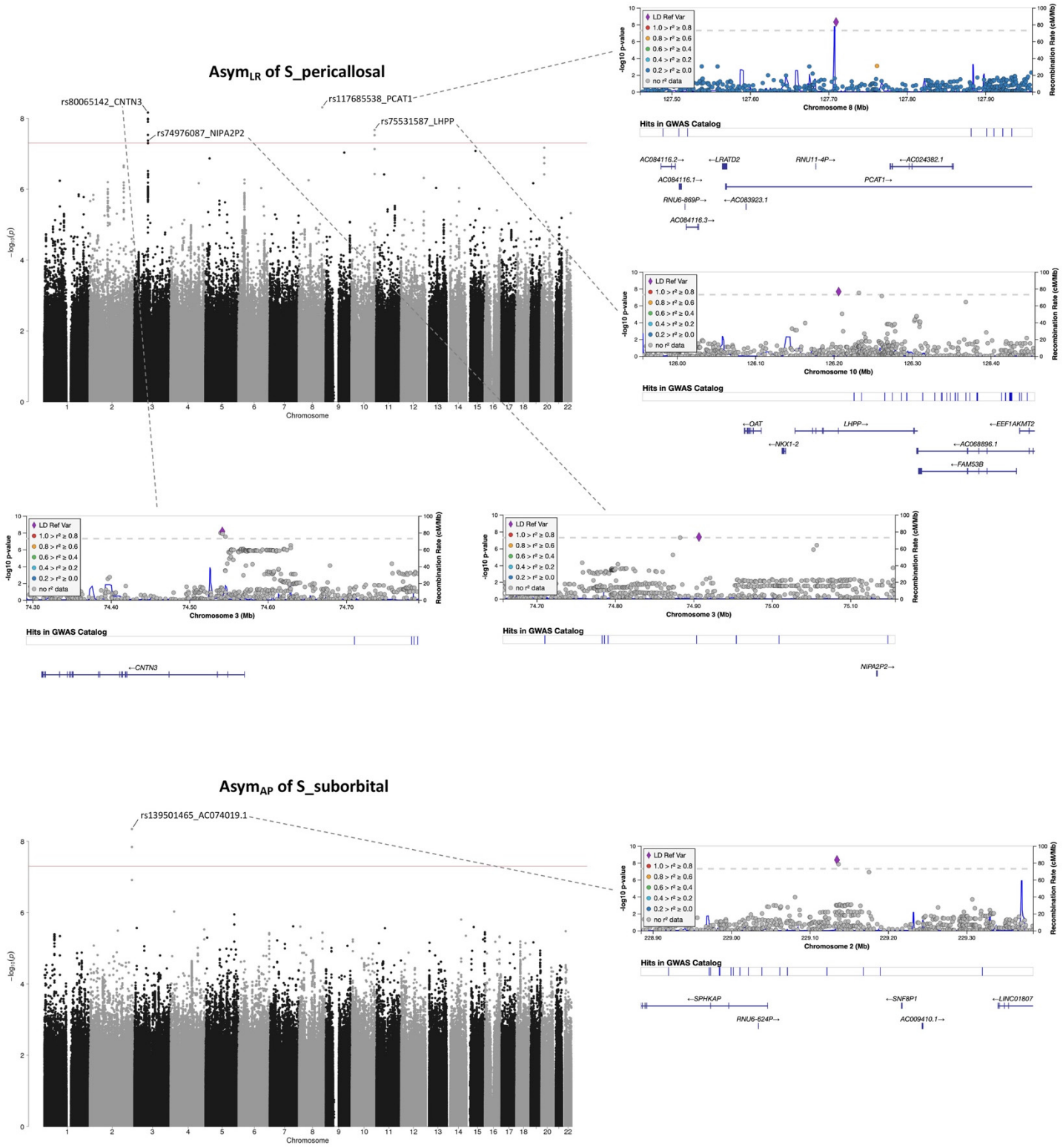

Figure S19 - Part 31. Manhattan plots of meta-GWAS summary statistics for the brain torque profiles showing significant genetic associations. Red and blue lines represent the significance levels of P < 5e-8 and P < 5e-8/348 = 1.44e-10 respectively. Independent lead variants are annotated with their SNP IDs and the closest genes. LocusZoom plots (purple diamond symbols indicate lead SNPs) are attached to show regional associations. For the abbreviations of brain regions, see Table S14.

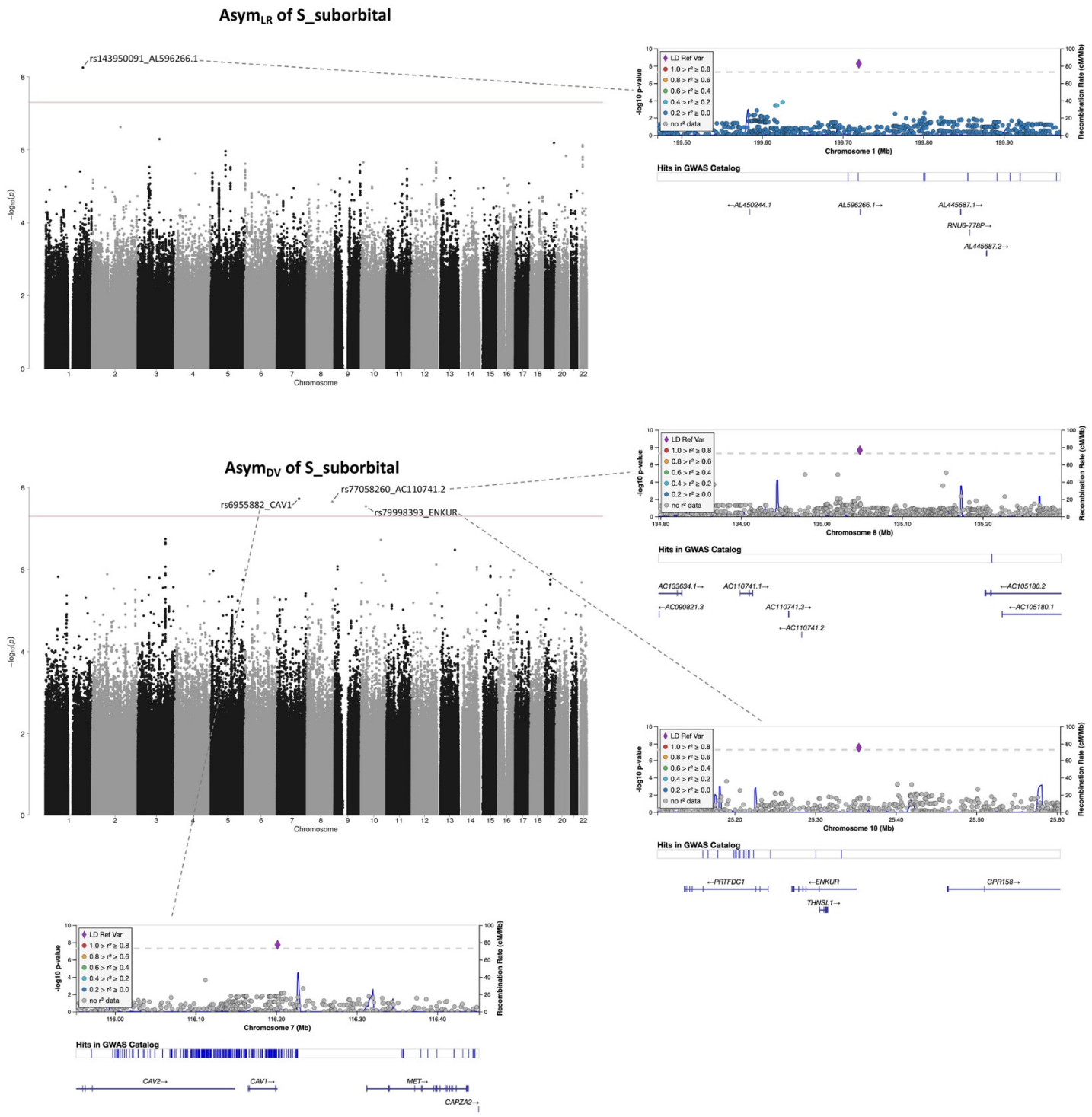

Figure S19 - Part 32. Manhattan plots of meta-GWAS summary statistics for the brain torque profiles showing significant genetic associations. Red and blue lines represent the significance levels of P < 5e-8 and P < 5e-8/348 = 1.44e-10 respectively. Independent lead variants are annotated with their SNP IDs and the closest genes. LocusZoom plots (purple diamond symbols indicate lead SNPs) are attached to show regional associations. For the abbreviations of brain regions, see Table S14.

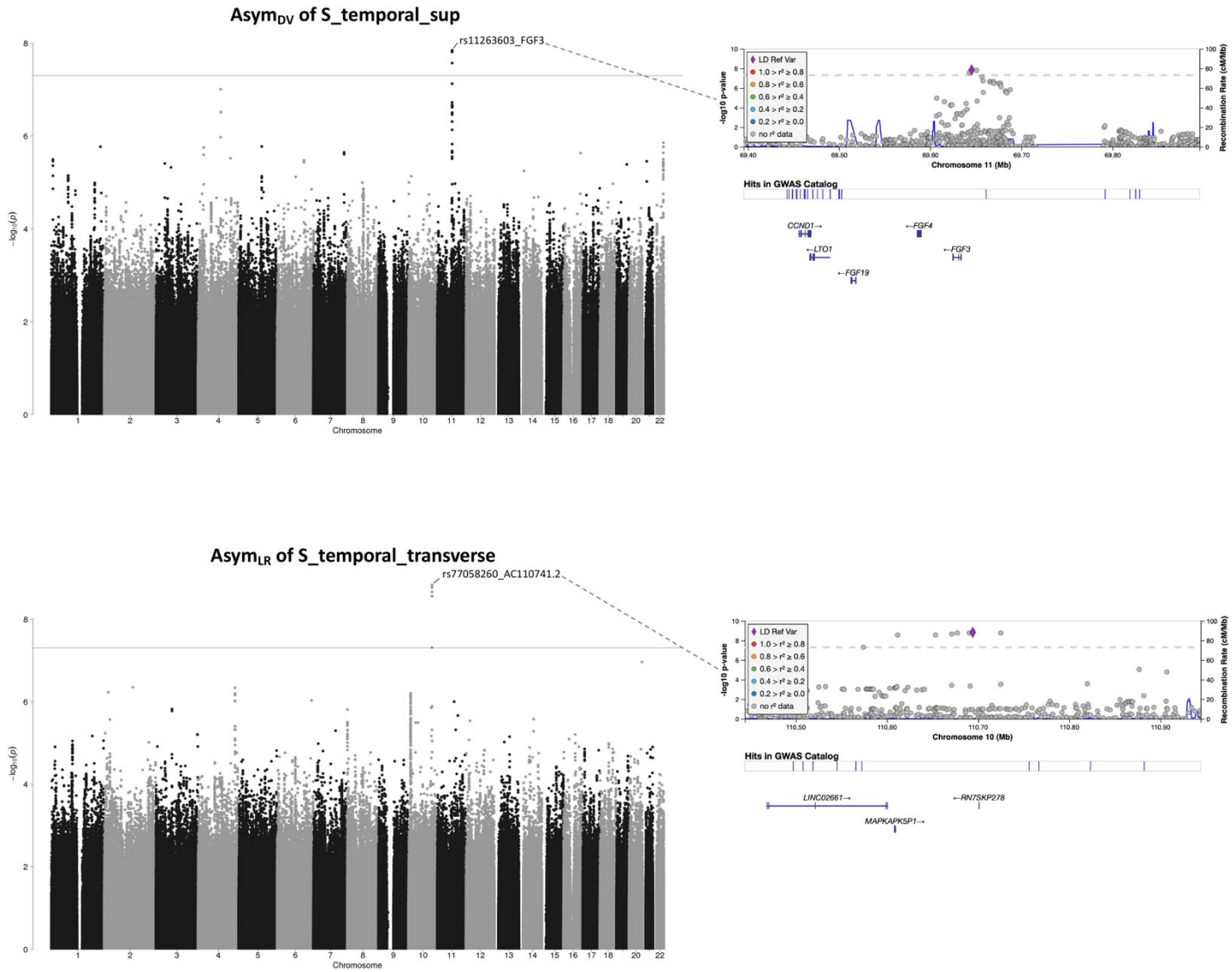

Figure S19 - Part 33. Manhattan plots of meta-GWAS summary statistics for the brain torque profiles showing significant genetic associations. Red and blue lines represent the significance levels of P < 5e-8 and P < 5e-8/348 = 1.44e-10 respectively. Independent lead variants are annotated with their SNP IDs and the closest genes. LocusZoom plots (purple diamond symbols indicate lead SNPs) are attached to show regional associations. For the abbreviations of brain regions, see Table S14.

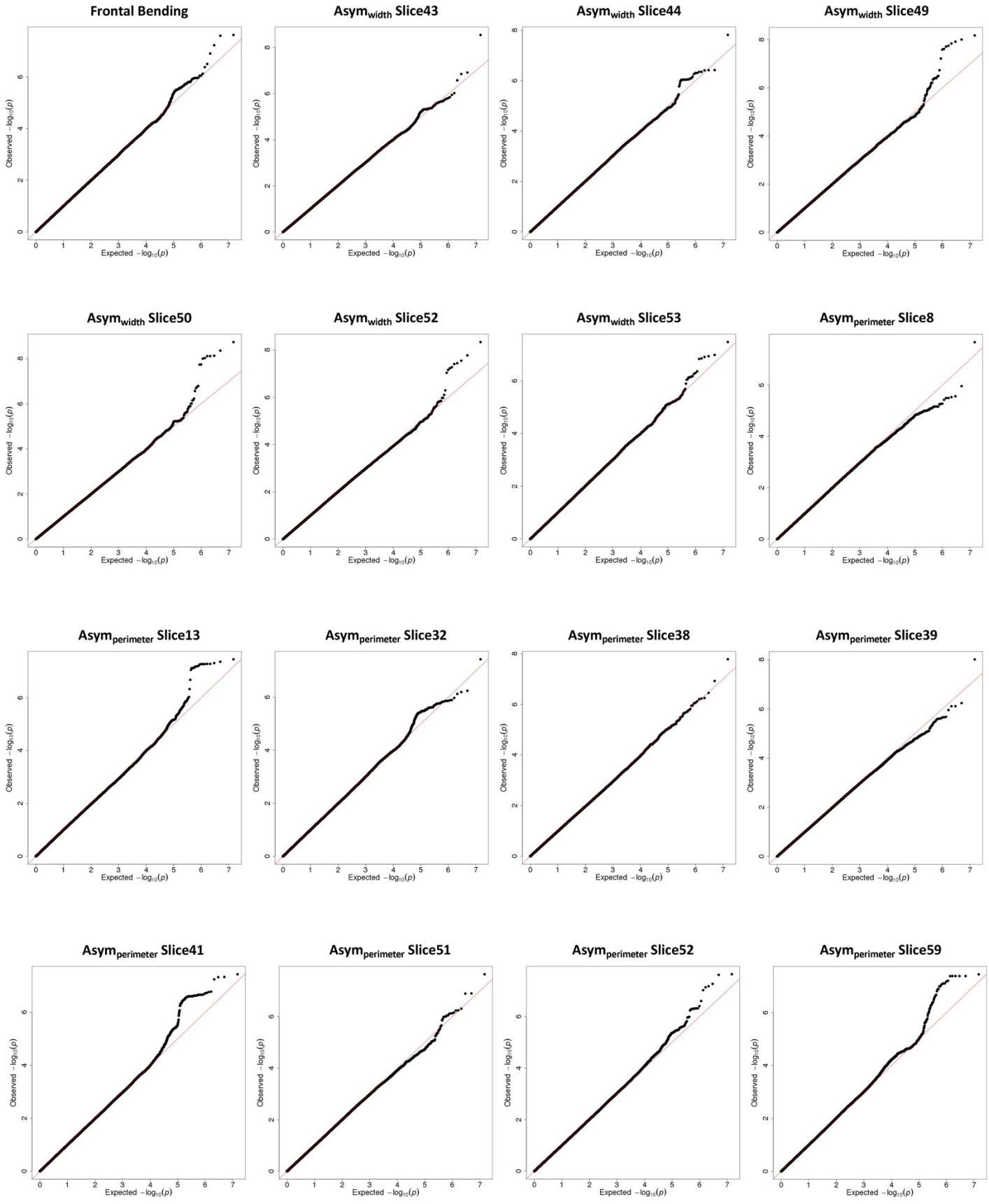

Figure S20 – Part 1. Q-Q plots of meta-GWAS summary statistics for the brain torque profiles showing significant genetic associations. For the abbreviations of brain regions, see Table S14.

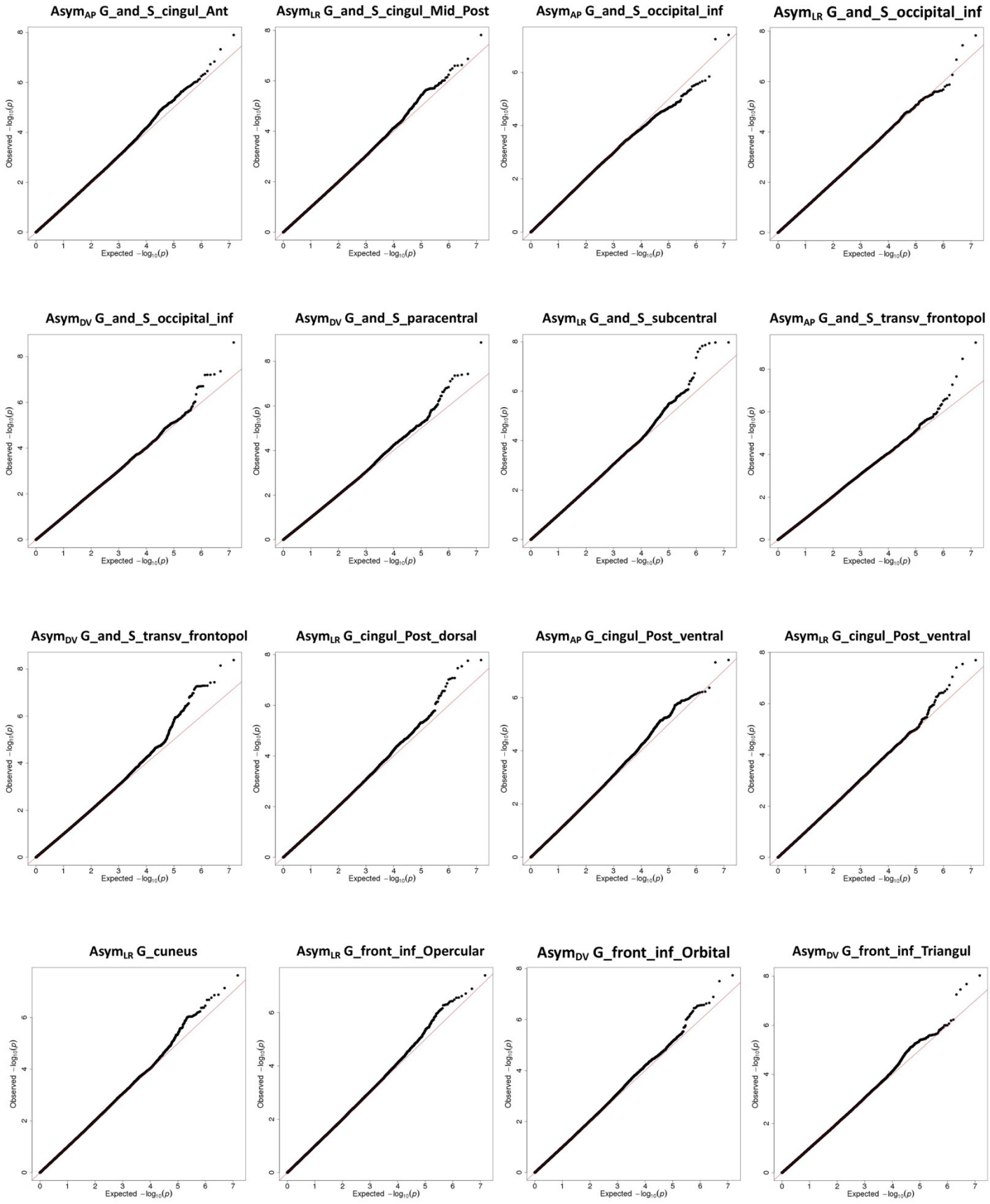

Figure S20 – Part 2. Q-Q plots of meta-GWAS summary statistics for the brain torque profiles showing significant genetic associations. For the abbreviations of brain regions, see Table S14.

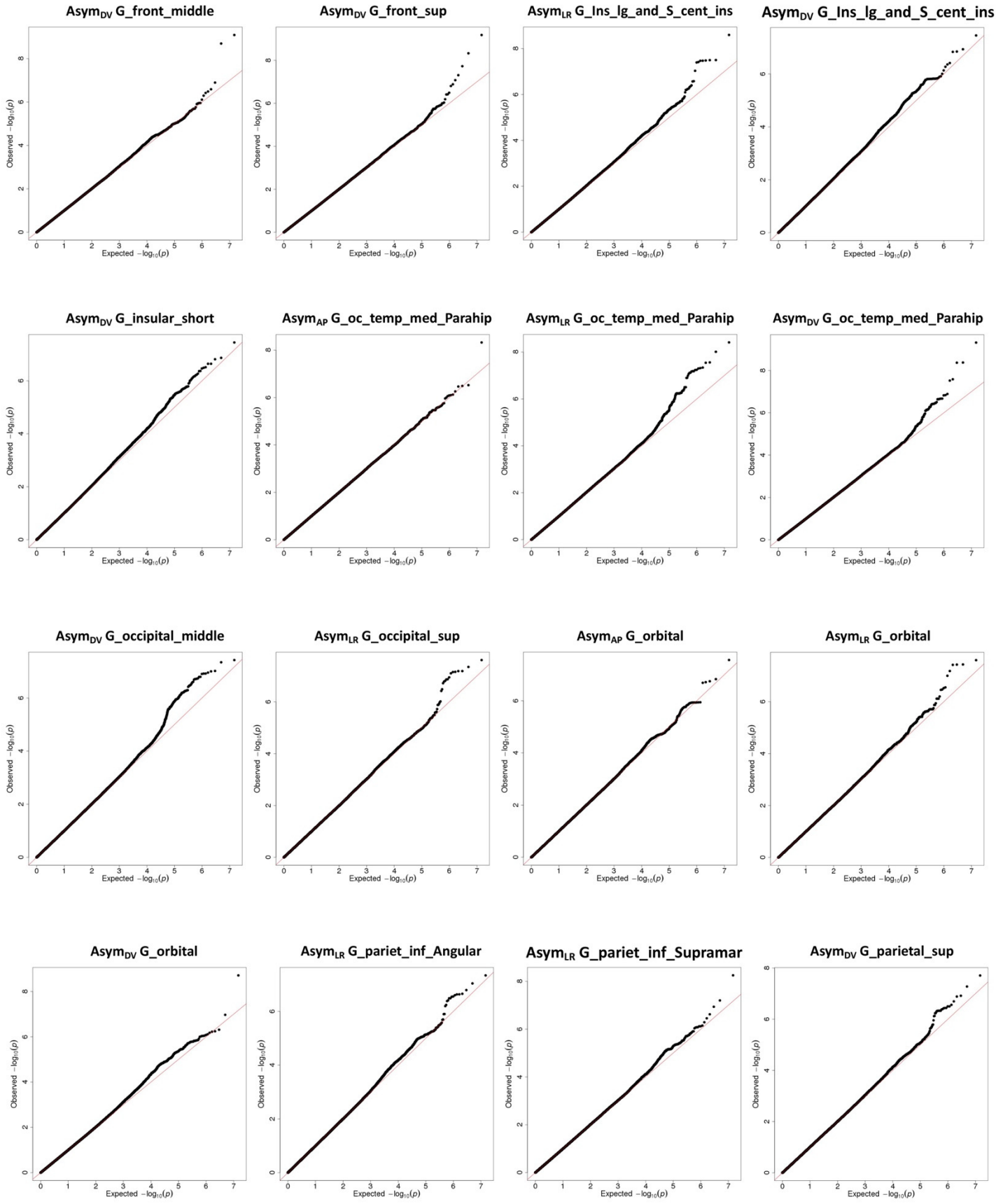

Figure S20 – Part 3. Q-Q plots of meta-GWAS summary statistics for the brain torque profiles showing significant genetic associations. For the abbreviations of brain regions, see Table S14.

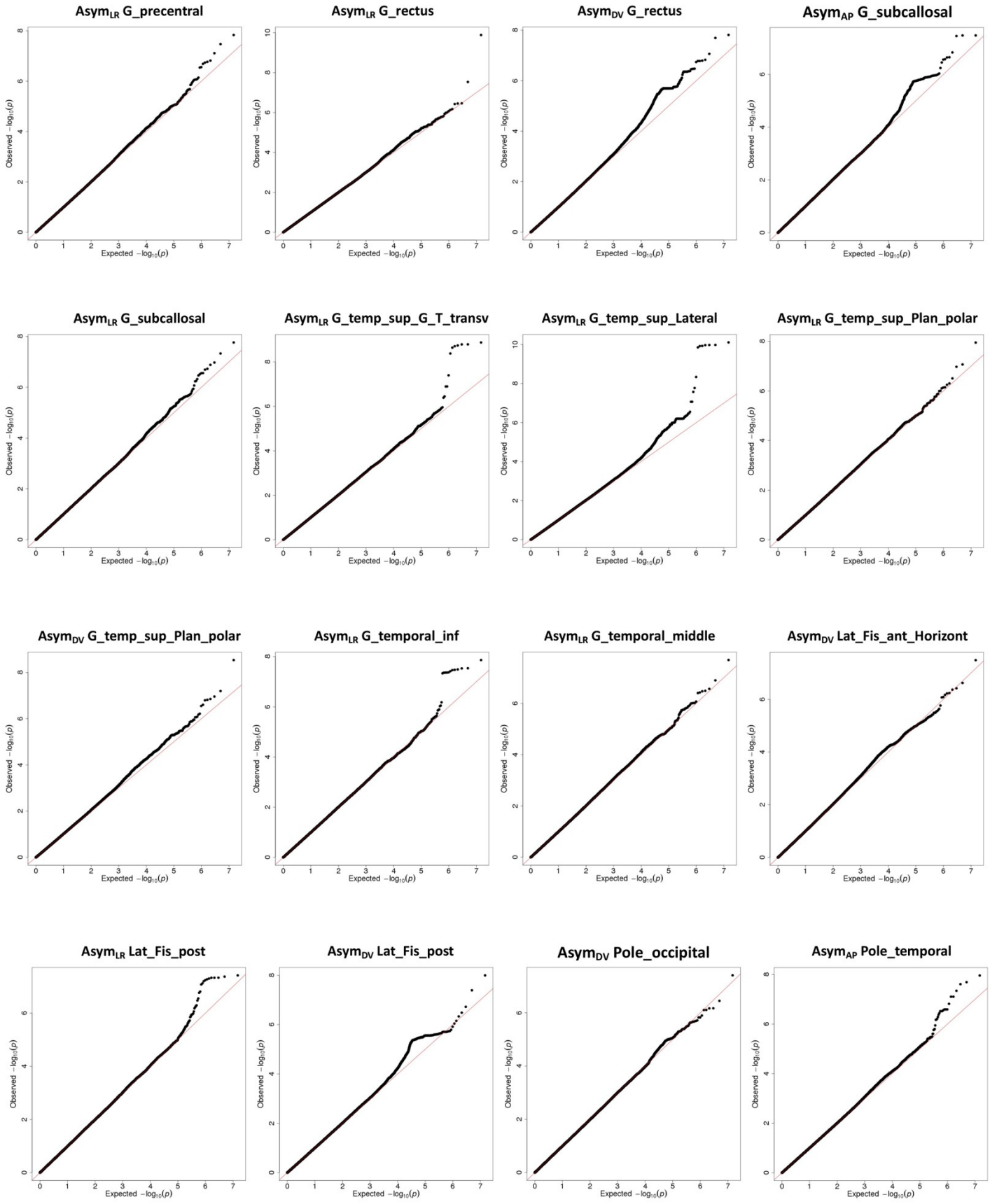

Figure S20 – Part 4. Q-Q plots of meta-GWAS summary statistics for the brain torque profiles showing significant genetic associations. For the abbreviations of brain regions, see Table S14.

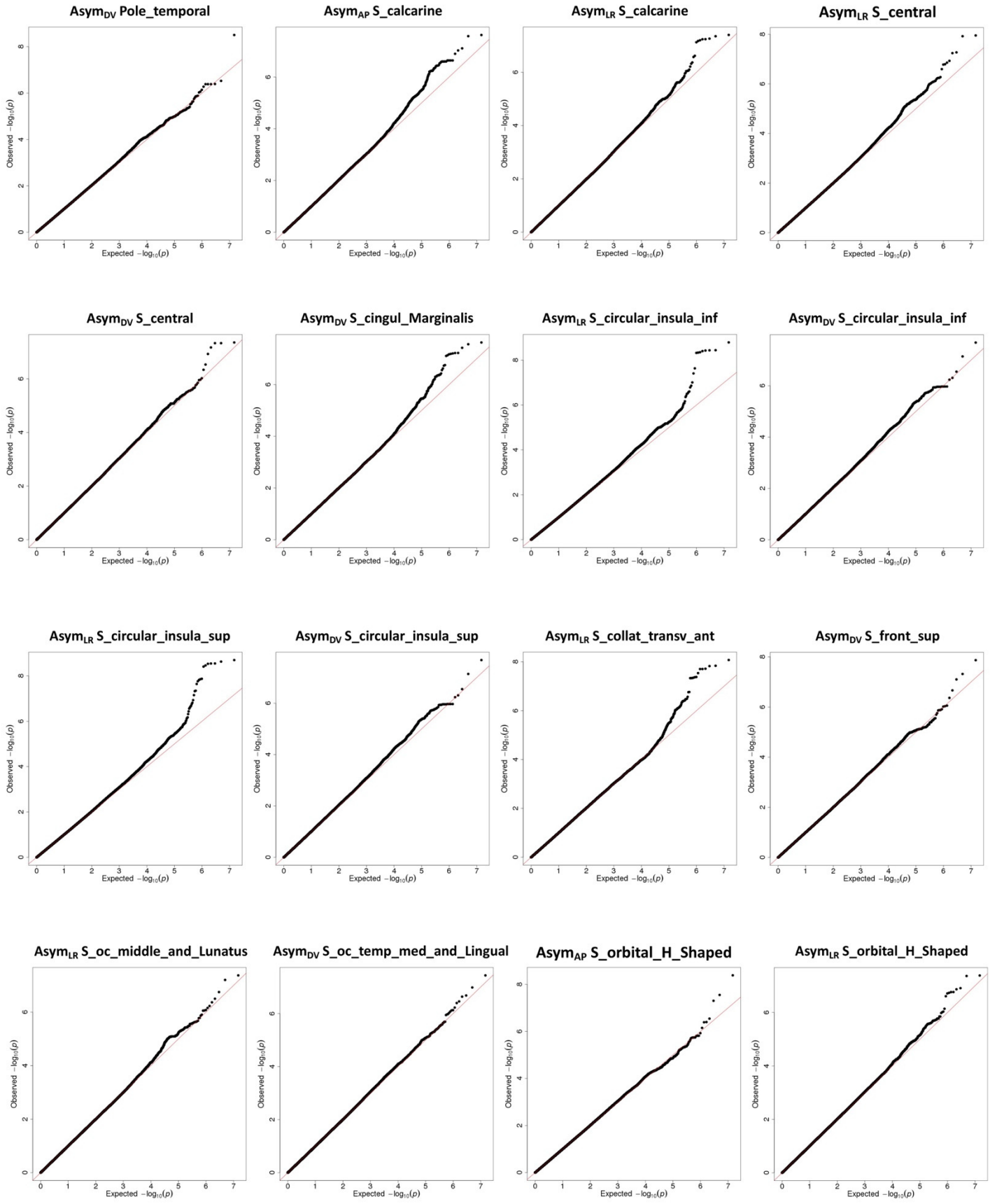

Figure S20 – Part 5. Q-Q plots of meta-GWAS summary statistics for the brain torque profiles showing significant genetic associations. For the abbreviations of brain regions, see Table S14.

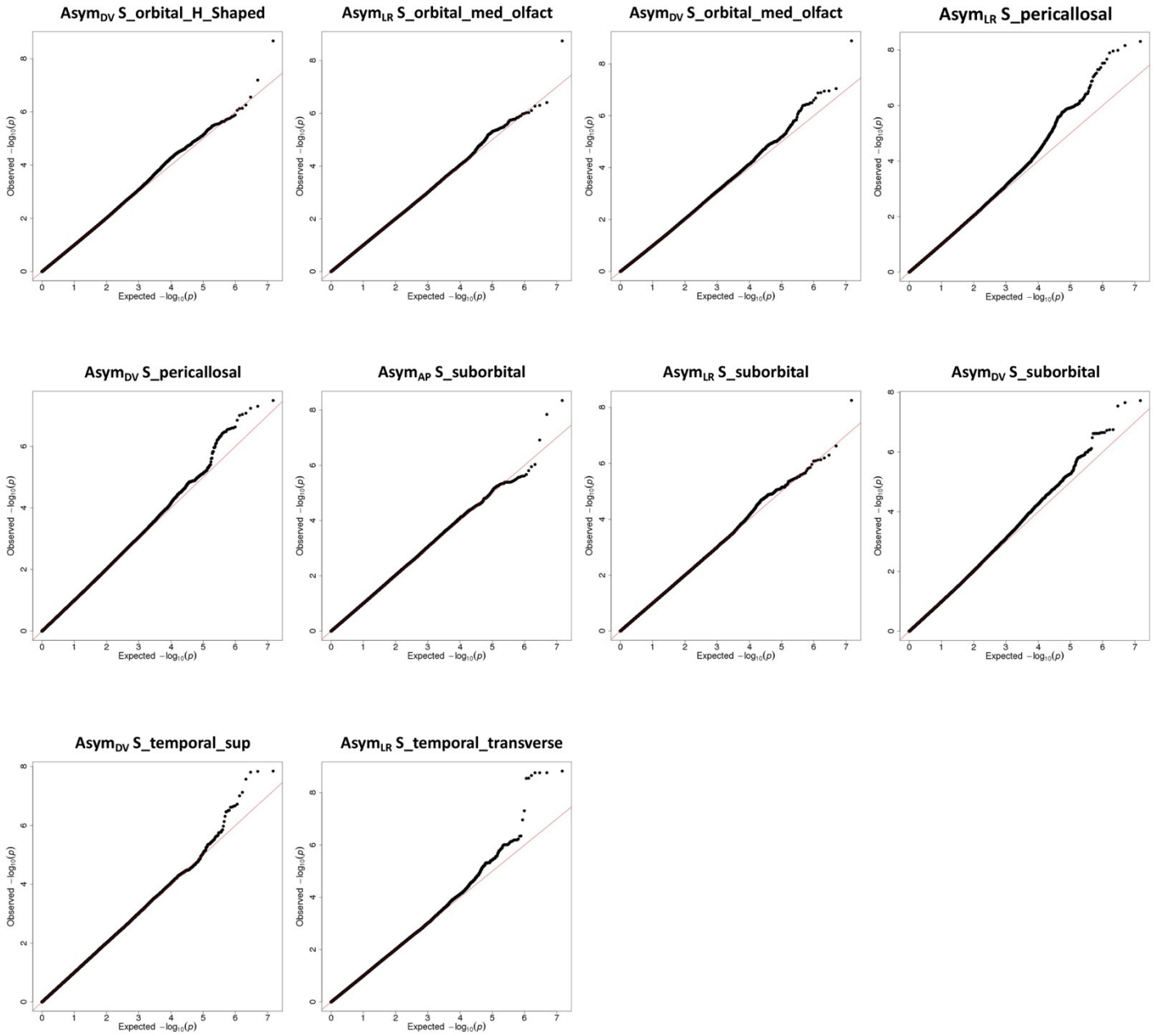

Figure S20 – Part 6. Q-Q plots of meta-GWAS summary statistics for the brain torque profiles showing significant genetic associations. For the abbreviations of brain regions, see Table S14.

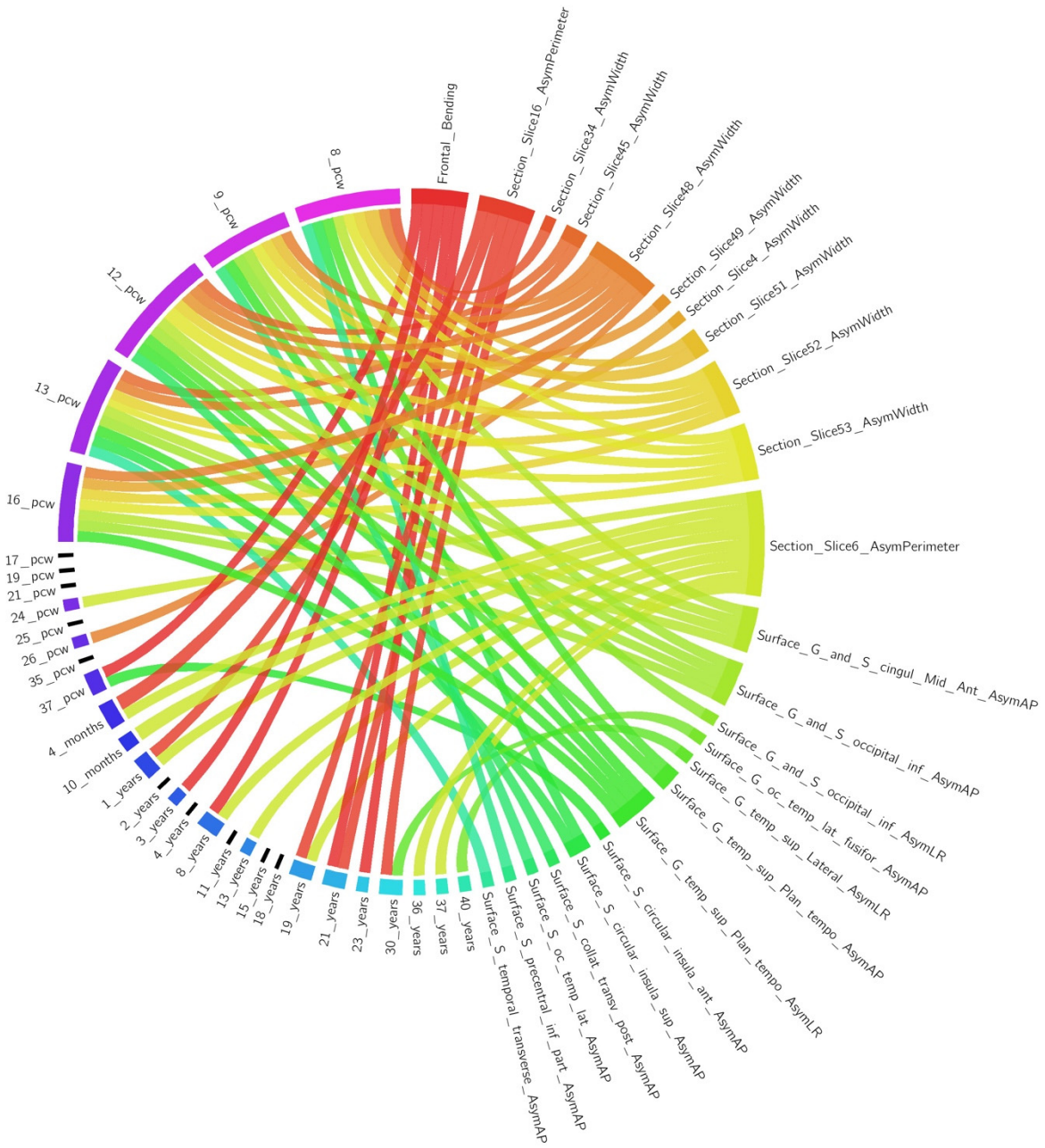

Figure S21. Overview of MAGMA gene-property analysis results with respect to the BrainSpan age-specific gene expression data. Ribbons in the connectogram plot illustrate associations (P < 0.05/31) of gene expression levels at 31 neurodevelopmental stages (left) with the genetic associations with brain torque (BT) profiles (right). Different colors represent different age stages or BT profiles. Ribbons are colored with the colors of linked BT profiles. Ribbon thickness represent the -log(P) value of the corresponding association. AsymWidth = Width Asymmetry, AsymPerimeter = Perimeter Asymmetry, AsymLR = asymmetry along left-right axis, AsymAP = asymmetry along Antero-Posterior axis, AsymDV = asymmetry along Dorso-Ventral axis. For the abbreviations of brain regions, see Table S14.

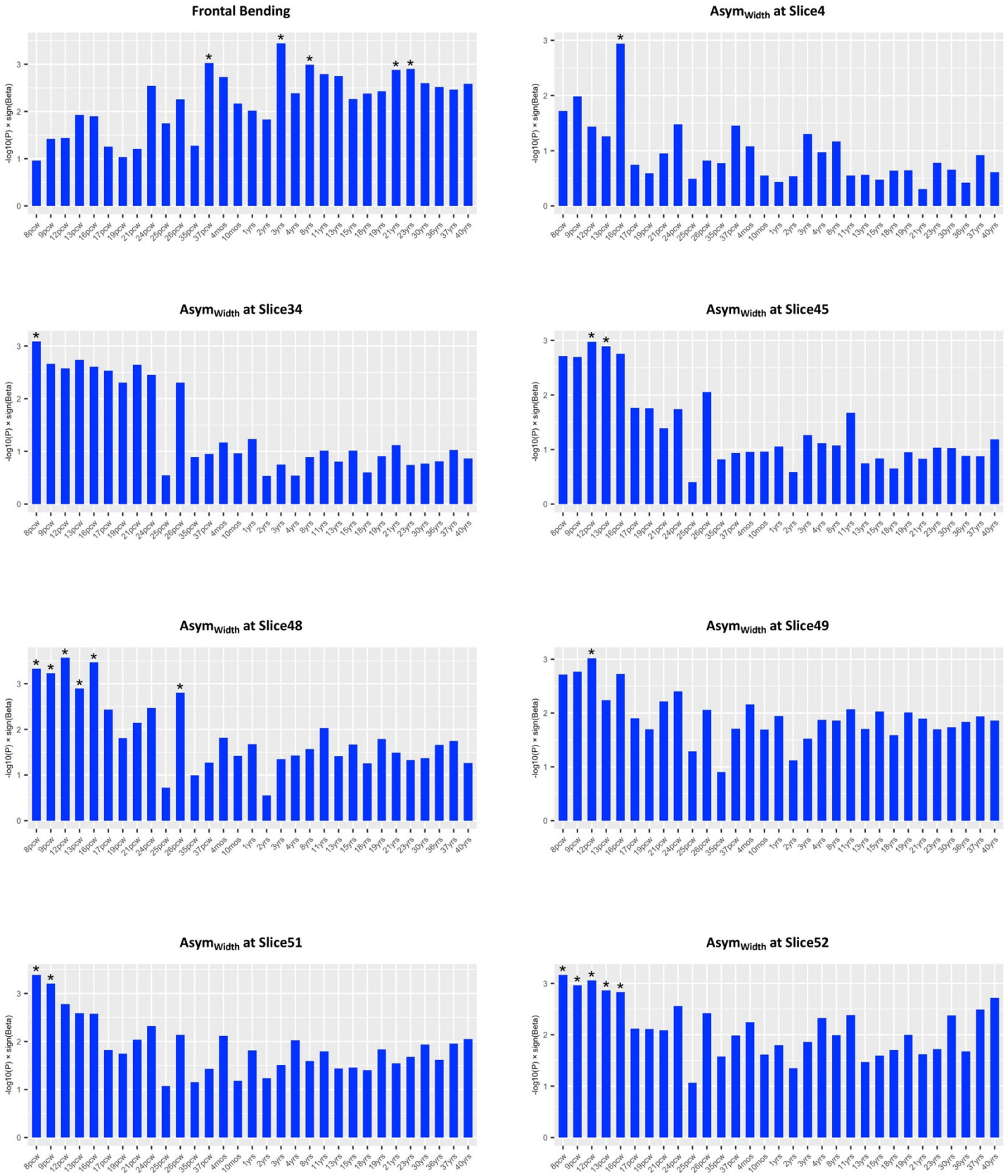

Figure S22 – Part 1. Relation between gene-based associations with brain torque features and higher gene expression levels in the brain at particular ages, using BrainSpan data from 31 age groups. Asterisks represent P < 0.05/31 = 0.0016. For the abbreviations of brain regions, see Table S14.

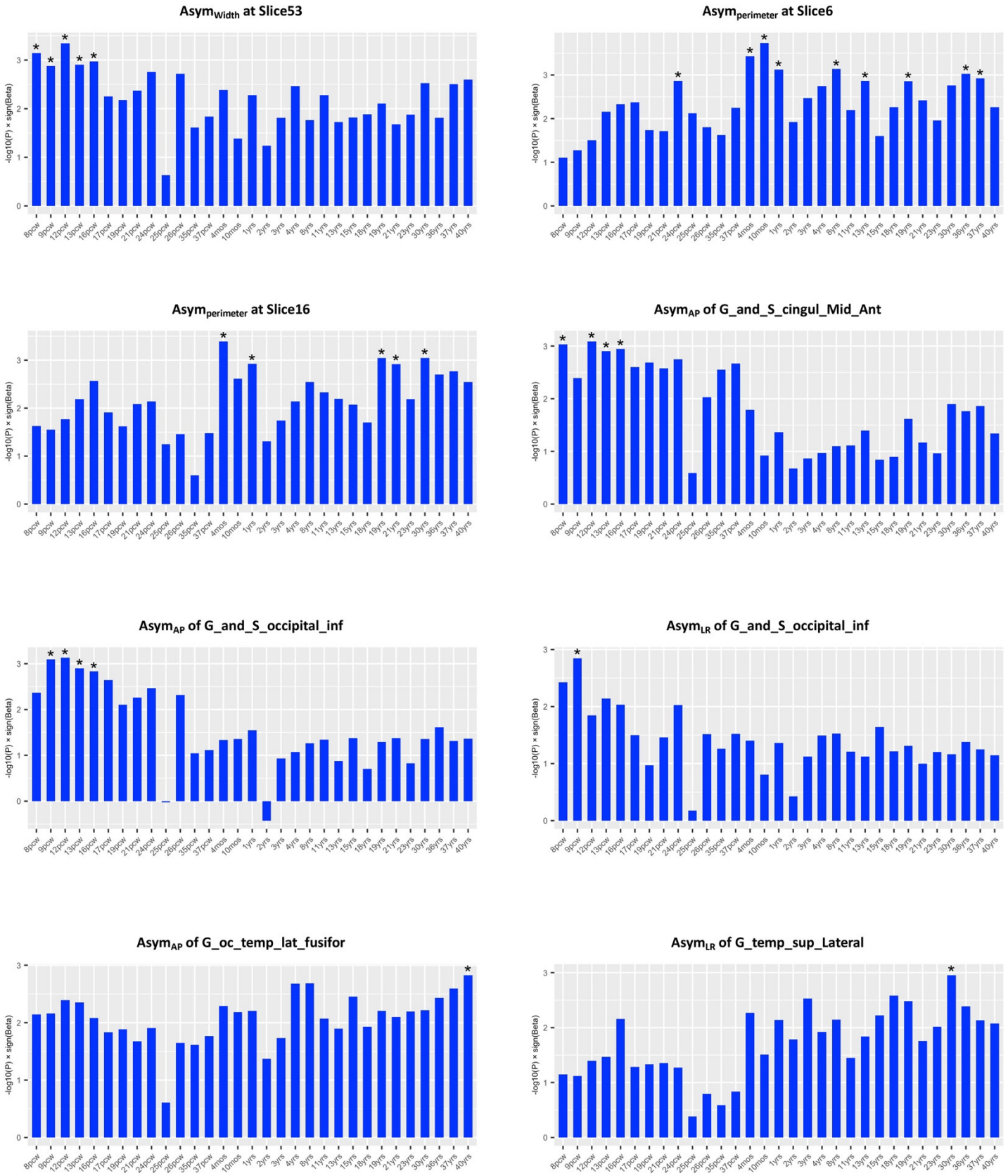

Figure S22 – Part 2. Relation between gene-based associations with brain torque features and higher gene expression levels in the brain at particular ages, using BrainSpan data from 31 age groups. Asterisks represent P < 0.05/31 = 0.0016. For the abbreviations of brain regions, see Table S14.

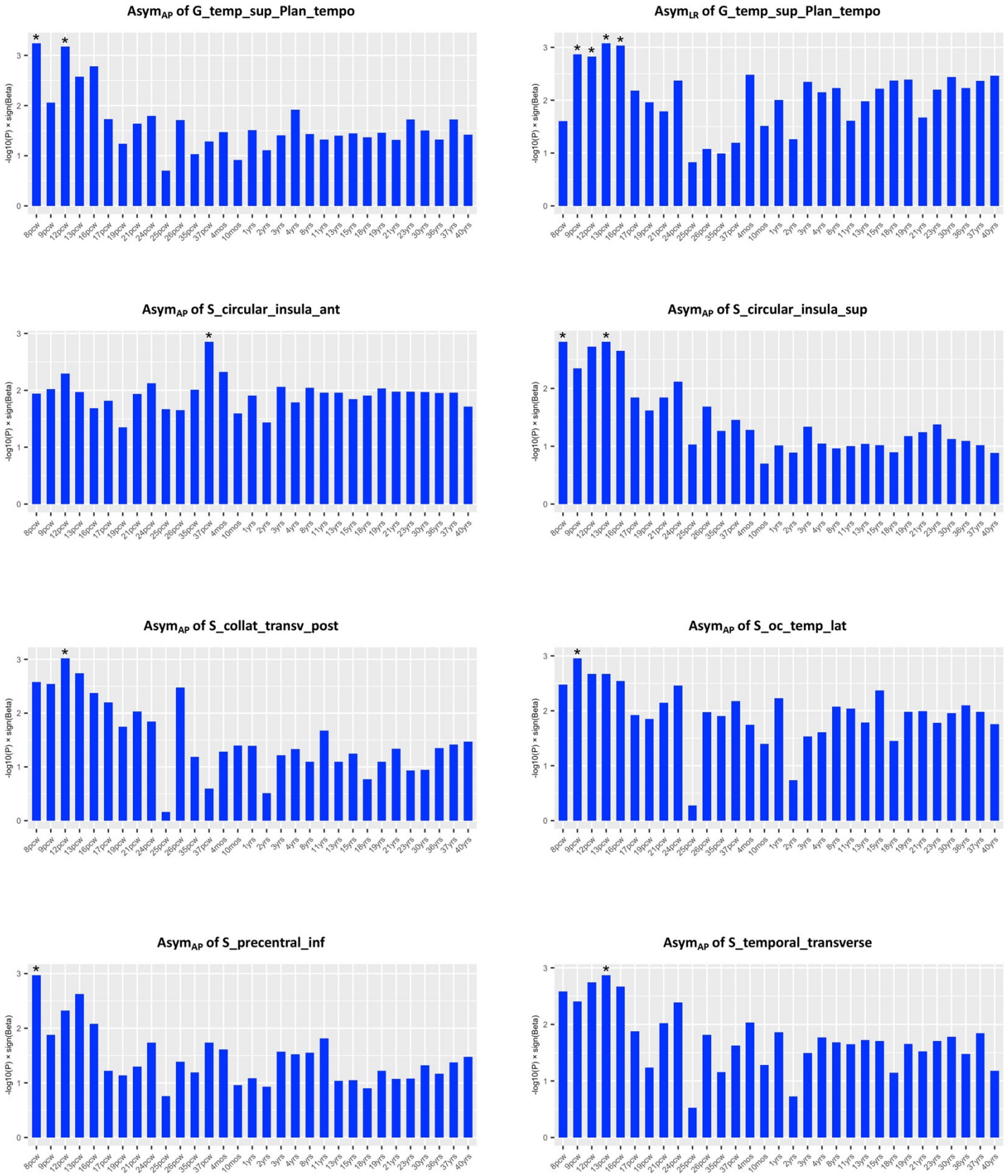

Figure S22 – Part 3. Relation between gene-based associations with brain torque features and higher gene expression levels in the brain at particular ages, using BrainSpan data from 31 age groups. Asterisks represent P < 0.05/31 = 0.0016. For the abbreviations of brain regions, see Table S14.

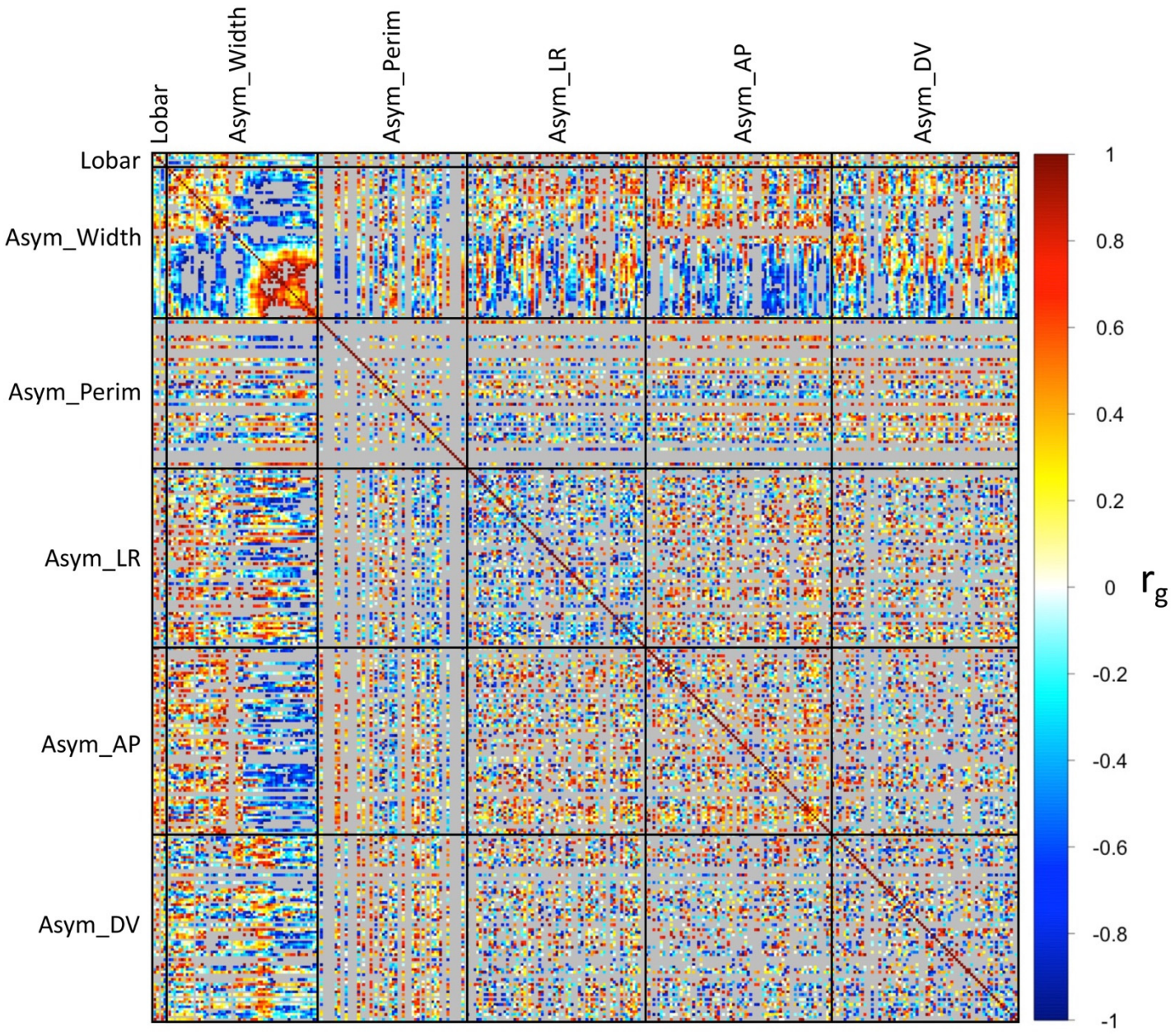

Figure S23: Heat map showing genetic correlations between brain torque (BT) profiles estimated using the meta-GWAS summary statistics. The BT profiles include lobar measures of frontal/occipital petalia, bending and shift, sectional asymmetries in hemispheric width (Asym_Width) and perimeter (Asym_Perim) and regional mean surface positional asymmetries along the left-right (Asym_LR), anterior-posterior (Asym_AP), and dorsal-ventral (Asym_DV) axes. Color bar represents genetic correlation coefficient r_g. Correlations with a P > 0.05 are shown in grey. Detailed statistics of these genetic associations are summarized in Table S27.

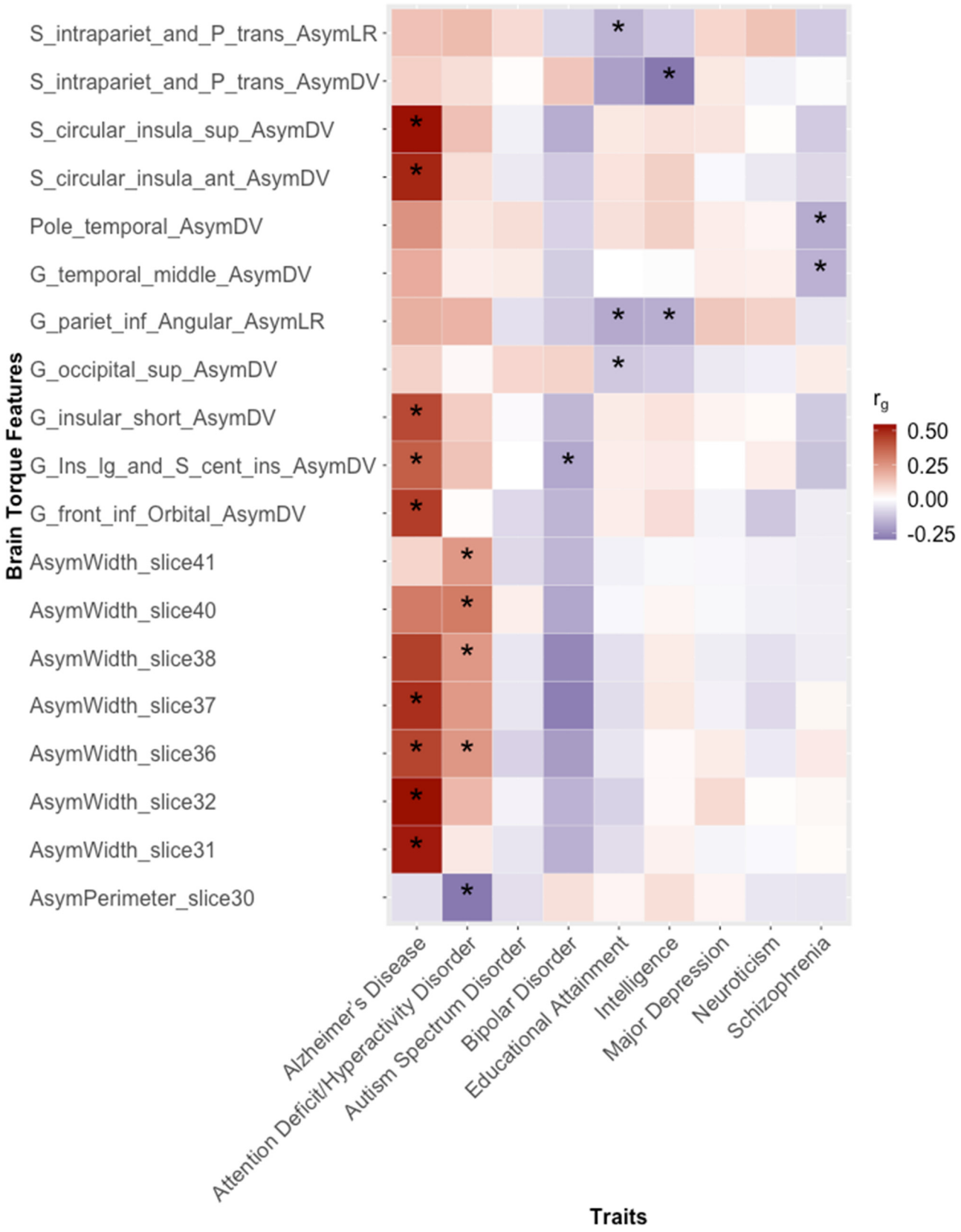

Figure S24. Genetic correlations between brain torque (BT) features and other traits. Only BT features showing at least one trend ($P < 0.05$) of genetic correlation (highlighted with asterisks) are included here. Color bar represents genetic correlation coefficient r_g. For the abbreviations of brain regions, see Table S14. Detailed statistics of these genetic associations are summarized in Table S28.

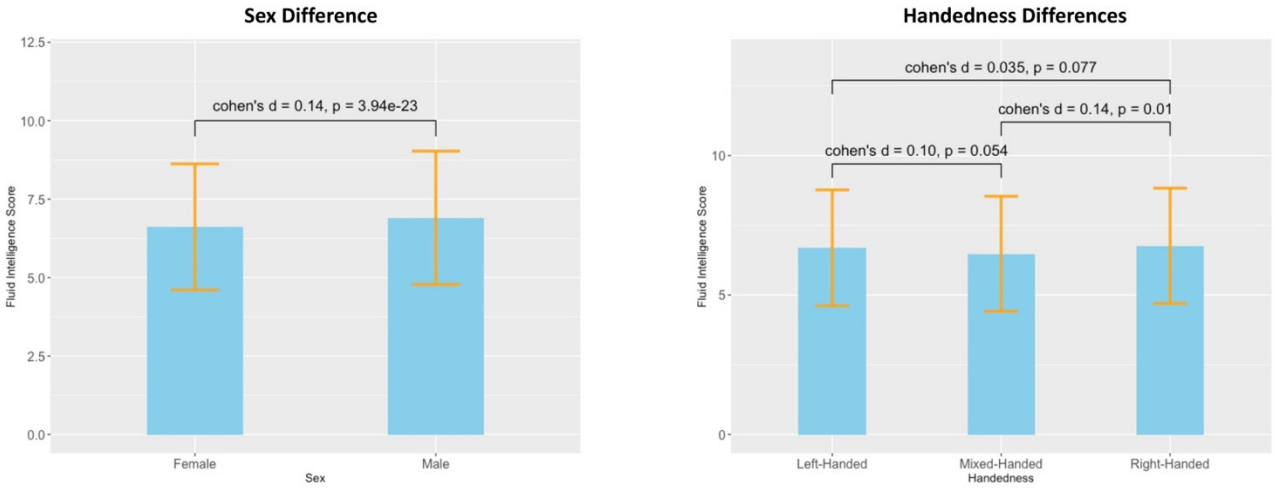

Figure S25. Sex and handedness differences in fluid intelligence (verbal-numerical reasoning) score in the UK Biobank cohort.

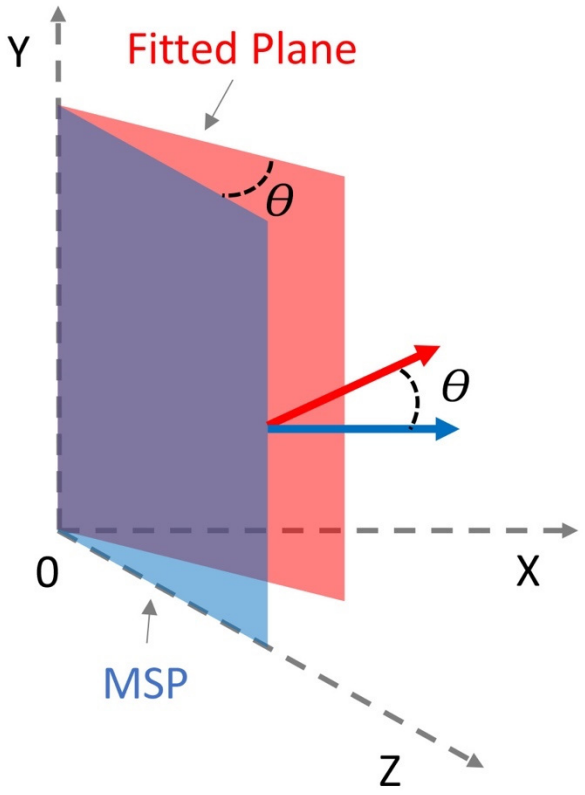

Figure S26: Example of unreliable normal-based bending measurement. In this example, the fitted plane (red plane) is rotated around the Y axis relative to the mid-sagittal plane (MSP, blue plane) only. No rotation in the other directions. The angle θ between the normals (red and blue arrows) of the two planes represents this rotation around the Y axis. However, the angle of the target bending (the rotation around the Z axis) is 0.

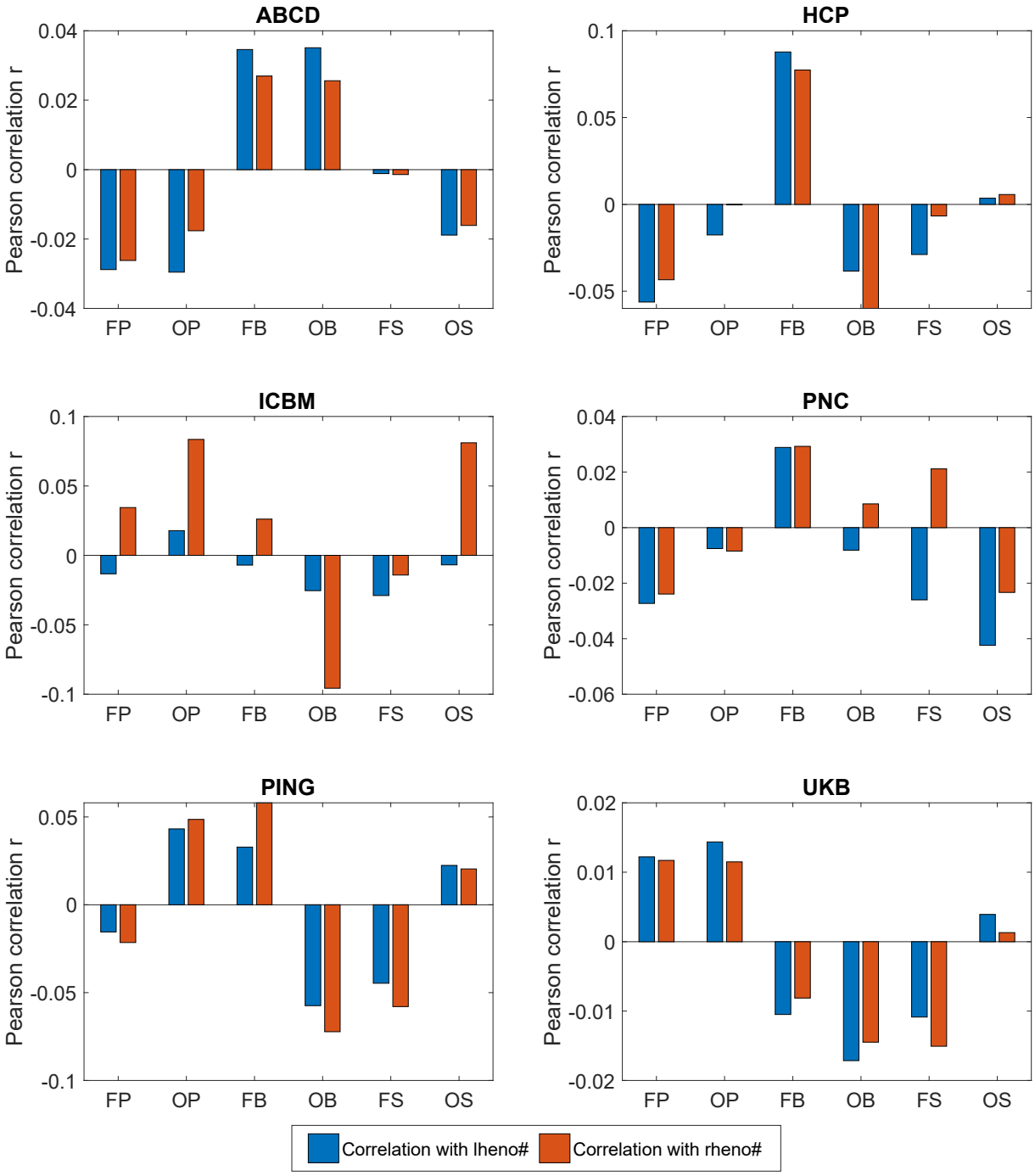

Figure S27: Correlations between lobar brain torque measures and FreeSurfer Euler number in each individual data set. No correlations were significant (P > 0.05/6). FP = Frontal Petalia, OP = Occipital Petalia, FB = Frontal Bending, OB = Occipital Bending, FS = Frontal Shift, OS = Occipital Shift, lheno# = Euler number of left hemisphere, rheno# = Euler number of right hemisphere.

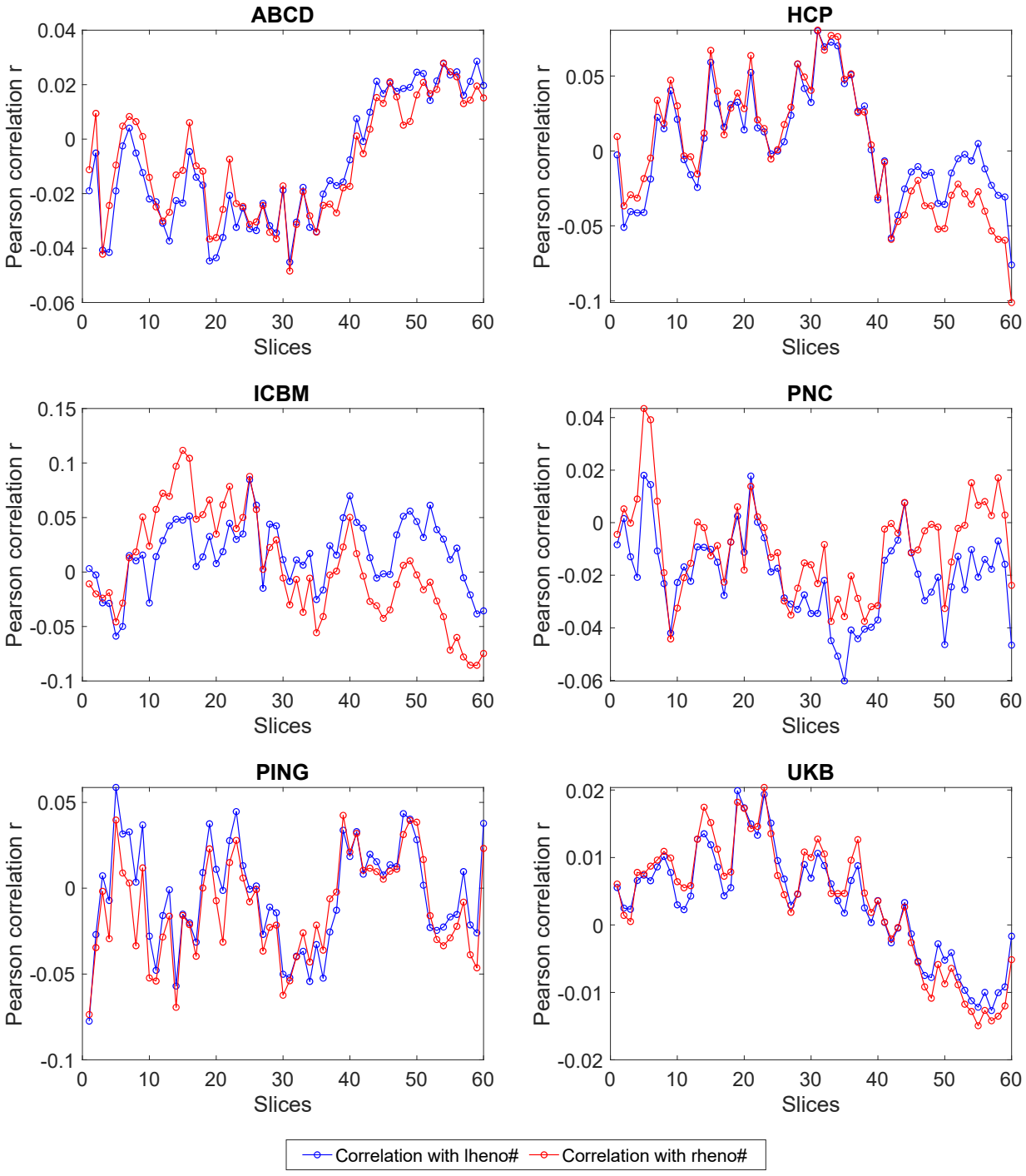

Figure S28: Correlations between sectional width asymmetries and FreeSurfer Euler number in each individual data set. No correlations were significant (P > 0.05/120). lheno# = Euler number of left hemisphere, rheno# = Euler number of right hemisphere.

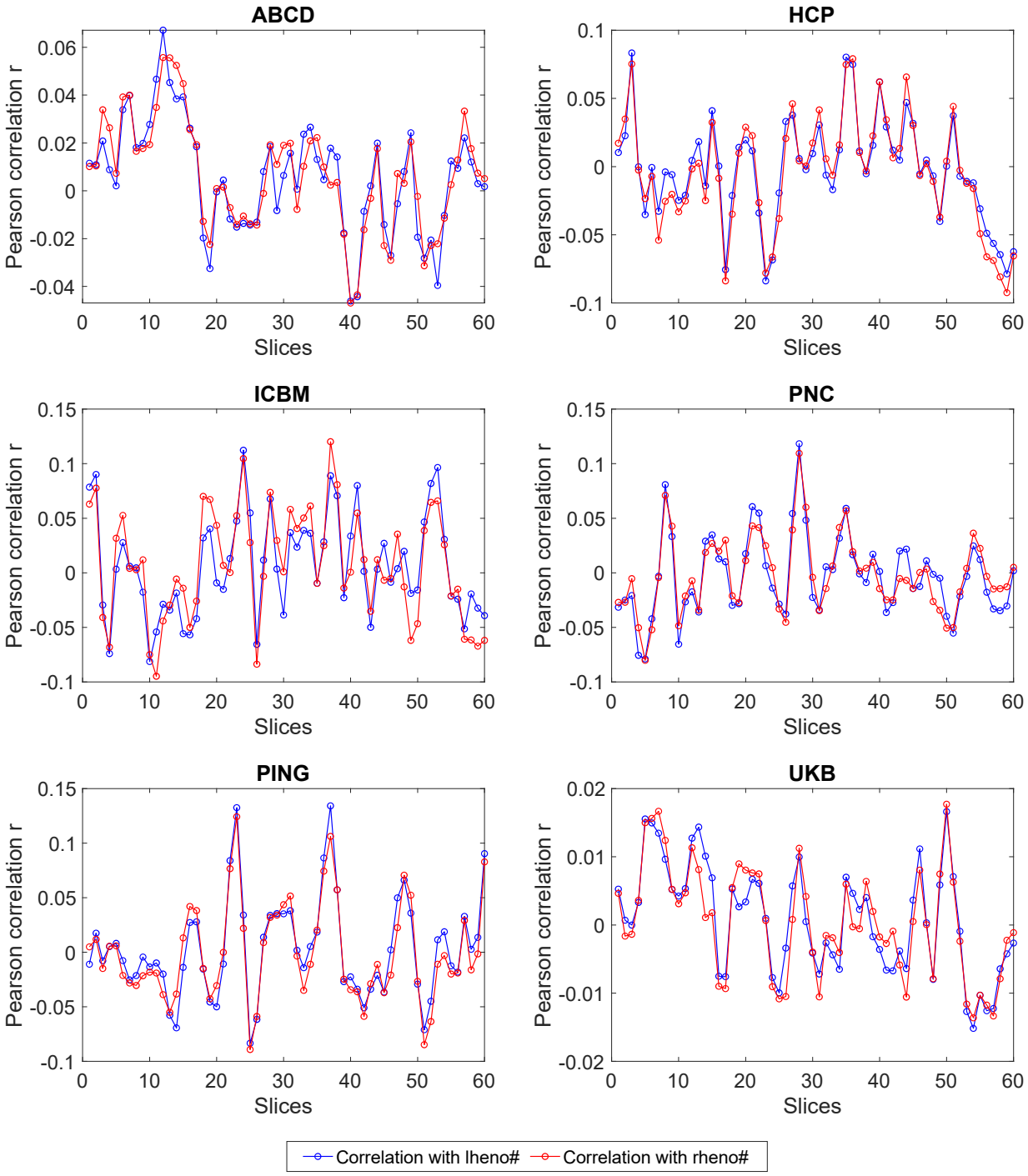

Figure S29: Correlations between sectional perimeter asymmetries and FreeSurfer Euler number in each individual data set. No correlations were significant (P > 0.05/120). lheno# = Euler number of left hemisphere, rheno# = Euler number of right hemisphere.

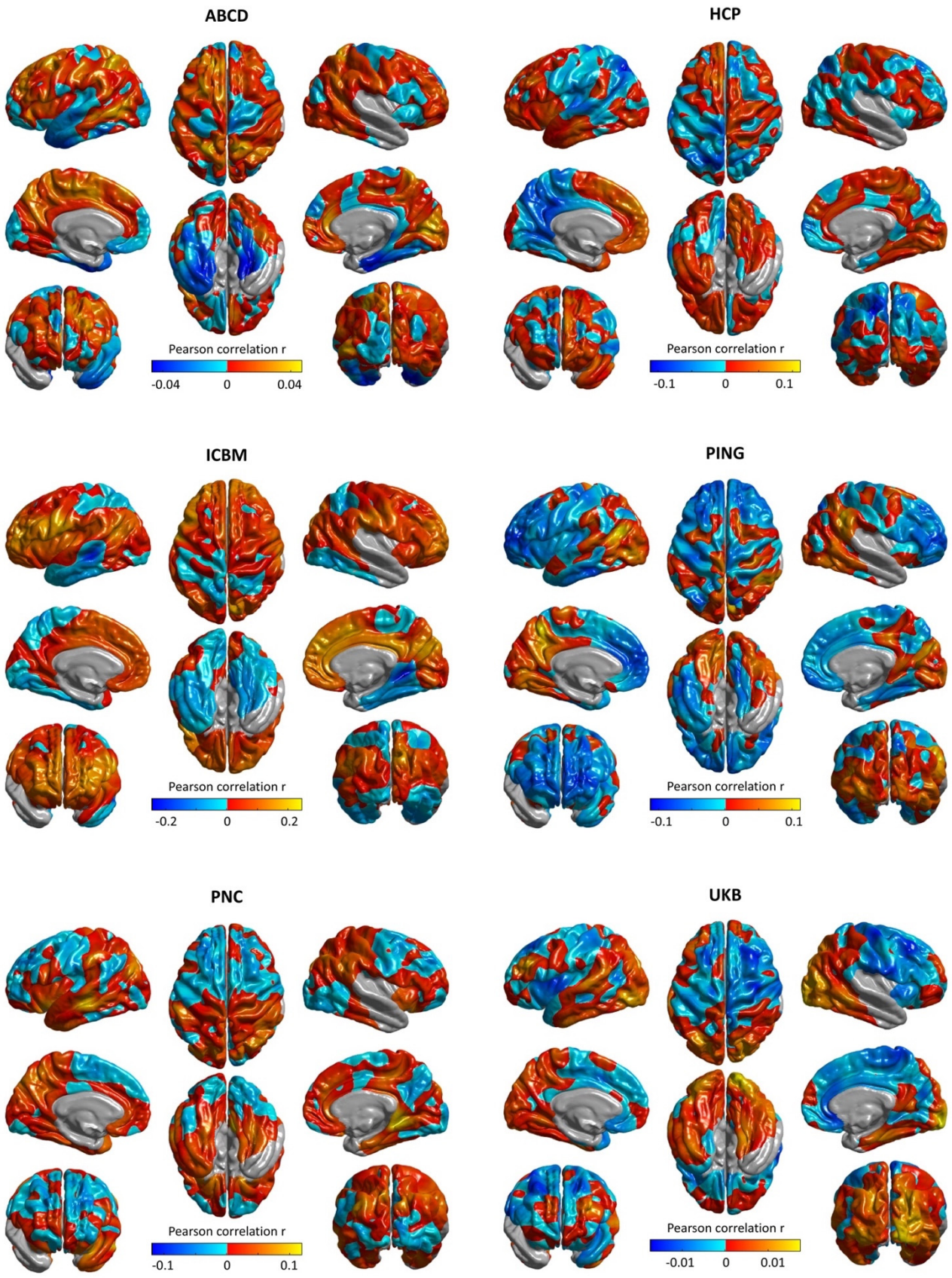

Figure S30: Correlations between surface positional asymmetries along the left-right axis and FreeSurfer Euler number in each individual data set. No correlations were significant (random field theory (RFT) corrected P > 0.05/3). lheno# = Euler number of left hemisphere, rheno# = Euler number of right hemisphere.

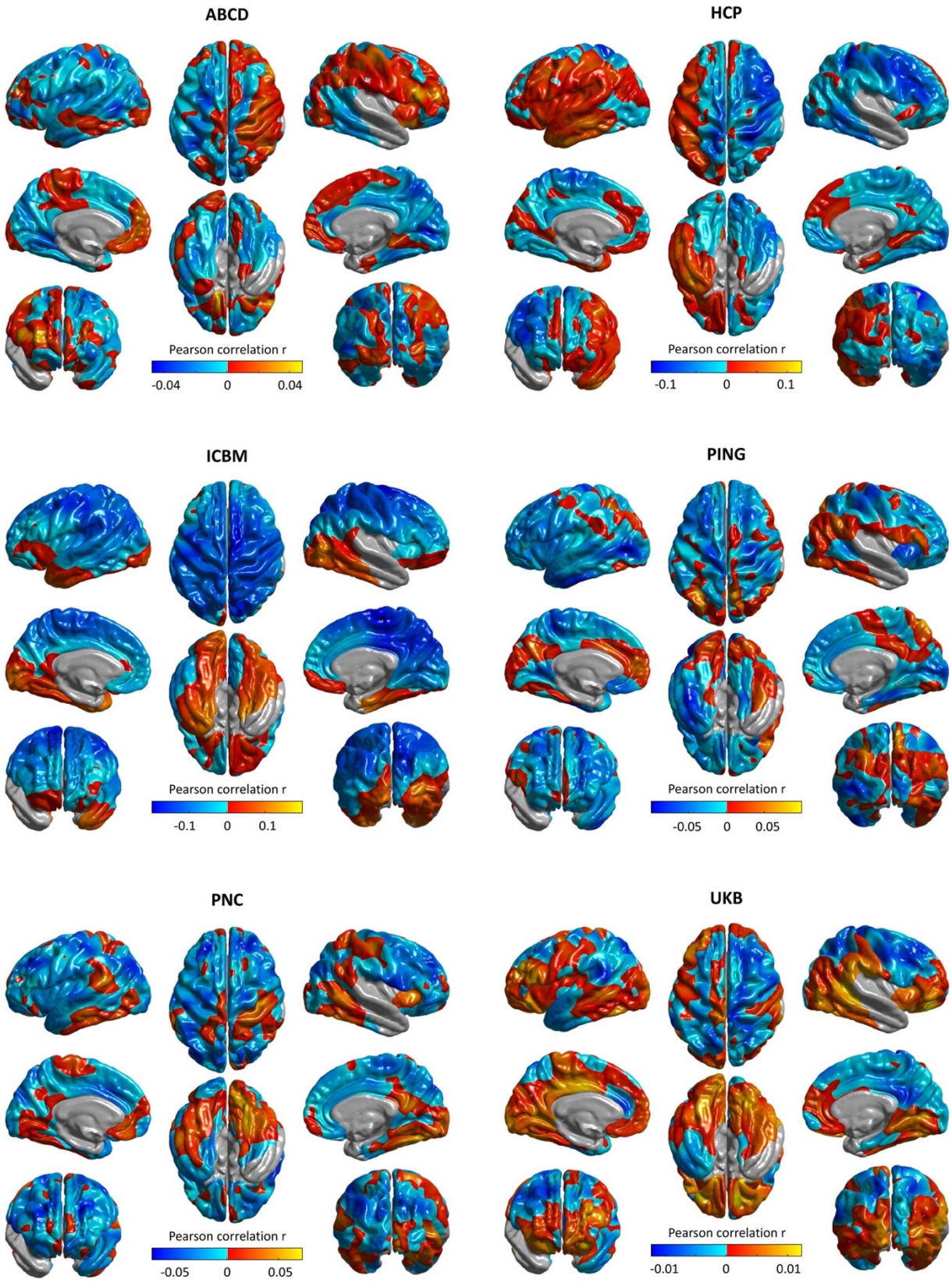

Figure S31: Correlations between surface positional asymmetries along the anterior-posterior axis and FreeSurfer Euler number in each individual data set. No correlations were significant (random field theory (RFT) corrected P > 0.05/3). lheno# = Euler number of left hemisphere, rheno# = Euler number of right hemisphere.

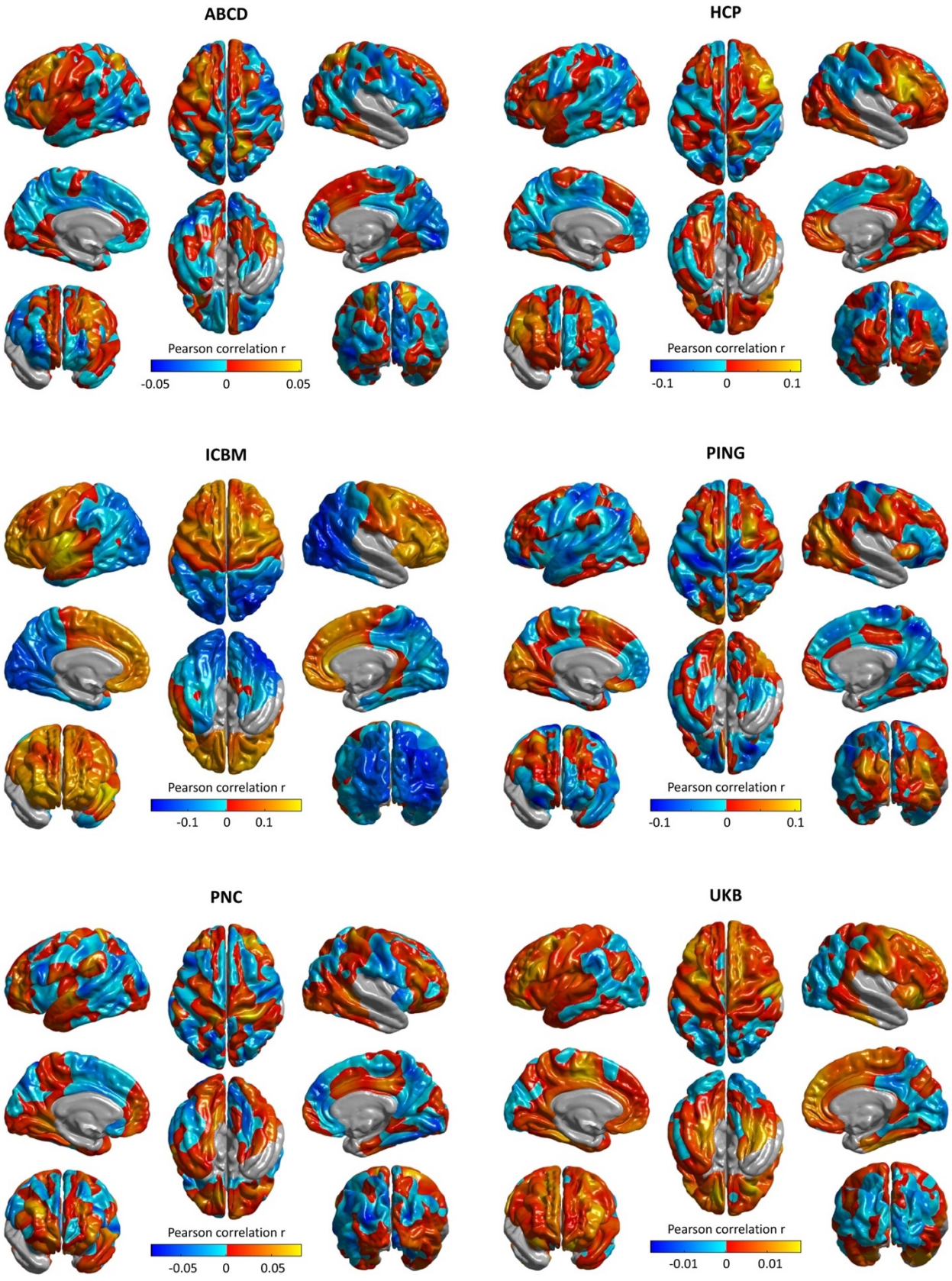

Figure S32: Correlations between surface positional asymmetries along the dorsal-ventral axis and FreeSurfer Euler number in each individual data set. No correlations were significant (random field theory (RFT) corrected P > 0.05/3). lheno# = Euler number of left hemisphere, rheno# = Euler number of right hemisphere.

Table S1. Sample characteristics in the individual and pooled datasets.

	ABCD	HCP	ICBM	PING	PNC	UKB	POOL
Sample size	2769	860	371	677	922	18513	24112
Age in years (M (SD), MED, min-max)	10 (0.61), 10, 9-10.92	28.81 (3.68), 29, 22-37	33.82 (14.01), 28, 18-80	12.05 (4.98), 11.42, 3.17-21	14.73 (3.42), 14.92, 8.25-22.58	62.65 (7.45), 63.20, 44.57-80.66	51.33 (21.65), 59.57, 3.17-80.66
Sex, male (%)	1449 (52.33%)	379 (44.07%)	193 (53.10%)	355 (52.44%)	428 (46.42%)	8908 (48.12%)	11716 (48.59%)
Handedness, RH/LH/MH	2189/196/392	627/45/188	333/34/4	577/70/30	796/126/0	16489/1747/277	21003/2218/891
Ethnicity, European (%)	1399 (50.52%)	630 (75.90%)	262 (70.62%)	515 (76.07%)	459 (49.78%)	15900 (85.88%)	19165 (79.48%)

Note: M = mean, SD = standard deviation, MED = median, min = minimum, max = maximum, RH = right-handed, LH = left-handed, MH = mixed-handed.

Table S2: Population-level average petalia, bending and shift in the individual and pooled datasets.

	Petalia				Bending				Shift			
	Frontal		Occipital		Frontal		Occipital		Frontal		Occipital	
	T-value	P-value	T-value	P-value	T-value	P-value	T-value	P-value	T-value	P-value	T-value	P-value
ABCD	25.76	1.30e-131	33.80	3.20e-210	12.42	8.22-35	33.84	9.88e-211	4.30	8.72e-6	13.92	5.98e-43
	Frontal vs Occipital				Frontal vs Occipital				Frontal vs Occipital			
	T = 13.91		P = 1.45e-43		T = -27.52		P = 1.10e-156		T = 4.56		P = 2.59e-6	
HCP	0.77	0.22	10.14	3.12e-23	10.52	9.71e-25	10.87	3.70e-26	0.069	0.47	-7.68	2.22-14
	Frontal vs Occipital				Frontal vs Occipital				Frontal vs Occipital			
	T = 7.90		P = 2.44e-15		T = 13.67		P = 9.84e-41		T = 4.63		P = 1.97e-6	
ICBM	-6.13	1.1e-9	-8.68	6.40e-17	0.32	0.38	9.19	1.45e-18	-0.080	0.47	-4.85	9.14e-7
	Frontal vs Occipital				Frontal vs Occipital				Frontal vs Occipital			
	T = 4.48		P = 4.23e-6		T = -8.71		P = 9.65e-18		T = 3.01		P = 0.0013	
PING	-11.69	3.38e-29	-18.44	4.27e-62	4.30	9.94e-6	18.86	2.15e-64	3.36	4.19e-4	-6.56	5.25e-11
	Frontal vs Occipital				Frontal vs Occipital				Frontal vs Occipital			
	T = 9.50		P = 4.74e-21		T = -16.64		P = 5.02e-57		T = 1.46		P = 0.071	
PNC	12.28	1.67e-32	-16.92	1.93e-56	3.10	9.82e-4	17.81	1.76e-61	-0.92	0.18	-7.41	1.42e-13
	Frontal vs Occipital				Frontal vs Occipital				Frontal vs Occipital			
	T = 8.05		P = 7.26e-16		T = -15.83		P =2.43e-53		T = 4.14		P = 1.81e-5	
UKB	-56.05	<2.23e-308	-86.93	<2.23e-308	21.57	3.33e-102	88.11	<2.23e-308	-7.14	4.72e-13	-39.93	<2.23e-308
	Frontal vs Occipital				Frontal vs Occipital				Frontal vs Occipital			
	T = 39.31		P < 2.23e-308		T = -72.60		P < 2.23e-308		T = 19.90		P = 6.05e-88	
POOL	-62.60	<2.23e-308	-96.48	<2.23e-308	22.98	7.33e-116	98.32	<2.23e-308	-8.51	9.40e-18	-44.29	<2.23e-308
	Frontal vs Occipital				Frontal vs Occipital				Frontal vs Occipital			
	T = 44.01		P < 2.23e-308		T = -82.17		P < 2.23e-308		T = 21.26		P = 4.25e-100	

Note: non-significant (P > 0.05/6) results are highlighted in blue.

Table S3: Prevalence of different configurations of frontal/occipital petalia, bending and shift in the pooled sample.

	Petalia				Bending				Shift			
Male		LFP (%)	RFP (%)			LFB (%)	RFB (%)			UFS (%)	DFS (%)	
	ROP (%)	17.07	8.70	25.77	LOB (%)	13.02	12.39	25.41	UOS (%)	18.39	19.65	38.04
	LOP (%)	15.70	58.53	74.23	ROB (%)	44.66	29.93	74.59	DOS (%)	28.73	33.24	61.97
		32.77	67.23			57.68	42.32			47.12	52.89	
Female		LFP (%)	RFP (%)			LFB (%)	RFB (%)			UFS (%)	DFS (%)	
	ROP (%)	17.13	10.23	27.36	LOB (%)	12.77	13.36	26.13	UOS (%)	18.69	19.42	38.11
	LOP (%)	18.29	54.36	72.65	ROB (%)	41.32	32.55	73.87	DOS (%)	29.81	32.08	61.89
		35.42	64.59			54.09	46.91			48.50	51.50	
Right Handed		LFP (%)	RFP (%)			LFB (%)	RFB (%)			UFS (%)	DFS (%)	
	ROP (%)	16.80	9.48	26.28	LOB (%)	13.00	12.71	25.71	UOS (%)	18.61	19.66	38.27
	LOP (%)	16.98	56.74	73.72	ROB (%)	43.33	30.96	74.29	DOS (%)	29.30	32.43	61.73
		33.78	66.22			56.33	43.67			47.91	52.09	
Left Handed		LFP (%)	RFP (%)			LFB (%)	RFB (%)			UFS (%)	DFS (%)	
	ROP (%)	19.07	8.56	27.63	LOB (%)	11.86	14.19	26.05	UOS (%)	17.95	19.16	37.11
	LOP (%)	17.21	55.16	72.37	ROB (%)	40.79	33.16	73.95	DOS (%)	29.35	33.53	62.88
		36.28	63.72			52.65	47.35			47.30	52.69	
Mixed Handed		LFP (%)	RFP (%)			LFB (%)	RFB (%)			UFS (%)	DFS (%)	
	ROP (%)	19.13	12.03	31.16	LOB (%)	12.83	13.75	26.58	UOS (%)	18.44	17.53	35.97
	LOP (%)	17.75	51.09	68.84	ROB (%)	39.40	34.02	73.42	DOS (%)	28.75	35.28	64.03
		36.88	63.88			52.23	47.77			47.19	52.91	
Whole Sample		LFP (%)	RFP (%)			LFB (%)	RFB (%)			UFS (%)	DFS (%)	
	ROP (%)	17.10	9.49	26.59	LOB (%)	12.89	12.89	25.78	UOS (%)	18.54	19.53	38.07
	LOP (%)	17.03	56.38	73.41	ROB (%)	42.95	31.27	74.22	DOS (%)	29.28	32.64	61.92
		34.13	65.87			55.84	44.16			47.82	52.17	

LFP: left-frontal petalia	LFB: leftward-frontal Bending	UFS: upward-frontal shift
RFP: right-frontal petalia	RFB: rightward-frontal Bending	DFS: downward-frontal shift
LOP: left-occipital petalia	LOB: leftward-occipital bending	UOS: upward-occipital shift
ROP: right-occipital petalia	ROB: rightward-occipital bending	DOS: downward-occipital shift

Prevalence rates of the most predominant configurations in each group are highlighted in red.

Table S4: Sex differences in variance of lobar brain torque profiles assessed in the pooled sample.

	var(Males)	var(Females)	VR	F	P
Frontal Petalia	2.51	1.96	1.28	144.8	2.98E-33
Occipital Petalia	4.96	4.46	1.11	38.91	4.51E-10
Frontal Bending	4.68	3.8	1.23	109.63	1.34E-25
Occipital Bending	25.38	24.93	1.02	1.45	0.228
Frontal Shift	19.68	18.82	1.05	4.2	0.0404
Occipital Shift	12.5	12.71	0.98	1.6	0.206

Var: Variance, VR: variance ratio
Significant sex differences in variances ($P < 0.05/6$) are highlighted in red.

Table S5: Sex and handedness differences in prevalence of brain torque configurations in the pooled sample.

Petalia Configuration								
	LFP/ROP		LFP/LOP		RFP/ROP		RFP/LOP	
	χ^2	P-value	χ^2	P-value	χ^2	P-value	χ^2	P-value
M vs F	0.015	0.90	27.60	1.49e-7	15.81	6.99e-5	41.28	1.32e-10
RH vs LH	7.07	0.0078	0.072	0.79	1.92	0.17	1.97	0.16
RH vs MH	3.23	0.073	0.36	0.55	6.29	0.012	10.88	9.71e-4
LH vs MH	0.0014	0.97	0.13	0.72	8.64	0.0033	4.15	0.042
Bending Configuration								
	LFB/LOB		LFB/ROB		RFB/LOB		RFB/ROB	
	χ^2	P-value	χ^2	P-value	χ^2	P-value	χ^2	P-value
M vs F	0.31	0.58	26.55	2.57E-7	4.85	0.028	18.60	1.6E-5
RH vs LH	2.62	0.13	5.10	0.024	3.77	0.052	4.42	0.036
RH vs MH	0.023	0.88	5.25	0.022	0.80	0.37	3.67	0.055
LH vs MH	0.55	0.46	0.50	0.48	0.10	0.75	0.21	0.65
Shift Configuration								
	UFS/UOS		UFS/DOS		DFS/UOS		DFS/DOS	
	χ^2	P-value	χ^2	P-value	χ^2	P-value	χ^2	P-value
M vs F	0.34	0.56	3.30	0.069	0.18	0.67	3.55	0.060
RH vs LH	0.56	0.46	0.0023	0.96	0.30	0.58	1.07	0.30
RH vs MH	0.016	0.90	0.12	0.73	2.41	0.12	3.09	0.079
LH vs MH	0.10	0.75	0.11	0.74	1.09	0.30	0.84	0.36

M: Male, F: Female, RH: right-handed, LH: left-handed, MH: mixed-handed.
LFP: left-frontal petalia; RFP: right-frontal petalia; LOP: left-occipital petalia; ROP: right-occipital petalia.
LFB: leftward-frontal Bending, RFB: rightward-frontal Bending, LOB: leftward-occipital bending, ROB: rightward-occipital bending.
UFS: upward-frontal relative shift, DFS: downward-frontal relative shift, UOS: upward-occipital relative shift, DOS: downward-occipital relative shift.
Typical brain torque configurations are highlighted in blue.
Significant sex/handedness differences ($P < 0.05/6$) are highlighted in red.

Table S6: Sex and handedness differences in prevalence of single brain torque profiles in the pooled sample.

Petalia								
	LFP		RFP		LOP		ROP	
	χ^2	P-value	χ^2	P-value	χ^2	P-value	χ^2	P-value
M vs F	18.16	2.03e-05	18.16	2.03e-05	7.52	0.0061	7.52	0.0061
RH vs LH	5.39	0.02	5.39	0.02	1.82	0.18	1.82	0.18
RH vs MH	3.59	0.058	3.59	0.058	10.23	0.0016	10.23	0.0016
LH vs MH	0.098	0.75	0.098	0.75	3.78	0.52	3.78	0.52
Bending								
	LFB		RFB		LOB		ROB	
	χ^2	P-value	χ^2	P-value	χ^2	P-value	χ^2	P-value
M vs F	30.38	3.56e-8	30.38	3.56e-8	1.59	0.21	1.59	0.21
RH vs LH	0.86	0.35	0.86	0.35	0.11	0.74	0.11	0.74
RH vs MH	5.71	0.017	5.71	0.017	0.32	0.57	0.32	0.57
LH vs MH	2.61	0.11	2.61	0.11	0.09	0.76	0.09	0.76
Shift								
	UFS		DFS		UOS		DOS	
	χ^2	P-value	χ^2	P-value	χ^2	P-value	χ^2	P-value
M vs F	4.44	0.035	4.44	0.035	0.014	0.91	0.014	0.91
RH vs LH	0.29	0.59	0.29	0.59	1.09	0.30	1.09	0.30
RH vs MH	0.17	0.68	0.17	0.68	1.88	0.17	1.88	0.17
LH vs MH	0.0029	0.96	0.0029	0.96	0.35	0.55	0.35	0.55

M: Male, F: Female, RH: right-handed, LH: left-handed, MH: mixed-handed.
LFP: left-frontal petalia; RFP: right-frontal petalia; LOP: left-occipital petalia; ROP: right-occipital petalia.
LFB: leftward-frontal Bending, RFB: rightward-frontal Bending, LOB: leftward-occipital bending, ROB: rightward-occipital bending.
UFS: upward-frontal relative shift, DFS: downward-frontal relative shift, UOS: upward-occipital relative shift, DOS: downward-occipital relative shift.
Typical brain torque features are highlighted in blue.
Significant sex/handedness differences ($P < 0.05/6$) are highlighted in red.

Table S7: Handedness differences in variance of lobar brain torque profiles. assessed in the pooled sample..

				RH vs LH			RH vs MH			LH vs MH		
	var(RH)	var(LH)	var(MH)	VR	F	P	VR	F	P	VR	F	P
Frontal Petalia	2.24	2.26	1.89	0.99	0.26	0.61	1.18	8.62	3.33E-3	1.19	8.34	3.91E-3
Occipital Petalia	4.74	4.77	3.73	0.99	0.01	0.92	1.27	14.52	1.39E-4	1.28	11.77	6.12E-4
Frontal Bending	4.24	4.23	3.79	1.00	0.64	0.42	1.12	3.95	0.047	1.12	5.01	0.025
Occipital Bending	25.31	25.34	20.97	1.00	0.03	0.86	1.21	15.64	7.70E-05	1.21	11.18	8.38E-4
Frontal Shift	19.22	18.95	20.36	1.01	0.13	0.72	0.94	0.15	0.703	0.93	0.28	0.60
Occipital Shift	12.63	12.98	11.22	0.97	1.42	0.23	1.13	7.74	5.41E-3	1.16	9.54	2.02E-3

RH: right-handed, LH: left-handed, MH: mixed-handed, Var: Variance, VR: variance ratio
Significant handedness differences ($P < 0.05/6$) are highlighted in red.

Table S8 (separate file, Table S8-S14.xlsx). Phenome-wide associations for frontal/occipital petalia, bending and shift identified using the UK Biobank dataset (P<0.05/6334=7.89e-6). Associations with P < 0.05/6334/348 = 2.27e-8 are highlighted in green.

Table S9 (separate file, Table S8-S14.xlsx). Phenome-wide associations for hemispheric width asymmetries identified using the UK Biobank dataset (P<0.05/6334=7.89e-6). Associations with P < 0.05/6334/348 = 2.27e-8 are highlighted in green.

Table S10 (separate file, Table S8-S14.xlsx). Phenome-wide associations for hemispheric perimeter asymmetries identified using the UK Biobank dataset (P<0.05/6334=7.89e-6). Associations with P < 0.05/6334/348 = 2.27e-8 are highlighted in green.

Table S11 (separate file, Table S8-S14.xlsx). Phenome-wide associations for surface positional asymmetries along the antero-posterior axis (Asym_AP) identified using the UK Biobank dataset (P<0.05/6334=7.89e-6). Associations with P < 0.05/6334/348 = 2.27e-8 are highlighted in green. For the abbreviations of brain surface regions, see Table S14.

Table S12 (separate file, Table S8-S14.xlsx). Phenome-wide associations for surface positional asymmetries along the left-right axis identified using the UK Biobank dataset (Asym_LR) (P<0.05/6334=7.89e-6). Associations with P < 0.05/6334/348 = 2.27e-8 are highlighted in green. For the abbreviations of brain surface regions, see Table S14.

Table S13 (separate file, Table S8-S14.xlsx). Phenome-wide associations for surface positional asymmetries along the dorsal-ventral axis identified using the UK Biobank dataset (Asym_DV) (P<0.05/6334=7.89e-6). Associations with P < 0.05/6334/348 = 2.27e-8 are highlighted in green. For the abbreviations of brain surface regions, see Table S14.

Table S14 (separate file, Table S8-S14.xlsx). List of anatomical parcellations defined by the FreeSurfer Destrieux atlas.

Table S15: Associations (P < 0.05/20) between brain torque (BT) features and child behavior checklist (CBCL) scales in the ABCD cohort. For the abbreviations of brain surface regions, see Table S14.

BT	CBCL measure	r	Beta	P
Asym_Width_Slice18	Social CBCL Syndrome Scale	6.31E-02	6.40E-02	8.97E-04
Asym_Width_Slice18	Thought CBCL Syndrome Scale	6.53E-02	6.70E-02	5.89E-04
Asym_LR-G_temp_sup-Plan_tempo	RuleBreak CBCL Syndrome Scale	-6.32E-02	-6.39E-02	8.78E-04
Asym_AP-S_central	RuleBreak CBCL Syndrome Scale	6.31E-02	5.92E-02	9.01E-04
Asym_AP-G_precentral	RuleBreak CBCL Syndrome Scale	5.84E-02	5.46E-02	2.13E-03
Asym_AP-S_central	Aggressive CBCL Syndrome Scale	5.86E-02	5.53E-02	2.04E-03
Asym_DV-S_orbital-H_Shaped	Aggressive CBCL Syndrome Scale	-5.78E-02	-5.71E-02	2.34E-03
Asym_DV-S_orbital_med-olfact	Aggressive CBCL Syndrome Scale	-6.11E-02	-6.18E-02	1.30E-03
Asym_DV-S_orbital_med-olfact	External CBCL Syndrome Scale	-6.91E-02	-7.06E-02	2.72E-04
Asym_DV-G_insular_short	External CBCL Syndrome Scale	-6.01E-02	-5.94E-02	1.56E-03
Asym_DV-G_insular_short	TotProb CBCL Syndrome Scale	-5.81E-02	-5.78E-02	2.23E-03
Asym_Width_Slice18	AnxDisord CBCL DSM5 Scale	5.84E-02	5.86E-02	2.11E-03
Asym_Perimeter_Slice40	SomaticPr CBCL DSM5 Scale	6.40E-02	6.36E-02	7.52E-04
Asym_DV-G_insular_short	ADHD CBCL DSM5 Scale	-6.17E-02	-6.16E-02	1.17E-03
Asym_DV-S_circular_insula_sup	ADHD CBCL DSM5 Scale	-6.07E-02	-6.02E-02	1.39E-03
Asym_DV-S_orbital-H_Shaped	Opposit CBCL DSM5 Scale	-6.96E-02	-6.92E-02	2.48E-04
Asym_DV-G_orbital	Opposit CBCL DSM5 Scale	-6.83E-02	-6.84E-02	3.22E-04
Asym_DV-S_orbital_med-olfact	Opposit CBCL DSM5 Scale	-7.20E-02	-7.33E-02	1.48E-04
Asym_DV-S_front_inf	Opposit CBCL DSM5 Scale	-5.77E-02	-5.62E-02	2.38E-03
Asym_DV-S_circular_insula_ant	Opposit CBCL DSM5 Scale	-6.20E-02	-6.03E-02	1.09E-03
Asym_DV-G_insular_short	Opposit CBCL DSM5 Scale	-6.31E-02	-6.32E-02	8.98E-04
Asym_Width_Slice47	Conduct CBCL DSM5 Scale	-6.24E-02	-5.76E-02	1.01E-03
Asym_Width_Slice48	Conduct CBCL DSM5 Scale	-6.46E-02	-5.95E-02	6.75E-04
Asym_Width_Slice49	Conduct CBCL DSM5 Scale	-5.79E-02	-5.28E-02	2.29E-03
Asym_Width_Slice50	Conduct CBCL DSM5 Scale	-6.18E-02	-5.70E-02	1.13E-03
Asym_Width_Slice51	Conduct CBCL DSM5 Scale	-5.98E-02	-5.48E-02	1.65E-03
Asym_Width_Slice52	Conduct CBCL DSM5 Scale	-6.23E-02	-5.72E-02	1.03E-03
Asym_Width_Slice53	Conduct CBCL DSM5 Scale	-5.82E-02	-5.28E-02	2.20E-03
Asym_LR-G_temp_sup-Plan_tempo	Conduct CBCL DSM5 Scale	-6.91E-02	-7.01E-02	2.72E-04
Asym_LR-G_precuneus	Conduct CBCL DSM5 Scale	-6.34E-02	-6.09E-02	8.51E-04
Asym_AP-S_central	Conduct CBCL DSM5 Scale	7.13E-02	6.79E-02	1.73E-04
Asym_AP-G_pariet_inf-Supramar	Conduct CBCL DSM5 Scale	5.86E-02	5.56E-02	2.05E-03
Asym_AP-G_postcentral	Conduct CBCL DSM5 Scale	6.43E-02	6.11E-02	7.17E-04
Asym_AP-G_precentral	Conduct CBCL DSM5 Scale	6.46E-02	6.12E-02	6.67E-04
Asym_AP-S_precentral-sup-part	Conduct CBCL DSM5 Scale	5.75E-02	5.50E-02	2.49E-03
Asym_DV-G_postcentral	Conduct CBCL DSM5 Scale	-5.84E-02	-5.56E-02	2.11E-03
Asym_Width_Slice18	Stress CBCL Scale2007 Scale	5.83E-02	5.88E-02	2.13E-03
Asym_Width_Slice20	Stress CBCL Scale2007 Scale	5.92E-02	6.06E-02	1.82E-03
Asym_DV-G_insular_short	Stress CBCL Scale2007 Scale	-5.80E-02	-5.79E-02	2.27E-03

Table S16: Associations (P < 0.05/112) between brain torque (BT) features and GOASSESS psychopathological measures in the PNC cohort. For the abbreviations of brain surface regions, see Table S14.

BT	Psychopathology measures	T	Beta	P
Asym_DV-S_front_sup	ADD011 (Attention Deficit Disorder: trouble paying attention)	-3.56	-0.12	1.96E-04
Occipital_Petalia	ADD012 (Attention Deficit Disorder: problems following instructions)	3.50	0.12	2.42E-04
Asym_AP-G_oc-temp_lat-fusifor	ADD012 (Attention Deficit Disorder: problems following instructions)	3.66	0.12	1.33E-04
Asym_AP-S_postcentral	ADD012 (Attention Deficit Disorder: problems following instructions)	3.71	0.12	1.08E-04
Asym_AP-S_oc-temp_med_and_Lingual	ADD012 (Attention Deficit Disorder: problems following instructions)	3.59	0.12	1.76E-04
Asym_DV-G_cingul-Post-dorsal	ADD015 (Attention Deficit Disorder: trouble making plans)	3.93	0.13	4.66E-05
Asym_LR-S_subparietal	ADD016 (Attention Deficit Disorder: trouble listening)	-3.41	-0.12	3.45E-04
Asym_LR-G_precuneus	ADD016 (Attention Deficit Disorder: trouble listening)	-3.36	-0.11	4.14E-04
Asym_AP-S_oc-temp_lat	ADD016 (Attention Deficit Disorder: trouble listening)	3.46	0.12	2.80E-04
Asym_AP-G_oc-temp_lat-fusifor	ADD016 (Attention Deficit Disorder: trouble listening)	3.74	0.13	9.81E-05
Asym_AP-G_and_S_occipital_inf	ADD016 (Attention Deficit Disorder: trouble listening)	3.83	0.13	6.95E-05
Asym_AP-G_front_middle	ADD016 (Attention Deficit Disorder: trouble listening)	3.59	0.12	1.73E-04
Asym_DV-G_oc-temp_lat-fusifor	ADD016 (Attention Deficit Disorder: trouble listening)	-3.41	-0.12	3.39E-04
Asym_LR-G_and_S_frontomargin	AGR007 (Agoraphobia: fear of car travel)	4.03	0.13	3.07E-05
Asym_Perimeter_Slice7	CDD001 (Conduct Disorder: lying or stealing)	3.50	0.12	2.40E-04
Asym_Width_Slice16	DEP004 (Depression: irritability)	3.43	0.11	3.18E-04
Asym_Width_Slice17	DEP004 (Depression: irritability)	3.66	0.12	1.35E-04
Asym_LR-S_precentral-inf-part	MAN002 (Manic Disorder: full of energy)	3.47	0.12	2.73E-04
Asym_LR-S_orbital_lateral	OCD002 (Obsessive Compulsive Disorder: thoughts of violence)	-3.34	-0.11	4.38E-04
Asym_AP-G_front_inf-Orbital	OCD002 (Obsessive Compulsive Disorder: thoughts of violence)	-3.49	-0.12	2.57E-04
Asym_Perimeter_Slice22	OCD003 (Obsessive Compulsive Disorder: thoughts of contamination)	3.82	0.13	7.26E-05
Asym_Perimeter_Slice30	OCD003 (Obsessive Compulsive Disorder: thoughts of contamination)	3.72	0.13	1.07E-04
Asym_DV-G_cingul-Post-ventral	OCD013 (Obsessive Compulsive Disorder: compulsive checking)	-3.45	-0.12	2.93E-04
Asym_DV-S_parieto_occipital	OCD013 (Obsessive Compulsive Disorder: compulsive checking)	-3.70	-0.13	1.13E-04
Asym_LR-S_orbital_med-olfact	OCD015 (Obsessive Compulsive Disorder: repeat routine activities)	3.34	0.11	4.30E-04
Asym_Width_Slice21	ODD002 (Oppositional Defiant Disorder: breaking rules)	3.36	0.11	4.01E-04
Asym_AP-S_front_inf	ODD002 (Oppositional Defiant Disorder: breaking rules)	3.40	0.12	3.49E-04
Asym_DV-G_front_middle	ODD002 (Oppositional Defiant Disorder: breaking rules)	-3.45	-0.12	2.92E-04
Asym_DV-S_suborbital	ODD003 (Oppositional Defiant Disorder: often annoy/blame others)	-3.45	-0.12	2.95E-04
Asym_AP-S_postcentral	ODD006 (Oppositional Defiant Disorder: irritability for unfairness)	3.41	0.12	3.43E-04
Asym_DV-G_and_S_subcentral	PAN001 (Panic Disorder: had panic attack)	3.51	0.12	2.33E-04
Asym_Width_Slice13	PAN004 (Panic Disorder: fear of losing control/dying)	3.38	0.11	3.77E-04
Asym_Width_Slice14	PAN004 (Panic Disorder: fear of losing control/dying)	3.73	0.12	1.00E-04
Asym_Width_Slice15	PAN004 (Panic Disorder: fear of losing control/dying)	3.70	0.12	1.12E-04
Asym_Width_Slice20	PHB001 (Specific Phobia: animal phobia)	3.55	0.12	1.99E-04
Asym_Width_Slice21	PHB001 (Specific Phobia: animal phobia)	3.68	0.12	1.23E-04
Asym_Width_Slice22	PHB001 (Specific Phobia: animal phobia)	3.48	0.12	2.60E-04
Asym_Width_Slice23	PHB001 (Specific Phobia: animal phobia)	3.74	0.12	9.61E-05
Asym_LR-Pole_temporal	PHB001 (Specific Phobia: animal phobia)	3.85	0.13	6.22E-05
Asym_LR-S_oc_sup_and_transversal	PHB001 (Specific Phobia: animal phobia)	-3.40	-0.11	3.55E-04
Asym_LR-G_occipital_middle	PHB001 (Specific Phobia: animal phobia)	-3.48	-0.12	2.63E-04
Asym_Perimeter_Slice41	PSY001 (Psychosis: auditory verbal hallucination)	-3.47	-0.11	2.68E-04
Asym_Perimeter_Slice52	SCR007 (General Problems: hospitalized for emotions/behaviors)	3.89	0.13	5.28E-05
Asym_LR-S_circular_insula_inf	SCR007 (General Problems: hospitalized for emotions/behaviors)	3.40	0.11	3.55E-04
Asym_LR-S_collat_transv_post	SEP510 (Separation Anxiety: worry about safety of self/family)	-3.39	-0.11	3.70E-04
Asym_Perimeter_Slice48	SEP511 (Separation Anxiety: fear of being alone)	3.67	0.12	1.31E-04
Asym_LR-G_rectus	SOC005 (Social Anxiety: fear of center of attention)	3.41	0.11	3.37E-04

Table S17: Effects of age by psychopathology on brain torque (BT) features in children and adolescents in the PNC cohort (P < 0.05/112). For the abbreviations of brain surface regions, see Table S14.

BT	Psychopathology	F	Beta	P
Asym_LR-Lat_Fis-ant-Horizont	ADD013 (Attention Deficit Disorder: dislike school/homework)	12.74	-0.24	3.79E-04
Asym_LR-G_temp_sup-Lateral	ADD022 (Attention Deficit Disorder: difficulty waiting turns)	13.59	0.30	2.42E-04
Asym_LR-S_calcarine	CDD008 (Conduct Disorder: threaten someone)	15.13	0.35	1.08E-04
Asym_LR-G_front_inf-Opercular	DEP001 (Depression: feeling sad)	12.44	0.30	4.41E-04
Asym_Perimeter_Slice38	MAN005 (Manic Disorder: overly excited)	20.17	-0.44	8.02E-06
Asym_Perimeter_Slice24	OCD005 (Obsessive Compulsive Disorder: hyper-responsibility)	13.03	-0.40	3.24E-04
Asym_AP-G_oc-temp_med-Lingual	PSY001 (Psychosis: auditory verbal hallucination)	14.33	-0.49	1.63E-04

Table S18: SNP-based Heritability of lobar brain torque features estimated using the LDSC and GCTA-GREML methods. LDSC was applied to the GWAS summary statistics for the UK biobank (UKB) cohort and the meta-GWAS summary statistics. GCTA-GREML was applied to the UKB genomic data.

	LDSC		GCTA-GREML
	UKB	**Meta-GWAS**	**UKB**
Brain Torque Profile	**h^2 [%95 CI] %**	**h^2 [%95 CI] %**	**h^2 [%95 CI] %**
Frontal Petalia	- (-)	2.74 [-1.59, 7.07]	0.11 [-13.22, 13.44]
Occipital Petalia	1.66 [-4.33,7.65]	2.97 [-1.03, 6.97]	7.4 [-5.54, 20.34]
Frontal Bending	- (-)	0.44 [-3.40, 4.28]	5.38 [-7.75, 18.51]
Occipital Bending	3.54 [-1.85, 8.93]	3.36 [-0.72, 7.44]	6.7 [-6.24, 19.64]
Frontal Shift	1.78 [-3.20, 6.76]	1.34 [-2.31, 4.99]	- (-)
Occipital Shift	- (-)	0.5 [-4.09, 5.09]	- (-)
CI: confidence interval; '-' presents nonsensical estimate of $h^2 < 0$.			

Table S19 (separate file, Table S19-S29.xlsx). Genetic associations identified in meta-GWAS at the significance level of P < 5e-8. Independent lead SNPs are highlighted in bold. Associations survived in further adjustment at P < 5e-8/348 = 1.44e-10 are highlighted in red.

Table S20 (separate file, Table S19-S29.xlsx). GWAS Catalog results for traits previously associated with identified genes (lead SNPs) influencing brain torque (BT).

Table S21 (separate file, Table S19-S29.xlsx). GWAS Catalog results for previously reported associations of the identified genes (lead SNPs) influencing brain torque (BT).

Table S22 (separate file, Table S19-S29.xlsx). Significant gene-based associations (P < 0.05/18359 genes = 2.72e-06) identified using MAGMA gene-based analysis.

Table S23 (separate file, Table S19-S29.xlsx). GWAS Catalog results for traits previously associated with the genes identified using MAGMA gene-based analysis.

Table S24 (separate file, Table S19-S29.xlsx). GWAS Catalog results for previously reported associations of the identified genes identified using MAGMA gene-based analysis.

Table S25 (separate file, Table S19-S29.xlsx). Significant gene-set associations (P < 0.05/7563 gene sets = 6.61e-6) identified using MAGMA gene-set analysis.

Table S26 (separate file, Table S19-S29.xlsx). Relations (P < 0.05/31 = 0.0016) between gene-based associations with brain torque features and higher gene expression levels in the human brain at particular ages.

Table S27 (separate file, Table S19-S29.xlsx). Genetic correlations between brain torque features (P < 0.05).

Table S28 (separate file, Table S19-S29.xlsx). Genetic correlations between brain torque features and other traits (P < 0.05).

Table S29 (separate file, Table S19-S29.xlsx). List of self-reported neurological and psychiatric disorders that were excluded in the UK Biobank cohort.